TUM School of Engineering and Design

INVESTIGATIONS ON METHANE OXIDATION LINKED WITH NITROGEN CYCLING PROCESSES IN THE SEASONALLY STRATIFIED LAKE FOHNSEE

Gisela Alejandra Peña Sanchez

Vollständiger Abdruck der von der TUM School of Engineering and Design der Technischen Universität München zur Erlangung des akademischen Grades einer

Doktorin der Naturwissenschaften (Dr. rer. nat)

genehmigten Dissertation.

Vorsitz: apl. Prof. Dr.sc.nat. habil. Hans Albert Gilg

Prüfer*innen der Dissertation:

1. Prof. Dr. rer. nat. Florian Einsiedl
2. Prof. Dr. rer. nat. Jürgen Geist

Die Dissertation wurde am 28.09.2022 bei der Technischen Universität München eingereicht und durch die TUM School of Engineering and Design am 09.12.2022 angenommen.

"Nothing in life is to be feared, it is only to be understood. Now is the time to understand more, so that we may fear less."

— **Marie Curie**

Abstract

Since the discovery of nitrite (n-damo) and nitrate-dependent anaerobic oxidation of methane (DAMO) in 2006, evidence has arisen about the occurrence of this process in freshwater ecosystems. Anaerobic oxidation of methane (AOM) linked with denitrification has been proposed to be a previously overlooked sink of methane in freshwater environments. However, the occurrence and relevance of DAMO in nature and, therefore, mitigating methane emissions to the atmosphere is so far largely unquantified. Nitrogen (N) loading in freshwater ecosystems is mitigated in redox transition zones by the processes of denitrification, dissimilatory nitrate reduction to ammonium, and the anaerobic oxidation of ammonium (anammox). DAMO and anammox have the potential to lower the nitrogen loading of aquatic ecosystems and to reduce methane emissions to the atmosphere. In this work, we investigated methane oxidation processes in the water column at lake Fohnsee, located in Southern Germany, during the summer stratification period. We determined the seasonal dynamics and quantitatively described the contribution of anaerobic and aerobic oxidation of methane removing CH_4 from the water column from April to December. Vertical concentration profiles and corresponding stable isotope ratios of methane ($\delta^{13}C$) and nitrate ($\delta^{15}N$ and $\delta^{18}O$), together with dissolved oxygen concentrations were measured and a numerical model was developed to evaluate whether anaerobic oxidation of methane coupled with denitrification is a key biogeochemical process at lake Fohnsee. Our data set together with the modeling results revealed a redox zone within the water column where both denitrification and anaerobic oxidation of methane are linked, contributing to approximately 70% of methane removal between June and September. Therefore, AOM linked with

denitrification represents the dominant methane sink in the water column of lake Fohnsee during summer stratification.

The data patterns also showed that the zone of anaerobic oxidation of methane was located near the lake bottom in May, and moved upwards following the seasonal vertical displacement of the oxycline and the availability of nitrate. This redox dynamic within the water column of lake Fohnsee also changed the distribution of nitrate through the water column and promoted the formation of a bacterial sulfate reduction zone close to the lake sediments.

Having identified the temporal and spatial dynamics of DAMO, in 2019 we investigated anaerobic methane oxidation linked with denitrification and anammox processes in the water column between April and September. Concentration profiles and stable isotope compositions of NO_3^- and NH_4^+, together with numerical modeling and quantification of the hydrazine synthase gene (*hzsB*) and nitrite reductase (*nirK* and *nirS*) genes, were used to identify the predominant nitrogen transformation processes at lake Fohnsee throughout the spring and summer periods. Water chemistry data, qPCR analysis, and increases of $\delta^{15}N$ and $\delta^{18}O$ values of nitrate from 7.0 to 41.0‰ and 2.0 to 28.0‰, respectively, showed that nitrate reduction to nitrite and NO occurs in an upward moving zone of the water column from June to September following the displacement of the oxycline caused by thermal stratification. We also observed an increase in $\delta^{15}N$ of ammonium from 15‰ to 28‰ in the anoxic water column. Modeling results suggest that this shift in $\delta^{15}N$-NH_4^+ is predominantly controlled by mixing between ammonium stemming from the oxic water column with $\delta^{15}N$ values of 25‰ and ammonium that is likely formed in the lake sediments by oxidation of organic matter with $\delta^{15}N$ values of 11‰. Observed gene abundances (*hzsB*, *nirK*, and *nirS*) in lake water samples collected in June and July indicated the co-occurrence of nitrate reduction and low rates of anammox, while the presence of sulfide in August

and September may have inhibited the activity of anammox bacteria near the sulfate reduction zone at the lake bottom.

This work shows that anaerobic oxidation of methane coupled with nitrate reduction is an overlooked process in the seasonally stratified lake Fohnsee leading to reduced emissions of methane to the atmosphere, and suggested that anammox has the potential to co-occur in the water column with DAMO after thermal stratification to eliminate N from the system.

Zusammenfassung

Seit der Entdeckung der nitrit- (n-damo) und nitratabhängigen anaeroben Oxidation von Methan (DAMO) im Jahr 2006 gibt es auch Hinweise auf das Vorkommen dieser Prozesse in Süßwasserökosystemen. Es wird in der Literatur daher spekuliert, dass die anaerobe Oxidation von Methan (AOM) gekoppelt mit der Denitrifikation ein bisher wenig beachteter Prozess zur Reduktion von Methanemissionen auch in Süßwasserhabitaten darstellt.

Das Vorkommen und die Bedeutung der AOM in Seen, gekoppelt mit der Denitrifikation bzw. mit Nitrit als Elektronenakzeptor und eine damit mögliche Verringerung der Methanemissionen in die Atmosphäre, sind jedoch bisher weitgehend unbekannt.

Eine Eliminierung von Stickstoff aus Süßwasserökosystemen kann an den in Seen häufig auftretenden Redox-Übergangszonen, insbesondere durch die Prozesse der Denitrifikation, gekoppelt mit der anaeroben Oxidation von Ammonium (Anammox) und mit Nitrit als Elektronenakzeptor, geknüpft sein. DAMO gekoppelt mit dem Anammox-Prozess haben das Potenzial, die Stickstoffbelastung aquatischer Ökosysteme zu verringern und gleichzeitig die Emission von Methan in die Atmosphäre zu reduzieren.

In dieser Arbeit untersuchten wir während der sommerlichen Stratifikationsperiode Methanoxidationsprozesse in der Wassersäule des Fohnsees, der in Süddeutschland in der Nähe von München liegt. Wir bestimmten seine saisonale Dynamik und quantifizierten mit Hilfe eines numerischen Modells gekoppelt mit den stabilen Isotopen für die Monate von April bis Dezember den Anteil der anaeroben und aeroben Oxidation von Methan in der Wassersäule des Fohnsees. Dafür wurden hochauflösende

vertikale Konzentrationsprofile und die entsprechenden stabilen Isotopenverhältnisse von Methan ($\delta^{13}C$) und Nitrat ($\delta^{15}N$ und $\delta^{18}O$) zusammen mit den Konzentrationen von gelöstem Sauerstoff in der Wassersäule für die Modellberechnungen gemessen.

Unsere Daten und die Ergebnisse des numerischen Modells zeigten eine Redoxzone in der Wassersäule, in der sowohl die Denitrifikation als auch die anaerobe Oxidation von Methan miteinander gekoppelt sind. Die numerischen Simulationen ergaben, dass zwischen Juni und September die AOM etwa 70% zum Methanabbau in der Wassersäul beiträgt. Daher stellt die anaerobe Oxidation von Methane in Verbindung mit der Denitrifikation die wichtigste Methansenke in der Wassersäule des Fohnsees während der Sommerperiode dar.

Die Daten zeigten auch, dass sich die Zone der anaeroben Oxidation von Methan im Mai zunächst in der Nähe des Seesbodens befand und sich entsprechend der saisonalen vertikalen Verschiebung des Sauerstoffgradienten und der Verfügbarkeit von Nitrat in Richtung der Seeoberfläche bewegte. Diese Redoxdynamik innerhalb der Wassersäule des Fohnsees hatte auch Auswirkungen sowohl auf die Relevanz der aeroben und anaeroben Oxidation von Methan im Fohnsee über den Betrachtungszeitraum, als auch auf die Ausbildung einer Sulfatreduktionszone nahe der Seesedimente.

Nach Bestimmung der zeitlichen und räumlichen Dynamik von DAMO am Fohnsee wurde die Bedeutung der anaerobe Methanoxidation in Verbindung mit Denitrifikation und Anammox-Prozessen in der Wassersäule des Fohnsees zwischen April und September untersucht.

Konzentrationsprofile und stabile Isotopenzusammensetzungen von NO_3^- und NH_4^+, zusammen mit der numerischen Modellierung und Quantifizierung der Hydrazinsynthase (hzsB)- und Nitritreduktase (nirK und nirS)-Gene wurden verwendet, um die vorherrschenden Stickstofftransformationsprozesse am Fohnsee während der Frühlings- und Sommerperioden zu identifizieren. Wasserchemische Daten, qPCR-Analysen und Erhöhungen der $\delta^{15}N$-Werte von Nitrat von 7,0 bis 41,0‰ bzw. für die $\delta^{18}O$-Werte des Nitrats von 2,0 auf 28,0‰ zeigten, dass die Nitratreduktion zu Nitrit und NO in einer sich aufwärts bewegenden Zone der Wassersäule von Juni bis September stattfindet, nachdem der Sauerstoffgradient in der Wassersäule durch die thermische Schichtung in Richtung Seeoberfläche wanderte. Wir konnten damit verbunden auch einen Anstieg des $\delta^{15}N$ –Werte von Ammonium von 15‰ auf 28‰ in der anoxischen Wassersäule beobachten. Unsere Modellierungsergebnisse deuten darauf hin, dass der beobachtete Isotopenschift im $\delta^{15}N$-NH_4^+ vornehmlich durch die Vermischung von Ammonium aus der oxischen Wassersäule mit $\delta^{15}N$-Werten von 25‰ und Ammonium, das vermutlich in den Seesedimenten bei der Oxidation von organischem Material mit $\delta^{15}N$-Werten von 11‰ gebildet wird, gesteuert wird. Die zusätzlich untersuchten Genhäufigkeiten (hzsB, nirK und nirS) in den im Juni und Juli entnommenen Wasserproben deuten aber auch auf das gleichzeitige Auftreten von Nitratreduktion und geringen AnammoxRaten hin, so dass der Anstieg im $\delta^{15}N$ vom Ammunium nicht alleine durch Mischung zu erklären ist sondern eine Koppelung beider Prozesse nahelegt. Das Auftreten von gelöstem Sulfid nahe des Seesedimente in den Monaten August und September könnte ein Grund für die beobachtete geringe Aktivität der Anammox-Bakterien darstellen.

Diese Arbeit zeigt, dass die anaerobe Oxidation von Methan in Verbindung mit der Nitratreduktion einen wichtiger Prozess für die Eliminierung von xi

Methan und Stickstoff in einem saisonal geschichteten See darstellt und dadurch zu einer Verringerung der Emission von Methan in die Atmosphäre führt. Außerdem deuten die Ergebnisse darauf hin, dass Anammox insbesondere in den Sommermonaten nach Ausbildung der thermischen Schichtung in der Wassersäule das Potenzial hat zusammen mit DAMO aufzutreten, um Stickstoff aus dem System zu eliminieren.

Structure of the thesis

The following work was developed within the framework of the research project: Anaerobic oxidation of methane, which was funded by the German Research Foundation (DFG). This thesis is divided into seven chapters as follows; the first chapter: The introduction comprehends the problem definition and motivation of the thesis. Chapter 2. State-of-the-art contains the most current scientific information that is relevant to the understanding of the thesis. Chapter 3. Aims and objectives contain the three specific objectives of this thesis. Chapter 4 covers all methods used. Chapter 5 contains the results and discussion of the specific objectives I and II, which were defined in Chapter 3. The results and discussion in Chapter 5 are also part of the first manuscript published within the scope of the DFG project. Chapter 6 contains the results and discussion of objective III. The results and discussion in Chapter 6 are part of the second manuscript published within the scope of the DFG project. Finally, Chapter 7. Synaptic discussions and Conclusions, contains the closing conclusions of the thesis, and additional scientific knowledge acquired during the project which was not part of the scope of Chapter 5 and 6, and that the author considers it was worth being discussed.

Publications

Some text, figures, and tables have appeared previously in the following scientific-peer-reviewed publications:

Analyzing seasonal variations of methane oxidation processes coupled with denitrification in a stratified lake using stable isotopes and numerical modeling.

Peña Sanchez, G. A., Mayer, B., Wunderlich, A., Rein, A., and Einsiedl, F. Geochim. Cosmochim. Acta (2022), Volume 323, 242-257

doi:10.1016/j.gca.2022.01.022

Author contributions: *Alejandra Pena (AP) and Florian Einsiedl (FE) have conceived and designed the study, AP has performed the field work with the support of Anja Wunderlich (AW). Measurement of methane isotopes, methane concentrations, anions, and cations were performed by AP under the supervision of AW. Instrumentation and methodology of nitrate isotopes were provided by Bernhard Mayer (BM) and measurements at the stable isotope laboratory of the University of Calgary in Canada. The modeling study was performed by AP and discussed with Arno Rein (AR). Interpretation of the complete data set was performed by AP and FE. The original manuscript was written by AP with the supervision of BM and FE. The final manuscript was reviewed and approved by all co-authors.*

Seasonal dynamics of anaerobic oxidation of ammonium and denitrification in a dimictic lake during the stratified spring–summer period

Peña Sanchez, G. A., Mayer, B., Wunderlich, A., Duffner C., Schulz S., Schloter M., and Einsiedl, F. Limnol. Oceanogr. 9999, 2022, 1–17
doi: 10.1002/lno.12067

Author contributions: *Alejandra Pena (AP) and Florian Einsiedl (FE) have conceived and designed the study, AP has performed the field work. Measurements of methane isotopes, methane concentrations, anions, and cations were performed by AP. Instrumentation and methodology for ammonium and nitrate isotopes were provided by Bernhard Mayer (BM) and measurements were performed by AP. qPCR analyses were performed by Clara Duffner (CD) with the support of Stefanie Schulz (SS). The modeling study was performed by AP. Interpretation of the complete data set was performed by AP and FE. CD, SS, and Michael Schloter (MS) helped in interpreting the microbiological results. CD wrote the methodology section for DNA extraction and PCR amplification in chapter 6.1.4. CD, SS, and MS contributed to the writing of the quantitative PCR results and discussion. The original manuscript was written by AP with the supervision of BM and FE. The final manuscript was reviewed and approved by all co-authors.*

Acknowledgments

This thesis would have not been possible without the collaboration and effort of some people. First, I would like to thank my supervisor Prof. Einsiedl for giving me the opportunity to work on this project and for his guidance during my Ph.D. I would like to thank my mentor Prof. Mayer for his support and for providing a different perspective when it was needed.

I must thank the Deutsche Forschungsgesellschaft (DFG) which funding made possible this study, and the International Graduate School of Science and Engineering (IGSSE) for providing the funding which made possible the collaborations with the Isotope science Lab of the University of Calgary in Canada, and the Research Unit for Comparative Microbiome Analysis at the Helmholtz Zentrum München. I would also like to thank the Chair of Aquatic system Biology for facilitating the use of the infrastructure of the research station in Iffeldorf and providing us with sampling equipment at the site of study Lake Fohnsee.

I would especially like to thank the entire Ph.D. team at the Chair of Hydrogeology and my closest friends there. Thanks to Anne, Tamara, Felix, Manuel, Florian, Lisa, Daniel, Fabian, Florian, Theis, and Alberto for all the good moments and encouragement of the last years. In this context, I would like to express my deepest gratitude to our lab manager Susanne Thiemann for all her technical support in this work.

Finally, I would like to thank my loved ones for all their support.

Contents

List of Figures

List of Tables

List of Abbreviations and acronyms

a	System specific constant
A	Area
AOA	Ammonia oxidizing archaea
AOB	Ammonia oxidizing bacteria
AOM	Anaerobic oxidation of methane
Asple	Peak area returned by the gas chromatograph for a specific sample
Astd	Peak area returned by the gas chromatograph for a specific standard
ATP	Adenosine triphosphate
BSR	Bacterial sulfate reduction
BSRZ	Bacterial sulfate reduction zone
C	Concentration
CDZ	Chemolithotrophic denitrification zone
D	Diffusion coefficient
DAMO	Nitrate dependent anaerobic methane oxidation
DL	Detection limit
DNRA	Dissimilatory nitrate reduction to ammonium
DO	Dissolved oxygen
Fz	Vertical flux
g	gravitational acceleration
GC	gas chromatography
hzs	Hydrazine synthase enzyme
IC	Ion chromatography
IPCC	Intergovernmental Panel on Climate Change
J	Dispersive max flux density
k	First order reaction term
Kz	Turbulent diffusion coefficient
MMO	Methane monooxygenase enzyme
Nap	Periplasmatic nitrate reductase enzyme
Nar	Nitrate reductase enzyme
n-damo	Nitrite dependent anaerobic methane oxidation
ni	concentration of substance I in a bottle
Nir	Nitrite reductase enzyme
NMTZ	Nitrate-methane transition zone
Nos	enzyme nitrous reductase

PDE	Partial differential equation
Pi	molar quantity of substance i
pMMO	Particulate form of the methane monooxygenase enzyme
Pstd	Partial pressure
qPCR	Quantitative polymerase chain reaction
R	Degradation rate
R*	Organic carbon chain
Ri	Isotope ratio at i
Rp	Isotope ratio product
Rs	Isotope ratio reactant
sMMO	Soluble form of the methane monooxyenase enzyme
SSI	Schmidt's stability index
t	Time
T	Temperature
Vw	Volume of the water in a bottle
x	Distance
α	Isotope fractionation
ε	Isotope enrichment factor
σ	Standard variation
ϱ	Density
ΔG	Gibbs free energy
$\Delta G°$	Gibbs free energy under standard conditions

Statement of Original Authorship

The work contained in this thesis has not been previously submitted to meet the requirements for an award at this or any other higher education institution. To the best of my knowledge and belief, the thesis contains no material previously published or written by another person except where due reference is made.

Signature: _____

Date: _____

Chapter 1: INTRODUCTION

1.1 RELEVANCE OF UNDERSTANDING METHANE OXIDATION PROCESSES AND THEIR LINK WITH THE N AND S-CYCLES

Methane (CH_4) is the second most important anthropogenic greenhouse gas after carbon dioxide (CO_2) (Houghton et al., 2001). Although concentrations of CH_4 in the atmosphere are only found in trace amounts, atmospheric methane is responsible for nearly 20% of global warming (IPCC, 2007). Atmospheric CH_4 concentrations have more than doubled since pre-industrial times and recent observations have suggested that global methane emissions have risen approximately 10% in the last two decades (Jackson et al., 2020).

Freshwater ecosystems are one of the major natural sources of methane (Louis et al., 2000; Bastviken et al., 2008; Luyssaert et al., 2012). Lakes alone contribute up to 16% of the global natural methane emissions, although they represent less than 3% of the land surface (Downing et al., 2006). Particularly in water bodies, swamps, ponds, and lake sediments with highly reducing redox conditions, CH_4 will be produced by methanogens during the last step of organic matter decomposition, i.e. methanogenesis (Conrad et al., 2009). However, a large portion of the methane produced in anoxic sediments of freshwater bodies can be oxidized by aerobic and anaerobic processes in the water column before it enters the atmosphere (Bastviken et al., 2002; Borrel et al., 2011).

It was thought for several decades that methane consumption in stratified lakes, which have reduced bottom waters and oxygenated surface waters, was solely the result of aerobic microbial methane oxidation close to the oxycline, either in the water column or near the lake sediments (Rudd et al., 1974;

Whiticar and Faber, 1986; Frenzel et al., 1990). More recently, nitrate (DAMO) and nitrite (n-damo) dependent anaerobic oxidation of methane has been found to constitute a new methane oxidation pathway with the potential of being an overlooked sink of methane in aquatic ecosystems (Raghoebarsing et al., 2006; Ettwig et al., 2010). Additionally, evidence that CH_4 might be as well oxidized using sulfate as the electron acceptor in freshwater ecosystems where sulfate concentrations are relatively high (2 mM SO_4^{2-}) has arisen in the last decade (Schubert et al., 2011).

Microbial oxidation of methane is among the most relevant processes in reducing methane emissions to the atmosphere (Valentine and Reeburgh, 2000; Orphan et al., 2002; Valentine, 2002; Lieberman and Rosenzweig, 2004; Knittel and Boetius, 2009), and thus it plays a fundamental role regulating global climate.

It is calculated that lakes in temperate latitudes are responsible for 31% of the emissions from inland waters in the world (Bastviken et al., 2011), making temperate lakes particularly relevant in terms of global CH_4 emissions.

Aerobic microbial oxidation of methane can occur under low oxygen concentrations (> 1 μmol L^{-1}) within the chemocline, as it has been previously documented for lake Lugano (Blees et al., 2014). Additionally, denitrification is mostly restricted to an area that is located near the oxic-anoxic interphase. Therefore, it remains challenging to differentiate to which extent aerobic oxidation of methane versus anaerobic oxidation of methane coupled with denitrification (DAMO) contributes to methane removal in natural ecosystems. Up to now, the identification of DAMO and n-damo, and their quantitative importance in the environment was mainly performed under laboratory conditions (Norði and Thamdrup, 2014; Roland et al., 2016; Naqvi et al., 2018) or molecular detection of the microorganisms known to mediate

these processes (Schouten et al., 2004; Schubert et al., 2011; Kits et al., 2015; Padilla et al., 2016; Weber et al., 2017).

Anaerobic oxidation of methane (AOM) with other electron acceptors such as SO_4^{2-} and Fe(III) may also be thermodynamically feasible (Ettwig et al., 2016; McGlynn, 2017), and the recycling of the newly formed reduced products (i.e. H_2S, Fe(II)) by denitrification can generate new pathways for AOM (Straub et al., 1996; Wenk et al., 2014). Thus, the occurrence and relevance of AOM coupled with denitrification in methane removal and therefore mitigating methane emissions in the environment is difficult to identify and quantify, and so far, largely unknown.

A diverse range of redox conditions is developed in the water column of temperate lakes as a consequence of thermal stratification in summer. In oxygen-deficient environments, microorganisms use different electron acceptors in order of their thermodynamic favorability, usually starting with NO_3^-, followed by Mn(IV), Fe(III), SO_4^{2-}, and CO_2 (Fenchel et al., 1999). Thus, the formation of distinctive redox zones in the water column determines the order in which biochemical processes occur during the year.

N load in natural ecosystems is mostly mitigated by microbially driven redox reactions taking place in oxygen-deficient waters. Until now, three anaerobic pathways are known to be involved in the transformation of fixed nitrogen (NO_3^-, NO_2^-, NH_4^+) in aquatic and terrestrial ecosystems: canonical denitrification (Delwiche and Bryan, 1976), dissimilatory reduction of nitrate to ammonium (DNRA) (Tiedje, 1988) and anaerobic oxidation of ammonium (anammox) (Thamdrup and Dalsgaard, 2002; Kuypers et al., 2003). Each of these processes fulfills a different function in the natural N-cycle. Anammox and denitrification lead to net ecosystem N-losses as N_2 / N_2O, while DNRA maintains N within the ecosystem as NH_4^+ (Cojean et al., 2020).

Moreover, sulfate-reducing conditions could be achieved during later summer at seasonally stratified lakes producing H_2S (Peña Sanchez et al., 2022). The presence of H_2S could potentially promote DNRA (Murphy et al., 2020) and be toxic for anammox bacteria thus inhibiting the anaerobic oxidation of ammonium (Russ et al., 2014). Therefore, it seems that interactions between the biochemical cycles are more complex than we thought, and research in the last decades has shown that our knowledge about anoxic processes is still incomplete. Fig 1. gives an overview of the possible redox processes taking place in the water column of a stratified lake that are relevant to this thesis. Therefore, the role of CH_4 as a source of carbon is highlighted.

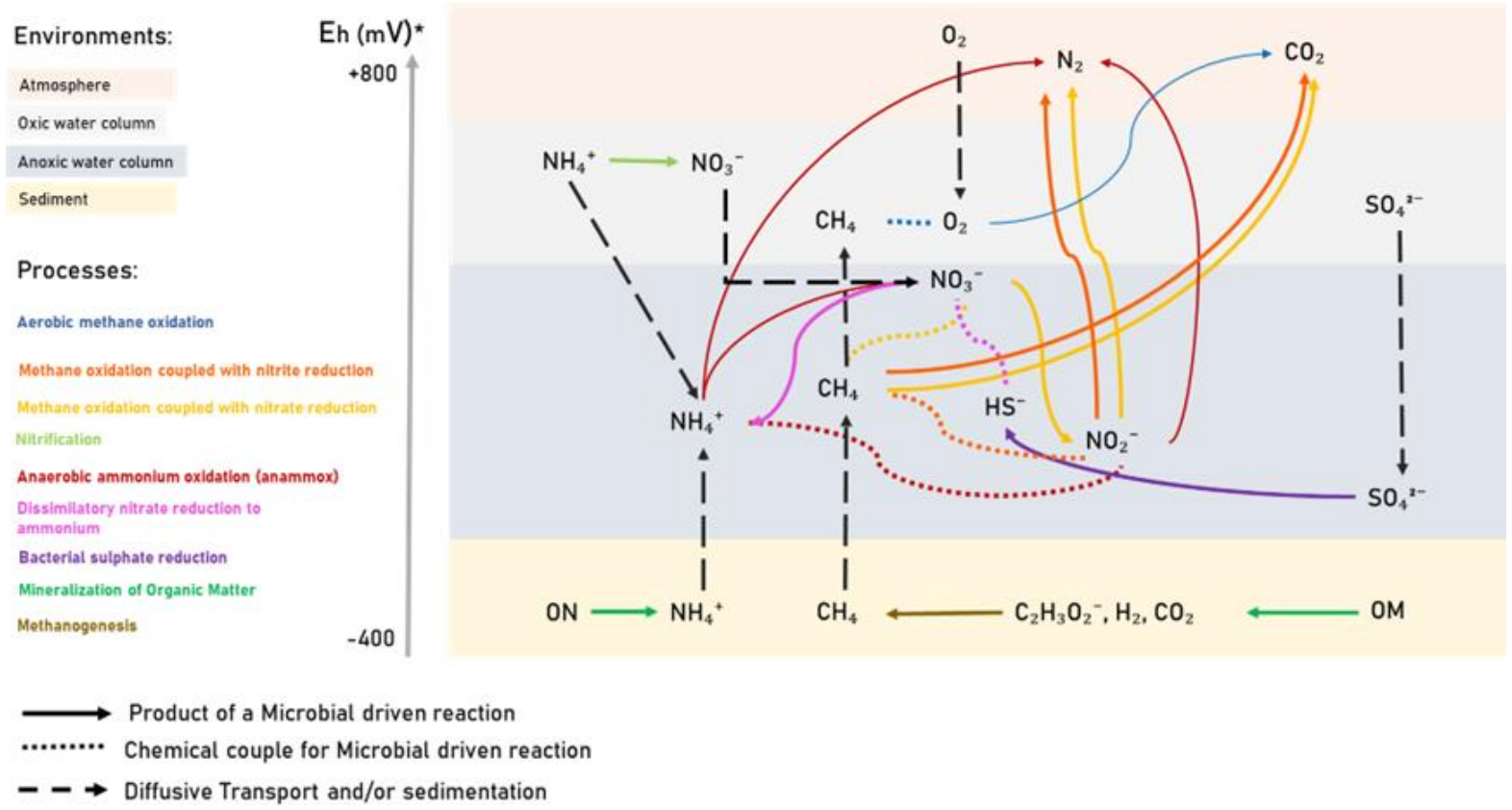

Figure 1.1 Potential interaction between redox processes in the water column of methane, ammonium, nitrate and sulfate at lake Fohnsee during summer stratification, and assumed transport mechanisms. Arrows point to the product of the redox reaction. Organic nitrogen (ON). Organic matter (OM).

It has been hypothesized that in sub-oxic and anoxic environments where CH_4, NO_3^- and, NH_4^+ are available, anammox and DAMO could simultaneously occur (Thauer and Shima, 2008; Zhu et al., 2010). Under this scenario, NO_2 may be produced during NO_3^- reduction with methane as an electron donor, and afterward, NO_2^- could be used by anammox bacteria to oxidize ammonium.

Therefore, anammox and anaerobic methane oxidizers organisms could co-exist and cooperate or could compete for substrate if NO_2^- is exclusively the result of denitrification with organic carbon. The coupling of anammox and DAMO have been observed in bioreactors (Peng et al., 2020; Fan et al., 2021), with the potential for increasing the sustainability of wastewater treatment processes (van Kessel et al., 2018). However, only a limited number of studies have suggested the co-occurrence of both processes in aquatic environments (Shen et al., 2014; Qin et al., 2018; Einsiedl et al., 2020).

Figure 2. summarizes the hypothesized paths of the coupling of DAMO and anammox, and the potential microorganism involved in freshwater environments.

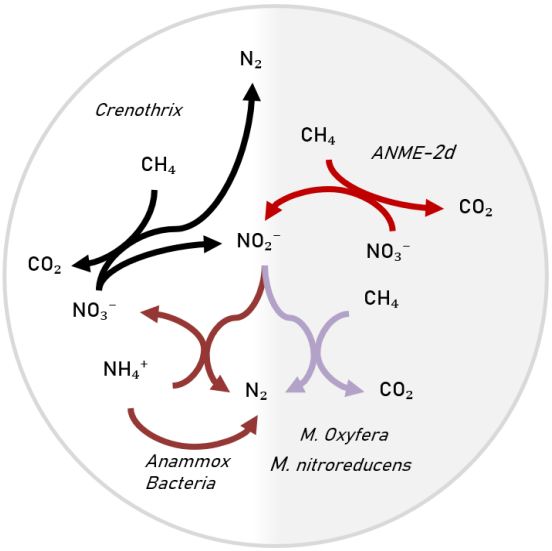

Figure 1.2 potential paths of anaerobic oxidation of methane with denitrification and coupled with anaerobic ammonium oxidation in freshwater environments

Briefly, in the first path of DAMO coupled with anammox, ANME-2d archaea reduce nitrate to nitrite (Haroon et al., 2013), thus supplying the substrate for anammox bacteria and the methane oxidizer *M. Oxyfera*. A second path involves the filamentous methane oxidizer bacteria bellowing to the family *Crenothrix*. *Crenothrix* bacteria contain the complete path for denitrification, including the genome *narK* responsible for the transformation of NO_3^- to NO_2^- (Oswald et al., 2017). Therefore, *Crenothrix* could also supply nitrite for anammox bacteria growth.

Chapter 2: STATE OF THE ART

2.1 LINKING MICROBIAL-DRIVEN TRANSFORMATIONS OF NITROGEN AND METHANE IN FRESHWATER ECOSYSTEMS

2.1.1 Methane production and methane oxidation processes in freshwater ecosystems

It is widely known that inland waters such as rivers, lakes, and wetlands are an important source of methane (ST. Louis et al., 2000). Methane in these environments is produced in the anoxic sediments during the final step of microbial degradation of organic matter i.e. methanogenesis. Complete mineralization of organic matter in the sediments can be achieved when other oxidants commonly present in freshwater ecosystems such as oxygen, nitrate, and sulfate have been completely depleted (Conrad, 2009). These conditions are commonly achieved in freshwater environments where transport mechanisms will minimize the renewal of oxidants from the water column to the sediments.

The pathway from organic matter to CH_4 requires the presence of diverse microbial communities performing different biochemical processes in sequence (Conrad, 2020). Methanogens belong mostly to the domain archaea (Borrel et al., 2011), however, they depend on the activity of other bacteria, eukaryotes, and archaea to degrade complex organic compounds into their substrate (i.e. acetate, hydrogen, and CO_2).

In the first step, polymeric organic matter such as proteins and lipids are transformed into less complex chains (i.e. monomers) by the process of hydrolysis (Conrad, 2020). Subsequently, monomers are broken into short

fatty acids such as acetate, formate, hydrogen, and CO_2. In the final step, methane is produced from acetate or by the conversion of H_2 and CO_2 to CH_4 (Conrad, 2020).

Methane production from acetate is denominated as acetoclastic methanogenesis while H_2 is the substrate for hydroclastic methanogenesis (Conrad et al., 2009). In addition, H_2 and CO_2 could be further combined to produce acetate during chemolithotrophic acetogenesis (Drake HL et al., 2006). Acetoclastic and hydroclastic methanogenesis are described by the following chemical reactions:

$$2CH_3COOH \rightarrow 2CH_4 + 2CO_2 \qquad (1)$$

$$4H_2 + CO_2 \rightarrow CH_4 + 2H_2O \qquad (2)$$

In most cases, CO_2 is not the limiting substrate in freshwater sediments (Praetzel et al., 2020). Thus, the relevance of each methanogenic pathway in a specific ecosystem will depend on the availability of both H_2 and acetate.

Finally, it is worth mentioning that although methanogenesis has been studied for decades, recent research has shown our knowledge about microbial methane production paths is still incomplete. For example, Grossart et al., (2011) observed the production of methane in lakes under oxygen-saturated conditions in the water column, breaking the paradigm that CH_4 could only be produced under strictly anaerobic conditions and increasing our understanding of the natural sources of methane.

Methane can be transported from the lake sediment to the atmosphere through the water column by four distinctive paths: Plant-mediated flux, ebullition,

advection, and diffusion, nevertheless, only methane transported advection and diffusion permit microbial CH_4 oxidation (Bastviken, 2009).

Microbial-driven methane oxidation is accomplished by methanotrophic microorganisms using methane as their terminal electron donor. It has been estimated that 30 to 99% (Bastviken, 2009) of the methane produced in freshwater sediments is oxidized in the water column by either aerobic or anaerobic methane oxidizers microorganisms(Rudy et al., 1976; Valentine, 2002; Deutzmann, 2020).

Methane oxidation was first described at beginning of the 20th century as an aerobic process by the following equation:

$$CH_4 + 2O_2 \rightarrow CO_2 + 2H_2O \qquad \Delta G^{\circ\prime} = -819kJ\ mol^{-1}\ \ CH_4 \qquad (3)$$

Sohngen et al (1906) suggested that the mismatch between the large production of methane in anoxic environments and the low concentrations of CH_4 found in the atmosphere should be the result of microbial consumption. Subsequently, Sohngen was able to isolate the first methanotrophic bacteria *"Bacillus methanicus"*.

Until now, there are four identified families of methanotrophic microorganisms: *Methylococcaceae, Methylocystaceae, Methylacidiphilaceae, and Beijerinckiaceae* (Bodelier et al., 2019), the last family is characterized by facultative methanotrophs belonging to the genera *Methylocella* and *Crenothrix*, among others (Stoecker et al., 2006). During the first step of CH_4 oxidation, one atom of the O_2 molecule is combined with CH_4 to form Methanol (CH_3OH), and the other oxygen atom is reduced to form H_2O (Hanson and Hanson, 1996). The conversion of methane to methanol is carried out by the enzymatic

complex *Monooxygenase (MMo)* (Anthony, 1983; Dalton, 1992; Lipscomb, 1994). MMo is found in all known methanotrophs in two forms MMOp and MMOs.

In freshwater ecosystems, aerobic methanotrophy will depend on the availability of both methane and oxygen, thus, optimal conditions occur in oxic/anoxic interfaces where opposite fluxes of CH_4 and O_2 may occur. Thus, maximum aerobic methane-oxidizing bacteria abundances and the highest aerobic methane oxidation rates are usually found at the oxic-anoxic interface (Rudd et al., 1976). Indeed, aerobic oxidation of methane has been observed at O_2 concentrations as low as 1 umolL^{-1} (Blees et al., 2014). Moreover, facultative methanotrophs of the family *Chrenothrix* located at the oxycline have been identified to be a relevant biological sink for methane at lake Zug in Switzerland (Oswald et al., 2017). Finally, it is worth mentioning that some strings of *Crenothrix* can grow using both O_2 and NO_3^-, giving them a huge competitive advantage over strictly aerobic methanotrophs.

Methane molecules have four C-H bonds which are highly stable making CH_4 the most inert hydrocarbon, thus, it was long thought that microbial-driven anaerobic oxidation of methane in nature was not possible (Yan et al., 2018). However, the oxidation of CH_4 is thermodynamically feasible with other electron acceptors besides O_2, such as NO_3^-, NO_2^-, Fe(III), Mn(IV), and SO_4^{2-} (Deutzmann, 2020).

First observations of anaerobic oxidation of methane were inferred from depth distributions of methane concentrations in anoxic marine sediments (Barnes and Goldberg, 1976; Martens and Berner, 1977; Reeburgh and Heggie, 1977) where sulfate was accounted to be the electron acceptor for AOM.

Possible anaerobic oxidation of methane reactions in freshwater ecosystems and associated Gibbs energies are described by the following equations:

$$CH_4 + 4NO_3^- \rightarrow CO_2 + 4NO_2^- + 2H_2O \quad (4)$$

$\Delta G^{\circ\prime} = -503kJ\ mol^{-1}\ CH_4$ (Raghoebarsing et al., 2006)

$$3CH_4 + 8NO_2^- + 8H^+ \rightarrow 3CO_2 + 4N_2 + 10H_2O \quad (5)$$

$\Delta G^{\circ\prime} = -928kJ\ mol^{-1}\ CH_4$ (Raghoebarsing et al., 2006)

$$CH_4 + 8Fe(OH)_3 + 15H^+ \rightarrow HCO_3^- + 8Fe^{2+} + 21H_2O \quad (6)$$

$\Delta G^{\circ\prime} = -572kJ\ mol^{-1}\ CH_4$ (Crowe et al., 2011)

$$CH_4 + 4MnO_2 + 7H^+ \rightarrow HCO_3^- + 4Mn^{2+} + 5H_2O \quad (7)$$

$\Delta G^{\circ\prime} = -789kJ\ mol^{-1}\ CH_4$ (Crowe et al., 2011)

$$CH_4 + SO_4^{2-} \rightarrow HCO_3^- + HS^- + H_2O \quad (8)$$

$\Delta G^{\circ\prime} = -16kJ\ mol^{-1}\ CH_4$ (Cui et al., 2015)

In contrast to marine environments, where AOM is mostly coupled with SO_4^{2-} reduction (Cui et al., 2015), nitrate and nitrite are more likely to serve as electron acceptors during AOM in freshwater ecosystems due to their availability in freshwater. Both nitrate and nitrite-dependent AOM are highly exergonic processes, thus, methane oxidation using NO_3^- and NO_2^- as electron acceptors are expected to be the most relevant reaction pathways for AOM in freshwater ecosystems. Anaerobic oxidation of methane coupled with nitrate reduction is reviewed in detail in Section **2.1.4.** Denitrification linked with methane oxidation.

2.1.2 Aerobic and anaerobic methane oxidation rates in the water column of freshwater systems

Direct measurements of aerobic and anaerobic oxidation of methane coupled with denitrification rates in-situ are challenging. Aerobic methane oxidation can take place under very low O_2 concentrations (> 1 μmol L^{-1}), most likely overlapping with zones in the water column where NO_3 has been simultaneously reduced. Thus, most oxidation rates reported in the literature have been measured from batch experiments (See Table 1). Standard conditions and dynamics between the microbial communities in batch incubations might significantly differ from in situ conditions. Therefore, oxidation kinetics parameters for methane oxidation derived from samples amended with methane provide only an estimate of potential, instead of oxidation rates in nature (Guerin and Abril 2007; Martinez-Cruz et al. 2015; Deshmukh et al. 2016).

In lakes' water columns and sediments, AOM rates are directly related to the amount of methane available in the system, and thus, they are also linked with methanogenesis rates in sediments (Sundh et al., 2005; Duc et al., 2010).

It has been reported that in shallow eutrophic lakes, methane consumption rates are the maximum in the late summer when methane production rates in sediments are also the highest (Utsumi et al., 1998). Furthermore, field and lab studies have shown that temperature (Hanson and Hanson, 1996; Conrad, 2009) as well as light (Oswald et al., 2015), might affect methane oxidation rates. Therefore, methane consumption rates can significantly vary throughout the year.

Moreover, temperature gradients, chemical conditions, and mixing patterns differ among lakes. In consequence, CH_4 oxidation rates may be difficult to compare among sites. Table 1. displays aerobic and anaerobic oxidation of

methane rates reported for lake water columns and their associated first-order rate constant (*k*). *k* values have been calculated from the oxidation rate and the methane concentration reported for each study.

Table 2.1 Reported aerobic and anaerobic oxidation of methane rates for different lakes' water columns

Oxidation Process	Lake mixing type	Time, depth	Method	Rate ($mgL^{-1}s^{-1}$)	Methane Concentration (mgL^{-1})	First order rate constant k (s^{-1})	Reference
Aerobic	Meromictic Lake (Experimental Lakes Area, Ontario)	May, 8m	incubations radiolabeled with 14C-CH_4 lake water, 50% distilled	4,40E-07	2,24E-01	1,96E-06	(Rudd et al., 1974)
		May, 14 m	incubations radiolabeled with 14C-CH_4 lake water, 50% distilled	7,07E-04	9,70E+00	7,29E-05	
Aerobic	Meromictic Lake Tanganyika	October	incubations radiolabeled with 14C-CH_4	3,55E-03	1,20E+00	2,96E-03	(Rudd, 1980)
Anaerobic	Meromictic Lake Tanganyika	October	incubations radiolabeled with 14C-CH_4, no added subtract	8,88E-04	1,60E-01	5,55E-03	
micro aerobic	Permanently stratified Lake Lugano	January-170m depth	incubations radiolabeled with 14C-CH_4	2,79E-07	4,80E-01	5,81E-07	(Blees et al., 2014)
		August, 170m depth		4,65E-07	7,20E-01	6,46E-07	
Anaerobic	Meromictic Lake Big Soda	October-mixolimnion	incubations radiolabeled with 14C-CH_4	1,86E-09	2,40E-01	7,75E-09	(Iversen et al., 1987)
		October-monolimnion		9,30E-09	9,60E-01	9,69E-09	
Aerobic		October (above 18m)		2,42E-10	1,60E-03	1,51E-07	
Aerobic	Holomictic Lake Mendota	April, 20m depth	incubations radiolabeled with 14C-CH_4	2,10E-10	3,04E-02	6,91E-09	(Harrits and Hanson, 1980)

		February 13-15 m Depth		3,72E-09	1,60E-01	2,33E-08	
Oxic-anoxic Interphase	Mono-lake	April 13m depth	Cell abundance	1,12E-08	1,60E-01	6,98E-08	(Carini et al., 2005)
		April 15m depth		1,86E-09	2,40E-01	7,75E-09	
		June 15m depth		7,44E-09	3,20E-01	2,33E-08	
Oxic-anoxic Interphase	Meromictic Lake Rotsee	November	measurements in enrichment cultures	1,86E-07	7,20E+00	2,58E-08	(Schubert et al., 2010)
		September		7,44E-07	4,80E+00	1,55E-07	
		April		1,02E-06	1,60E+00	6,40E-07	
		February		9,86E-07	1,60E+00	6,16E-07	

2.1.3 Aerobic and anaerobic transformation of nitrogen in freshwater ecosystems

Nitrogen (N) load in natural ecosystems is mostly mitigated by microbially driven redox reactions taking place in oxygen-deficient waters (Wenk et al., 2013). NH_4^+ in the water column is oxidated to NO_3^- during nitrification. Nitrate is consequently removed in the anoxic zone together with other fixed nitrogen compounds (NO_2^-, NH_4^+) through the production of nitrogen gases (N_2, N_2O) by mean of two anaerobic pathways: canonical denitrification (Delwiche and Bryan, 1976) and anaerobic oxidation of ammonium (anammox) (Thamdrup and Dalsgaard, 2002; Kuypers et al., 2003), or converted again to ammonium by dissimilatory reduction of nitrate to ammonium (DNRA) (Tiedje, 1988). Each of these processes fulfills a different function in the natural N-cycle. Anammox and denitrification lead to net ecosystem N-losses as N_2 / N_2O, while nitrification and DNRA conserve N within the ecosystem as NH_4^+ (Cojean et al., 2020).

Ammonium is released from the anoxic sediments as a result of the mineralization of organic matter (Morin and Morse, 1999; Beutel, 2006; Wang et al., 2008). The release of NH_4^+ by the degradation of biomass is considered one of the most important factors influencing N concentration in lakes (Morin and Morse, 1999; Wang et al., 2016), due to the fundamental role of ammonium in maintaining the trophic status of the lake ecosystem (Kaiserli et al., 2002)

Production of NH_4^+ is carried out by two main steps: first, microorganisms break down complex proteins into simpler amino acids, amides, amines, and CO_2 (aminization) as follows:

$$proteins \rightarrow R * -NH_2 + CO_2 \qquad (9)$$

Second, NH_2 groups are transformed into NH_3 or NH_4^+ during ammonification. Subsequently, ammonium is available to be assimilated by plants or used for metabolic purposes (Strock, 2008).

The ammonium diffusing from the sediments into the water column will most likely be oxidized in the aerobic water column to NO_3^- during nitrification. Nitrification refers to the oxidation of ammonium to nitrate via nitrite with oxygen as an electron acceptor. It occurs in two steps; first NH_4^+ is oxidized to NO_2^- by Ammonia Oxidizing Bacteria (AOB) and as recently discovered Ammonia Oxidizing Archaea (AOA) (Schleper and Nicol, 2010), consecutively, NO_2^- is oxidized to NO_3^- by chemolithotrophic bacteria bellowing to the genus *Nitrobacter* as follows:

$$NH_4^+ + 3O_2 \rightarrow 2NO_2^- + 2H_2O + 4H^+ \qquad (10)$$

$$O_2 + 2NO_2^- \rightarrow 2NO_3^- \qquad (11)$$

Thought nitrification was described as a two steps process already in 1890 by Winogradsky (Winogradsky, 1890), recent studies have shown that some single microorganisms might be able to carry out complete nitrification (Daims et al., 2015).

Nitrification leads to the formation of NO_3^-. Nitrate is considered inert in the presence of O_2, and thus, nitrate is usually the most abundant form of fixed N in oxygenated zones (Ward, 2003). Nevertheless, NO_3^- will act as a strong electron acceptor in oxygen-deficient waters, fueling a wide variety of anaerobic metabolisms such as denitrification and dissimilatory nitrate reduction to ammonium (DNRA).

Evidence for dissimilatory nitrate reduction to ammonium (DNRA) has been available for more than 30 years, however, its significance as a nitrate removal pathway on an ecosystem scale has increased interest only within the last decade.

This microbially mediated pathway involves the dissimilatory transformation of NO_3^- to NH_4^+, in contrast to assimilatory processes that incorporate N into cellular constituents (Giblin et al., 2013). Compared to nitrate, ammonium is usually a more biologically available and less mobile form of inorganic N. Thus, DNRA fulfills a retention function in the environment in contrast with denitrification, which end product is the natural attenuation of N load in ecosystems. DNRA can be carried out with organic carbon as the electron donor (fermentative) or with reduced inorganic substrates such as sulfide (chemoautotrophic)(van den Berg et al., 2017). Although the environmental factors determining the balance between denitrification to N_2 and DNRA are not fully understood, some major controls have been identified in the last

years. These include the availability of NOx, temperature, organic carbon loading as well as the C/N ratio, and the presence of reductants (Bonaglia et al., 2016; van den Berg et al., 2017; Callbeck et al., 2021). Limited NO_3^-/NO_2^- conditions, as well as the availability of carbon sources such as glucose and glycerol tent to favor DNRA (Nizzoli et al., 2010; Carlson et al., 2020). Additionally, low temperatures (~10°C) tend to favor denitrification in nature (Gruca-Rokosz et al., 2009, King & Nedwell, 1985; Ogilvie et al., 1997).

In freshwater environments, sulfide as an e-donor for DNRA can be supplied by bacterial sulfate reduction (BSR) taking place in a redox zone just below the denitrification zone. The presence of HS^- might enhance DNRA by inhibiting other bacteria competing for NO_3^- and NO_2^- (Burgin and Hamilton, 2007), and by sustaining chemoautotrophic nitrate-reducing bacteria. Additionally, sulfide has been shown to inhibit the enzymes responsible for the final two reduction steps in denitrification (Burgin and Hamilton, 2007). Thus, it is likely that DNRA will be present in environments with low NO_3^- and where sulfate reduction is taking place.

Besides ammonium oxidation taking place in the aerobic water column, it was for long believed that ammonium was chemically inert in the absence of oxygen and its activation was exclusively performed by monooxygenases enzymes (Kuenen, 2008). The first evidence of potential anaerobic oxidation of ammonium was observed in a laboratory-scale fluidized bed reactor using ^{15}N-labelled ammonium where the production mixed $^{14-15}N$-N_2 gas was detected (Van De Graaf et al., 1997). Later, ^{15}N-labelling experiments revealed that the combination of ^{15}N -NO_2^- and ^{15}N-NH_4^+ resulted in mixed $^{14-15}N$-N_2 gas, as well as experiments carried out with amended ^{15}N-hydroxylamine and ^{15}N-NH_4^+. This last experiment showed that during anaerobic oxidation of

ammonium, hydroxylamine or a related compound (e.g hydrazine) reacted with ammonium (Van De Graaf et al., 1997), contrary to aerobic ammonium oxidation, where NH_4^+ is oxidized first to Hydroxylamine. Production of hydrazine from ammonium oxidation proceeds as follows:

$$NH_2OH + NH_4^+ \rightarrow N_2H_4 + H_2O + H^+ \qquad (12)$$

In the following years, a growing culture made of 70% anammox microorganisms was enriched. Mass balance showed that the microorganism in this culture produced biomass using NO_2^- to reduce carbon dioxide. From these observations, the current anammox equation was derived (Strous 1998):

$$NH_4^+ + 1.32NO_2^- + 0.066HCO_3^- + 0.13H^+ \rightarrow 1.02N_2 + 0.26NO_3^- + 2.03H_2O + 0.066CH_2O_{0.5}N_{0.15} \qquad (13)$$

In the last 20 years, anammox bacteria have been extensively studied, and have been found almost ubiquitously in every type of environment, including marine freshwater and terrestrial ecosystems, for both natural and artificial environments. Field and laboratory studies have consistently shown that anammox may play a significant role in the nitrogen cycle of marine ecosystems removing up to 50% of the N load from the ecosystem (Dalsgaard et al., 2003; Engström et al., 2005; Hamersley et al., 2007). Recent research indicates that the anammox process might be as well ubiquitous in freshwater ecosystems (Gao et al., 2018). However, in contrast to ecosystems, the significance of anammox in freshwaters varies significantly in each environment (Schubert et al., 2006; Wenk et al., 2013; Zhao et al., 2015). Crowe et al. (2017) showed that anammox was responsible for up to 50% of N_2

released in Lake superior, whereas results obtained from Lake Kivu suggest that anammox account for only around 1% of N loss (Roland et al., 2018).

Anammox bacteria have been detected in nature with the use of molecular biomarkers (Lipsewers et al., 2016; Meng et al., 2016; Wang et al., 2016; Nie et al., 2018). The evidence of several study ecosystems has resulted so far in the identification of 5 genera of anammox bacteria bellowing to the family Brocadiaceae: "Candidatus Brocadia," "Candidatus Kuenenia," "Candidatus Scalindua," "Candidatus Anammoxoglobus," and "Candidatus Jettenia" and one genus identified in bioreactors bellowing to the family Planktomycetaceae: "Candidatus Anammoximicrobium.

Most recently, Wang et al. (2012) developed a suitable primer (hzsB_396F and hzsB_742R) for quantitative PCR of anammox bacteria. The *hzsB* primer targets a subunit of the hydrazine synthase, which is until now, the only known path for the anaerobic oxidation of ammonium, and thus, a key step in the anammox process (Kartal et al., 2011; Harhangi et al., 2012).

2.1.4 Denitrification linked with the anaerobic oxidation of methane (DAMO)

The addition of various forms of reactive N to the environment has been predominantly used to enhance food production. Eventually, some reactive N ends up in the environment polluting groundwater, rivers, and lakes (Rockström et al., 2009). Denitrification is still without discussion one of the most important microbially driven redox reactions taking place in oxygen-deficient waters mitigating N loading in natural ecosystems.

Respiratory denitrification is carried out by facultative bacteria that use NO_3^- or NO_2^- as an electron acceptor to produce N_2, NO, or N_2O. Denitrification is considered to occur widely in terrestrial, freshwater, and marine sub-oxic and

anoxic environments where NO_3^- is available, and sufficient organic matter is present (Ramesh Reddy and DeLaune, 2008).

Complete reduction of NO_3^- to N_2 is carried out in four main reaction steps: i) Nitrate reduction to nitrite which is catalyzed by the enzyme nitrate reductase encoded by the narGHJI operon, ii) nitrite reduction to nitric oxide catalyzed by nitrite reductase encoded by nirS and/or nirK, this reaction differentiates denitrifiers from other bacteria respiring NO_3^-. iii) NO is further transformed to N_2O by the enzyme nitric-reductase (Nor). iv) the last step involves the reduction of N_2O to N_2 which is catalyzed by the enzyme nitrous reductase (Nos). From all the genes involved during denitrification, functional markers for nitrite reductase genes (*nirK and nirS*) have been intensely used for investigating the diversity of denitrifying bacteria in lake sediments (Zhu et al., 2017), and in the water columns of varied freshwater environments (Wei et al., 2015; Pajares et al., 2017)

Denitrification can be differentiated into heterotrophic and chemolithoautotrophic denitrification, depending on the type of electron used for NO_3^- reduction. Chemolithoautotrophic denitrification uses inorganic compounds as electron donors such as hydrogen (H2), reduced sulfur compounds (e.g. HS^-, elemental sulfur, and thiosulfate), ferrous iron (Fe^{2+}), iron sulfides (e.g. FeS, FeS_2), arsenite (As(III)) and manganese (Mn(II)) (Di Capua et al., 2019); while heterotrophic denitrification uses organic compounds, including low-molecular-weight organics (e.g. acetate, methanol, glucose, benzene, methane) and high-molecular-weight organics (e.g. cellulose, polylactic acid, polycaprolactone, etc.) (Wang and Chu, 2016).

The following is a detailed review of the anaerobic oxidation of methane coupled with NO_3^-.

The coupling of anaerobic oxidation of methane with reduction of NO_3^- is a quite novel process linking the product of the last step of organic matter mineralization (i.e CH_4) and the principal path of N_2 return to the atmosphere.

Anaerobic oxidation of methane was believed to be carried out only with sulfate as an electron acceptor until 2006 when an enriched microbial consortium from anoxic sediment was capable to perform oxidation of methane using NO_3^- and NO_2^- under strictly anoxic conditions (Raghoebarsing et al., 2006). After Raghoerbarsing observations, it was speculated that anaerobic oxidation of methane coupled with nitrate reduction operated in a similar way that AOM with sulfate reduction, where AOM is mediated by a consortium of anaerobic methanotrophic Archaea (ANME 1 – ANME 2) working via reversal methanogenesis and sulfate-reducing bacteria (Hoehler et al., 1994).

However, AOM in freshwater ecosystems might work through another methane oxidation mechanism. The Bacterium *M.Oxyfera* bellowing to the phylum NC10 can perform nitrite-dependent methane oxidation without the presence of an archaeon partner (Ettwig et al., 2009). Candidatus *M.Oxyfera* bacteria exhibited a new intra-aerobic pathway where nitric oxide is broken into O_2 and N_2, and successively, the produced O_2 is used to oxidize methane (Ettwig et al., 2010).

In 2013, Haroon et al. (2013), performed Metagenomic single-cell genomic analyses combined with ^{13}C and ^{15}N-labelling experiments in a reactor feed principally with NO_3^-. After 350 days, a stable microbial community capable to perform complete NO_3^- reduction using methane as an electron donor was obtained. In this reactor, nitrite used by M. *Oxyfera* was supplied by the archaeon *Candidatus Methanoperedens nitroreducens*, which was principally responsible for the reduction of NO_3^- to NO_2^- using methane as an electron donor.

Bacteria members of the phylum NC10 have been found to be spread in different freshwater ecosystems. *M.oxyfera* bacteria have been identified in Coastal aquifers (López-archilla et al., 2007), peatlands (Zhu et al., 2012) lake sediments (Kojima et al., 2012; Deutzmann et al., 2014), paddy fields soils (Ding et al., 2015) and in river sediments (Shen, Liu, et al., 2014; Yan et al., 2015), moreover, the presence of *Candidatus Methanoperedens nitroreducens* has been reported in freshwater ecosystems like peatlands (Zhu et al., 2012), paddy fields soils (Ding et al., 2015), lake water columns (Naqvi et al., 2018), lake sediments (Deutzmann and Schink, 2011), river sediments (Shen, Zhu, et al., 2014; Yan et al., 2015) and wetlands sediments (Wang et al., 2016).

Additionally, stable isotope labeling experiments in combination with single-cell imaging mass spectrometry revealed methane-dependent growth of the lacustrine strain Crenothrix in the presence of NO_3^- , and it was suggested, that these methanotrophs act as a relevant biological sink for methane in lake Zug in Switzerland (Oswald et al., 2017). Most recently, Crenothrix were also observed to reach their peak abundance below the oxycline of lake Fohnsee in Germany, where microbial AOM coupled with denitrification was the most likely explanation for the observed microbiological and isotope data (Einsiedl et al., 2020).

2.1.5 Anaerobic oxidation of methane (AOM) coupled with anammox in freshwater ecosystems

Studies conducted in the last decades have shown that our knowledge about the anoxic process of carbon and nitrogen taking place in natural ecosystems are still incomplete. As described before, if ammonium is also present due to organic matter mineralization taking place in the sediment, NH_4^+ may be anaerobically oxidated using NO_2^- as an electron acceptor in the process known as anammox.

Anammox and methane oxidation coupled with denitrification were both observed to take place in different habitats only a few decades ago. Anammox might significantly contribute to N loading mitigation in anoxic environments, while DAMO might be an overlooked sink of the strong green house (e.i methane). Thus, both processes may have major implications for nitrogen as well as the global carbon cycle.

It has been hypothesized that in sub-oxic and anoxic environments where methane, NO_3^- , and NH_4^+ are available, anammox and DAMO could simultaneously occur (Yang et al., 2012; Einsiedl et al., 2020). The co-existence of AOM and anammox bacteria has been already documented in bioreactors. Enriched co-cultures of anammox bacteria and M. Oxyfera have been reported by Luesken et al. in a sequential batch reactor fed with nitrite, ammonium, and methane. Additionally, cultures containing M. nitroreducens, M. Oxyfera, and anammox bacteria have been enriched from samples taken from a membrane biofilm reactor supplied with NO_3^-, NH_4^+, and CH_4.

In nature, studies have reported the co-existence of n-damo bacteria and anammox bacteria in peatland sediments (Zhu et al., 2012) and paddy field soils (Ding et al., 2015; Shen, 2014). Nordi and Thamdrup (2014) observed in freshwater sediments the consumption of ammonium within the nitrate reduction zone and speculated that anammox bacteria could compete against other denitrifies for nitrite as an electron acceptor in natural systems.

In reactor studies conducted by Hu et al. (2015), using inoculum containing both anammox and n-damo microorganisms, Candidatus Methanoperedens nitroreducens became primarily responsible for the reduction of nitrate to nitrite while nitrite reduction to N_2 was performed solely by anammox bacteria.

Einsiedl et al. (2020) conducted a single sampling campaign at the seasonally stratified lake Fohnsee. An isotopic enrichment in $\delta^{13}C$ of methane, $\delta^{15}N$ of

nitrate, ammonium, nitrite, and $\delta^{18}O$ of nitrate together with an observed inverse isotope effect between $\delta^{15}N$ nitrate and nitrite (preferential removal of ^{15}N from the nitrite pool during oxidation to nitrate), coupled with the detection of different microbial communities that consist of bacteria known to be involved in denitrification with AOM (Crenothrix and NC10), and anammox (*'Candidatus Anammoximicrobium'*), strongly suggested that anaerobic oxidation of ammonium together with denitrification with methane as e-donor has occurred in the anoxic water column of Lake Fohnsee. However, the significance of these processes for studies conducted only during one single month and in the absence of bacterial sulfate reduction during the sampling campaign in 2016 may be unresolved if the dynamics of redox processes in seasonally stratified lakes are not considered.

2.2 THERMAL STRATIFICATION IN LAKES AND THERMODYNAMICS OF REDUCTION-OXIDATION REACTIONS IN FRESHWATER ENVIRONMENTS

2.2.1 Thermal stratification and its effect on the redox dynamics in seasonally stratified lakes

In contrast with permanently stratified lakes, in temperate latitudes, redox conditions in lakes can change dramatically during the year due to seasonal thermal stratification (Dake and Harleman, 1969). Several processes contribute to the heat transport through the lake water column vertically as well as horizontally, such as heat flux related to evaporation and precipitation, longwave radiation of surface waters and atmosphere, inflow and outflow of surface and groundwater, and solar radiation atmosphere (Imboden and Wüest, 1995).

In temperate lakes, surface waters are exposed directly to solar radiation and heat loss by thermal contact with the atmosphere (Imboden and Wüest, 1995).

In contrast, layers near the sediment are protected from the major sources of heat influx. Thus, heat transport in the deepest layers depends solely on diffusive forces on a molecular level, which can be very slow. Usually, heat is transmitted to deep water layers through wind stress at the lake's surface. When surface waters are warmer and hence less dense than deeper water layers, vertical mixing can only occur to a limited depth, which depends on the energy supplied by wind speed. The thermal stratification period in lakes starts when a thermal gradient (thermocline) and a density gradient have been established atmosphere (Imboden and Wüest, 1995). Generally, thermal stratification holds until late autumn when ambient temperatures force the circulation of deep waters atmosphere (Imboden and Wüest, 1995). Parameters such as Hutchinson's stability index and Schmidt's stability index (SSI) are used to evaluate physical stratification strength and determine the physical state and characteristics in lakes based on the estimation of the amount of energy required to mix the entire water column.

During thermal stratification, two distinct zones are formed in the water column; a surface water layer called epilimnion, and a colder water layer beneath, called hypolimnion.

The epilimnion exchanges volatile substances (e.g gases) with the atmosphere. On the other hand, volatile and dissolved substances can only enter the hypolimnion through the epilimnion by diffusive transport during the stratification period (Elçi, 2008). Transport of dissolved substances across the vertical density gradient of the thermocline is normally limited. Under these conditions, only the settling of particles can carry larger quantities of substances across the thermocline (Stone and English, 1993).

Gas exchange with the atmosphere and primary production taking place in the epilimnion replenishes O_2 in the surface waters. On the other hand, nutrients can accumulate in the hypolimnion by organic matter deposition

which is associated with oxygen consumption. The decomposition of organic material can cause the depletion of oxygen, resulting in the establishment of anoxic environments. In consequence, the vertical distribution of dissolved substances occurs through the water column is denominated chemical stratification.

After oxygen is depleted in the hypolimnion, redox reactions should be carried out using alternative electron acceptors such as nitrate, nitrite, and sulfate. The order which these electron acceptors are used is explained in the following section.

2.2.2 Thermodynamics of redox reactions in freshwater ecosystems

Microorganisms use the energy released from redox reactions for their metabolism (Jin and Bethke, 2007). They transport electrons from reducing agents called electron donors inside their cell membrane to synthesize adenosine triphosphate (ATP). Consecutively, the electrons are transferred to an oxidizing agent denominated terminal electron acceptor (Jin and Bethke, 2007).

Redox reactions are carried out in sequence from the highest to the lowest energy yields, described by the Gibbs free energy (ΔG). The Gibbs free energy at standard conditions ($\Delta G°$) can be used to compare the relative strength of potential oxidants and reductants to derive the thermodynamic favorability of a combination of half-reactions. Microbial communities growing on reactions with higher thermodynamic feasibility i.e higher ΔG will be favored (Burgin et al., 2011). Thus, microbes will oxidize organic carbon (including CH_4) using electron acceptors in the following order: O_2, NO_3^-/NO_2^-, followed by Mn(IV), Fe(III), SO_4^{2-} and CO_2 (Fenchel et al., 1999), also known as the energetic "ladder".

2.3 USING STABLE ISOTOPES OF CH_4, NO_3^-, NH_4^+ AND SO_4^{2-} TO STUDY PROCESSES IN FRESHWATER ECOSYSTEMS

2.3.1 Theoretical and analytical basics of stable isotope fractionation

Stable isotope techniques have been widely used to identify microbially driven processes in the carbon, nitrogen, and sulfur cycles of freshwater ecosystems, revealing the occurrence of denitrification (Cline and Kaplan, 1975; Mariotti et al., 1981), bacterial sulfate reduction (Harrison and Thode, 1958), and AOM (Whiticar and Faber, 1986). The principal mechanism of stable isotope fractionation is based on the fact, that organisms consume substrates with lighter isotopes (e.g. ^{12}C) at a higher rate than those with heavier isotopes (e.g. ^{13}C) of an element, leaving the residual substrate pool enriched in the heavier isotope, and the newly formed product enriched in the lighter isotope (Whiticar, 1999). Therefore, analysis of isotope compositions of methane, ammonium, and nitrate are a promising tool for identifying AOM and other nitrogen transformations in natural ecosystems.

Isotope fractionation due to microbial consumption occurs at a rate that can be associated with kinetic isotope fractionation. Generally, kinetic isotope fractionation is a distinct characteristic related to the mechanism used for splitting chemical bonds inside the cell of a microorganism employing a chemical compound (Barker and Fritz, 1981). However, in nature, the isotope fractionation associated with a biochemical reaction can be influenced by masking effects, e.g. by changing rates of determining steps such as substrate transport into the cell or diffusion limitation (Elsner, 2010). In consequence, observed kinetic isotope fractionation, also called apparent kinetic isotope effect (AKIE) might be significantly lower than the isotope fractionation on the cellular level (Brunner et al., 2013; Wenk et al., 2014).

Isotope fractionation factor α is defined as follows:

$$\alpha = {}^{R_p}\!/_{R_s} \qquad (14)$$

where Rp and Rs are the ratios of the heavy to light isotope in the product and substrate (reactant), respectively, Consequently, an isotope enrichment factor can be defined as follows:

$$\varepsilon = (\alpha - 1) * 1000 \quad (15)$$

In the following section, isotope signatures of the studied compounds (i.e. NO_3^-, NH_4^+ , and CH_4) and enrichment factors associated with the processes of methane oxidation, ammonium oxidation, and nitrate reduction are presented.

2.3.2 C isotope effects during methane production and methane oxidation

As mentioned above, methane can be produced in sediments from acetate and CO_2 or hydrogen and CO_2. The dominant methanogenic pathway will determine the final isotope composition of the CH_4 diffusing from the sediments into the water column. Understanding the final composition of methane is required for the quantification of not only methane emissions from freshwater ecosystems sediments but for the identification of subsequent methane transport mechanisms and transformations taking place in the water column, such as microbial-driven methane oxidation.

Generally, methane produced from CO_2 and H_2 tends to be less enriched in the heavy isotope of carbon (^{13}C) than methane produced from acetate as CO_2 is usually more depleted in ^{13}C than acetate (Conrad, 2020).

Methane produced exclusively from acetate is commonly assumed to have a signature in $\delta^{13}C$ between -27‰ to -60‰ (Conrad et al., 2009). These values are calculated under the assumption that the organic matter present in the sediment has $\delta^{13}C$ values between -34‰ and -23‰. On the other hand, carbon fractionation during the production of methane from H_2 and CO_2 seems to be significantly larger than methane from acetate (Conrad et al., 2009). In other words, very depleted values of $\delta^{13}C$ in methane of up to -80‰ might be an indication for CO_2-dependent methanogenesis in freshwater sediments.

After methane is produced, it is available to other microbial communities to be used as a carbon source. Microbial-driven methane oxidation occurs following two paths; Type I methanotrophs; assimilate formaldehyde via the ribulose- monophosphate pathway, whereas type II methanotrophs use the serine pathway. The first step in both oxidation pathways involves the oxidation of methane to methanol, which is catalyzed by the enzyme monooxygenase (MMO). MMO is present in all methane-oxidizing microorganisms in one of the two known forms; pMMO and sMMO.

Research has suggested that pMMO and sMMO produce similar carbon and hydrogen isotope fractionation, indicating that pMMO and sMMO have a similar reaction mechanism regarding their carbon isotope discrimination during CH_4 oxidation (Conrad et al., 2009). However, isotope enrichment factors for $\delta^{13}C$ have been reported within a range from -10‰ up to -35‰ (Barker and Fritz, 1981; Coleman and Risatti, 1981; Happell et al., 1994; Bergamaschi and Harris, 1995; Ree- burgh et al., 1997; Bergamaschi et al., 1998; Zyakun and Zakharchenko, 1998; Snover and Quay, 2000; Templeton et al., 2006; Kinnaman et al., 2007; Powelson et al., 2007).

Lately, Rasigraf et al (2012) have determined isotope enrichment factors associated with ^{13}C-CH4 discrimination during anaerobic oxidation of

methane for Candidatus M. Oxyfera. The authors calculated an enrichment factor ε of -29.2 +/- 2.6 ‰

2.3.3 N and O stable isotope effects during nitrification and denitrification

A series of culture experiments have investigated the nitrogen and oxygen isotope effects of N cycling processes. For example, during the aerobic oxidation of ammonium to nitrite and nitrate, the newly formed NO_3^- is depleted in ^{15}N relative to the substrate NH_4^+. Literature values for nitrogen enrichment factors for nitrification are commonly in the range of +12‰ to +38‰ (Mariotti et al., 1981; Horrigan et al., 1990; Casciotti et al., 2003).

Contrary to nitrification, the residual NO_3^- pool will be enriched in the heavier isotope ^{15}N due to denitrification. Most ^{15}N enrichment factors were reported for denitrification in different environments ranging from +10 to +30‰ (Brandes et al., 1998; Voss et al., 2001). These values are consistent with ε values derived from enrichment cultures (Wellman et al., 1968; Mariotti et al., 1981; Barford et al., 1999; Granger et al., 2008).

Coupled nitrate N and O isotope ratios measured in marine environments revealed a 1: 1 covariation of the N and O isotope enrichments associated with nitrate assimilation (Casciotti et al., 2002; Wunderlich et al., 2012), similar to laboratory experiments with pure cultures. Indeed, this dual isotope enrichment is considered a distinctive indication of denitrification. On the other hand, in freshwater environments, linear trajectories of ^{15}N:^{18}O display slopes between 0.5–0.8 in a 2D isotope plot (Böttcher et al., 1990; Wild et al., 2018) (Kendall et al., 2008). The discrepancy between the $\delta^{18}O$: $\delta^{15}N$ slope of nitrate observed in freshwater ecosystems in comparison to pure culture experiments has been attributed (among others) to the activity of anammox bacteria. These isotope effects are discussed in the next section

2.3.4 $\delta^{15}N\text{-}NH_4^+$ and $\delta^{15}N\text{-}NO_3^-$ isotope signatures during anaerobic oxidation of ammonium

Under aerobic conditions ammonium is produced as a result of the mineralization of organic matter. The processes of aminization and ammonification are the two main steps for mineralization. Both processes are associated with a small N isotope fractionation (+-1‰) (Kendall, 1998).

In the anoxic water column, ammonium might be oxidated to nitrogen gas during anammox. Recently, kinetic nitrogen isotope effects during the conversion of NH_4^+ to N_2 by anammox bacteria of -29.1‰ +/- 0.7 and -23.5‰ +-0.6 have been reported in batch culture experiments (Brunner et al., 2013). In contrast, ^{15}N enrichment factors attributed to anaerobic oxidation of ammonium in a lake water column have been significantly lower (-5‰) (Wenk et al., 2014). Thus, it seems that the isotope effect of anammox in $\delta^{15}N$ that is observed in-situ could be masked by other coupled N-cycling processes (e.g nitrification and DNRA) or by transport processes (e.g diffusion, sedimentation).

Moreover, it has been proposed the activity of anammox will influence the $\delta^{18}O$: $\delta^{15}N$ the slope of nitrate observed in freshwater ecosystems. As shown in Eq. 13, 0.26 mol of NO_3^- will be produced for each oxidized mol of NH_4^+, thus, also influencing the values of $\delta^{15}N$ in the NO_3^- pool. The formation of NO_3^-, during anammox, is characterized by an inverse kinetic isotope effect. Usually formed compounds will be depleted in the heavy isotope in comparison with the subtract. However, during anammox, the resulting nitrate is strongly enriched in $\delta^{15}N$ (Brunner et al., 2013; Kobayashi et al., 2019). In addition, when NO_2^- is oxidized to NO_3^- as a result of the anammox process, one oxygen molecule from water with a $\delta^{18}O$ value of around -10‰ is added to the newly

formed NO_3^-. Finally, $\delta^{18}O$ values of nitrite are lowered due to rapid oxygen isotope exchange with water oxygen (C Buchwald and Casciotti, 2010; Casciotti et al., 2010). In consequence, NO_3^- will be further enriched in the heavier isotope ^{15}N while $\delta^{18}O$ values of nitrate are lowered by oxygen exchange, and thus, the trajectory $\delta^{18}O$: $\delta^{15}N$ will decrease.

2.4 MODELING AS A TOOL FOR UNDERSTANDING BIOGEOCHEMICAL PROCESSES IN FRESHWATER ECOSYSTEMS

Temporal and spatial evolution of the chemical and physical properties of natural systems can be represented by differential equations. Increasing computer power in the last decades to solve and simulate these equations has made hydrodynamic and water quality models essential tools for both science and management.

Models can be used to evaluate and test hypotheses about the potential biochemical reactions affecting the state of a system, but also, they can be used to derive more realistic in-situ parameters in comparison with parameters derived from experiments under laboratory conditions.

The following section describes one of the models derived from the general mass transport and mass balance basic equations and the main model implemented in this thesis; the diffusion-reaction equation.

2.4.1 The diffusion-reaction equation

The diffusion-reaction equation arises as a model to describe the development of the concentration of substances in time and space, which changes depending on two principal mechanisms: 1) mass transport processes causing particle movement through space by Brownian motion (molecular diffusion),

or by the random motion of the fluid (turbulent diffusion), 2) reaction of the substance with their surroundings in a way that affects the substance current concentration.

The fundamental quantity in the study of diffusion is the flux, i.e. the mass of a concentration that passes a unit area per unit of time. Dispersive flux can be described by Fick's law, which states that the mass movement resulting from diffusion happens at a rate inversely proportional to the gradient of mass concentration, in other words, particles will move in direction of decreasing concentration.

$$J = -D\frac{dC}{dx} \qquad (16)$$

Where J is the dispersive mass flux density, C is the concentration of the substance, x is the distance and D represents the diffusion coefficient.

Considering the conservation of mass, equation 16 can be written as the classic diffusion equation as follows:

$$\frac{\partial C}{\partial t} = D\frac{\partial^2 C}{\partial x^2} \qquad (17)$$

The diffusion coefficient D accompanying the right part of the equation 17 (second derivative), might refer to the transport process due to the random motion of the chemical molecules (molecular diffusion), the random motion of the chemical carrier (turbulent diffusion), or a combination of both.

Changes in the substance concentration due to biochemical reactions are described by adding a reaction term on the right side of the equation as follows:

$$\frac{\partial C}{\partial t} = D\frac{\partial^2 C}{\partial x^2} \; -/+ \; R_i \quad (18)$$

The subtraction and addition symbol of the reaction term will represent if the substance is being consumed (negative) or is being produced (+). For biochemical reactions depending on only one limiting substrate, R is described as a first-order reaction term (k) multiplied by the substrate concentration.

The solution of this equation requires one initial condition and two boundary conditions. Implementation of this model for our case study is in detail explained in Chapter methods 4.6 and 4.7.

Chapter 3: AIMS AND OBJECTIVES

Because of the relevance of methane on climate change and the increase of nitrate concentrations in freshwater, the understanding of the fate of methane and nitrogen and its alleviation is of great importance. The coupling of anaerobic oxidation of methane with denitrification and anammox has not only the potential to eliminate N load from ecosystems to N_2 but also for reducing methane emissions to the atmosphere.

Therefore, the objective of this thesis was to investigate the dynamics of aerobic and anaerobic oxidation of methane, and the co-occurrence of DAMO with anammox at the seasonally stratified lake Fohnsee. The following specific objectives have been formulated: i) identifying and qualitatively describing the seasonal dynamics and vertical variations of the aerobic oxidation of methane and anaerobic oxidation of methane ii) evaluating and quantitatively describing whether denitrification coupled with anaerobic oxidation of methane (DAMO) is a key biogeochemical process at lake Fohnsee leading to reduced methane fluxes within the hypolimnion and constitutes a substantial sink for nitrate. iii) establishing if anammox is an important driver for NH_4^+ oxidation and co-occurs with DAMO in the water column and are thus overlocked processes in freshwater lakes.

To reach these goals sampling campaigns were performed monthly for nearly one year. From April to December 2018 and from May to September 2019. This thesis shows a combined approach using high depth-resolved isotope values of methane (δ^{13}C-CH4), ammonium (δ^{15}N-NH_4^+), nitrate (δ^{15}N and δ^{18}O-NO_3^-), and sulfate (δ^{34}S-SO_4^{2-}) and water chemistry data and to support our

interpretation with numerical modeling and quantitative PCR (qPCR) results for the functional genes for anammox (*hszB*) and denitrification (*nirK, nirS*).

Chapter 4: MATERIALS AND METHODS

4.1 STUDY SITE; LAKE FOHNSEE

Lake Fohnsee is one of the pre-Alpine lakes of the district Osterseen located in Southern Germany. This chain consists of 19 hydrologically interconnected lakes that drain to the north into Lake Starnberg. Lake Fohnsee has a surface area of approximately 211,900 m² with a water depth between 5 and 23 m and it is mostly fed by subsurface groundwater inflow (Braig, 2015).

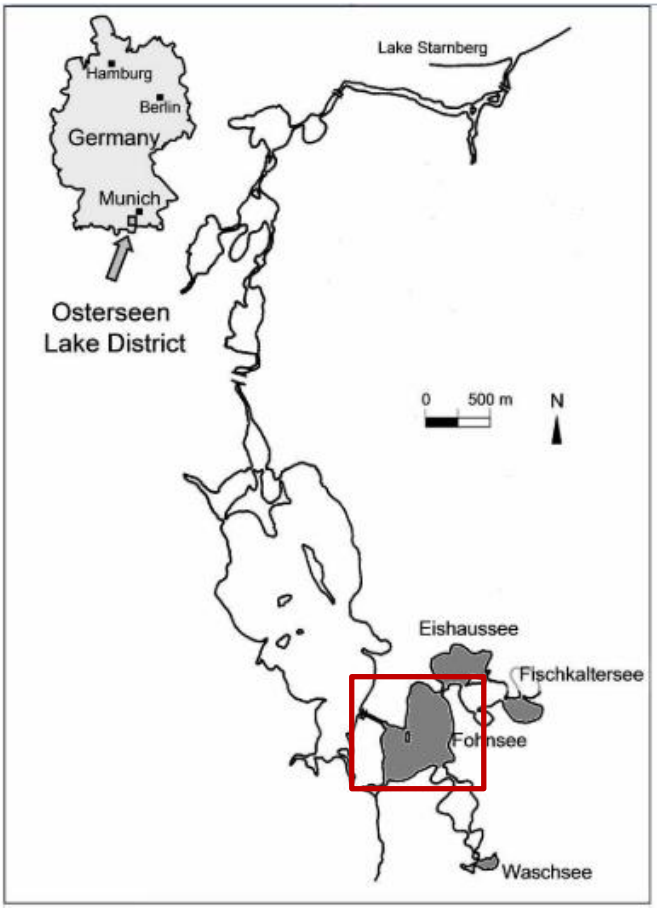

Figure 4. 1 Location map of Lake Fohnsee

Lake Fohnsee belongs to oligotrophic lakes with low nutrient content. Due to

its mixing patterns, it is classified as dimictic with two periods of mixing; one at the beginning of spring, when the shelf ice formed during winter melts, and the second one during autumn when thermal stratification vanishes. The lake develops a very stable hypolimnion, with high resistance to mechanical mixing in the water column (Braig et al., 2010). During the months of thermal stratification, oxygen is depleted near the lake sediment resulting in anoxic conditions from 8 m depth.

4.2 SAMPLING STRATEGY

4.2.1 Water column sampling

Sampling campaigns were conducted at Fohnsee from April to December 2018, and from April to September 2019 to obtain depth-resolved water samples from the water column of the lake to a depth of 22 m.

The sampling set-up consists of 4 peristaltic pumps at a land elevation that is connected to a set of plastic probes. These plastic probes are attached on the other extreme to a PVC tube which allows the submerging of the sampling probes. The system is portable and can be easily transported to the sampling point located in the middle of lake Fohnsee (WGS84: latitude: 11.31370, longitude: 47.78028). Sampling is conducted starting from the deeper layers towards the surface. Water is pumped at a very low flow rate to avoid disturbances in the water depth of the sample (Lane et al., 2003).

Water oxygen content and water temperature T (°C) were measured with a multi-parameter probe Multi 350i (WTW, Weilheim, Germany) prior to water sampling with a depth resolution of 1m and up to 0.1 m in the zone of greater interest. The detection limit of the O_2 sensor is 0.3 μmol L^{-1} whereas the analytical error is smaller than 0.5%.

4.3 HYDROCHEMICAL ANALYSIS AND METHANE CONCENTRATIONS

4.3.1 Hydrochemical Analysis

Water samples for NO_2^-, NO_3^-, NH_4, and SO_4^{2-} concentration analysis were field-filtered with a 0.22 μm syringe filter and transported in glass vials. Preservation of the samples was performed by adding 0.1 ml of Nitric acid for the cations samples and sodium hydroxide for the anions samples. Samples are subsequently analyzed by ion chromatography (IC) with an IC 1000 device (Thermo Fischer Scientific, MA, USA) including a Dionex IonPac AS9-HC analytical column (4×250 mm) for anions and a Dionex IonPac CS 12A analytical column (4×250 mm) for cations. Ion concentrations were measured in triplicates, and the values presented in this thesis correspond to the mean value of these measurements. The detection limit (DL) and standard deviation (σ) of the data presented are as follow: for NO_3^-, DL of 0.010 and σ of 0.001 mmol L^{-1}; for NO_2^-, DL of 0.006 and σ of $3.5*10^{-5}$ mmol L^{-1}; for SO_4^{-2}, DL of 0.008 and σ of $2*10^{-4}$ mmol L^{-1}.

4.3.2 Measurements of hydrogen sulfide

Water samples for H_2S concentration measurements were taken and preserved as described elsewhere (Grasshoff et al., 1978). Briefly, the plastic probe of the water sampler is placed at the bottom of the glass bottle where the water sample will be taken. The bottle is filled and overflowed with at least three volumes making sure to not draw any air bubbles into the sample. Samples are preserved with Zinc acetate, which precipitates the sulfide as zinc sulfide. The measurements are performed in a spectrophotometer Spectroquant® Prove 100 (Merck KGaA, Germany), method: photometric 0.020-1.5 mg L^{-1}

spectroquant, reference: 114779. Reagents contained in this method dissolve the precipitate and the color for photometric analysis develops normally.

4.3.3 Measurement of methane concentrations

Duplicate lake water samples for concentration and isotopic composition analysis of methane were collected in 120 mL glass bottles, allowing an overflow of three times the volume of the bottle to ensure that air bubbles were not trapped within the sample. Water samples were then fixed with 20µl NaOH 10M to stop the microbial activity and immediately sealed with a butyl rubber stopper. Zn-acetate was added to precipitate potentially occurring H_2S in the form of ZnS, in order to avoid interference during the subsequent gas analyses.

Methane concentrations were measured using a static equilibration headspace method as described by Kampbell et al., (2006). 20 mL of the 120 mL of the water sample in the capped bottles was replaced by synthetic air (80% N_2, 20% O_2) followed by outgassing of the dissolved gases from the water sample into the headspace for 2 h at 30ºC. The bottles are shaken for at least 5 minutes during the process to ensure gas equilibration.

Afterward, headspace gas is analyzed using a TRACE™ 1300 gas chromatograph with flame ionization detection, GC-FID (Thermo Fisher Scientific Inc, MA, USA). Measurements were performed three times. Values presented in this thesis correspond to the mean value of these measurements (average coefficient of variance: 0.0012 mmol L^{-1}).

The methane concentration in a bottle (n_{CH_4}) is obtained by summing the amount of methane in the head space (n_{CH_4HS}) and dissolved in water (n_{CH_4w}).

$$n_{CH_4} = n_{CH_4w} + n_{CH_4HS} \quad (19)$$

The concentration of methane in water at the time of the sampling is calculated as follows:

$$C - CH_4 = \frac{n_{CH_4}}{V_w} \quad (20)$$

Where Vw is the volume of the water in the bottle. The molar quantity in the head space is calculated with the partial pressure of methane in the headspace as follows:

$$P_{CH_4\,HS} = \frac{Pstd * A\,sple}{Astd} \quad (21)$$

Where Astd and Asple are the peak area returned by the Gas Chromatograph for the standard and the sample, respectively. The formula above is used to establish a calibration curve. Subsequently, the molar quantity of methane in the head space can be calculated by using the ideal gas law:

$$n_{CH_4\,HS} = \frac{P_{CH_4HS} * V_{HS} * P_{HS}}{R(273{,}15 + T)} \quad (22)$$

where V_{HS} is the volume of the headspace created in the bottle, P_{HS} is the pressure in the head space and R is the ideal gas constant.

4.4 STABLE ISOTOPE MEASUREMENTS OF METHANE ($\delta^{13}C$), NITRATE ($\delta^{15}N$, $\delta^{18}O$), SULFATE ($\delta^{34}S$, $\delta^{18}O$) AND AMMONIUM ($\delta^{15}N$)

The carbon isotopic composition of methane was determined from headspace gas (generated as described above), using cavity ring-down spectroscopy (G2201-i Isotopic Analyzer for CO_2/CH_4, Picarro Inc, California, USA). Reference materials were pure methane $\delta^{13}C$: -18‰ and 69‰ vs. VPDB
Measurements are done three times, the values presented in this thesis are the mean values of the measurements.

Samples for isotope analysis of nitrate ($\delta^{15}N$, $\delta^{18}O$) and sulfate ($\delta^{34}S$, $\delta^{18}O$) were field-filtered with 0.2 μm PES filters and stored in PE vials and kept frozen prior to analysis. The nitrogen and oxygen isotope ratios of nitrate dissolved in water were determined using the denitrifier method as described by Sigman et al., (2001) and Casciotti et al., (2002). This method consists of the bacterial reduction of NO_3^- to nitrous oxide gas (N_2O) via a bacterial that lacks nitrous oxide reductase. For this study, *P.aureofaciens* bacteria were grown in a special tryptic soy broth prepared in advance. Batches containing the broth are inoculated ensuring sterility and allowing 7 days of growth, after which time the bacteria will have reached maximum population density.

The bacteria are then harvested and subdivided into individual 20ml, crimp sealed sample vials (pre-flushed with inert N_2 for ~3-4 hours to lower the atmospheric blank). Standards and raw sample waters are then injected into individual vials in a pre-set order and left overnight at room temperature. Each vial is lysed by injecting 0.15mL of 10 N NaOH and the vials are mounted in an autosampler for automated analysis.

Subsequently, the produced N_2O gas was measured using an HP 6890 gas chromatograph with a PreCon® device coupled to a Finnigan Mat Delta+XL mass spectrometer. Each set of sample vials is prepared together with 4 reference materials for $\delta^{15}N$ and $\delta^{18}O$ respectively, as follows: IAEA NO_3^-: -4-7 ‰ +/- 0.2, USGS 32: +180‰ +/-1, +25‰ +/- 0.4, USGS 34: -1.8‰ +/-0.2, -27.9‰ +/- 0.6 and USGS 35: n/a*, +57‰ +/-0.6. standards are placed at the beginning and the end of each sampling rack. Precision and accuracy as σ (n = 10) were 0.5 and 1.0‰ for $\delta^{15}N$ and $\delta^{18}O$ of nitrate, respectively.

Water samples for nitrogen isotopic composition of dissolved ammonium were taken in HDPE bottles and filtered through a 0.45 μm filter directly into the bottle leaving a small head space. Samples were preserved adding ammonium free concentrated sulfuric acid (H_2SO_4) until samples reached a pH equal to 2. Consequently, $\delta^{15}N$-NH_4^+ was determined using the "diffusion-method" as described by Sebilo et al. (2004). Dissolved NH_4^+ is converted into NH_3 by raising the pH and subsequently the gas is trapped as $(NH_4)_2SO_4$ on a small strip of polypropylene previously saturated with $NaHSO_4$. The filter is then combusted in a EA-IRMS (Elemental Analyzer - isotope ratio mass spectrometry) system along with a full suite of Reference Materials (IAEA N_2: +20.3‰, ISL KNO_3: -1.32‰, USGS 40: -4.5‰, USGS 41: +47.6‰). The EA converts total nitrogen in a solid sample into N_2 gas. The IRMS is capable of detecting ion beams with mass/charge from N_2 (m/z 28 = $^{14}N^{14}N$, m/z 29 = $^{14}N^{15}N$, and m/z 30 = $^{15}N^{15}N$). $\delta^{15}N$ and $\delta^{18}O$ values are calculated by the instrument software (ISODAT 3.88).

Water samples for stable isotope composition analysis of SO_4^{2-} were pretreated with Zn-acetate to precipitate H_2S as ZnS and avoid re-oxidation. After the removal of potentially occurring ZnS, dissolved sulfate was precipitated as

pure $BaSO_4$ as described by Andersson et al., (1992). Subsequently, $\delta^{34}S$ and $\delta^{18}O$ values of SO_4^{2-} were determined using continuous-flow isotope ratio mass spectrometry (CF-EA-IRMS) at the Isotope Laboratory at the University of Calgary using a Thermo Delta+XL® coupled with a Carlo Erba NA 1500® elemental analyzer for sulfur isotope analyses and a HekaTech pyrolysis reactor for oxygen isotope analyses via a Conflo-III® device. Precision and accuracy as σ (n = 10) were 0.3 and 0.5‰ for $\delta^{34}S$ and $\delta^{18}O$ of sulfate, respectively.

Isotope results are expressed in per mil notation relative to the international standards V-PDB, AIR, V-SMOW and V-CDT for carbon, nitrogen, oxygen and sulfur isotope ratios. For an approximation of the observed carbon isotope enrichment factors (ε) of methane oxidation a closed system Rayleigh model was used (Mariotti et al., 1981).

4.5 CLOSED-SYSTEM RAYLEIGH MODEL

For an approximation of the observed carbon isotope enrichment factors (◎) of C methane, N and O for nitrate, and S and O for sulfate, apparent enrichment factors were calculated using a closed-system Rayleigh model (Mariotti et al., 1981).

$$ln\frac{R_i}{R_0} = \varepsilon * lnf \qquad (S1)$$

where ε is the isotope enrichment factor associated with the microbial consumption of the reactant, f is the unreacted portion of the substrate described by the relation C_i/C_0, and R_0 and R_i are the isotopic ratios of the substrate before alteration (index 0) and at a given time t (index *i*), respectively.

4.6 DEVELOPMENT OF A DIFFUSION-REACTION MODEL FOR CONCENTRATIONS AND STABLE ISOTOPES OF METHANE

4.6.1 Determination of methane and oxygen fluxes and calculation of the turbulent diffusion coefficient for Lake Fohnsee

Vertical fluxes (F_z) of chemical compounds in the water column were estimated from concentration gradients dC/dz, and the turbulent diffusion coefficient Kz applying Fick's first law of diffusion:

$$F_z = -K_z \frac{dC}{dz} \qquad (3)$$

Coefficients for turbulent diffusive transport (K_z) were calculated using the buoyancy frequency (Jassby and Powell, 1975) as described also for lake Lugano (Wenk et al., 2013; Blees et al., 2014) using density profiles, that were derived from the temperature profiles measured in Lake Fohnsee from May to December in 2018 and April to September at water depths between 8 m and 22 m:

$$K_z = a_0 \left(-\frac{g}{\rho_z} \frac{d\rho}{dz} \right)^{-0.5} \qquad (4)$$

where g is gravitational acceleration and ρ_z is water density at a given depth z. The system-specific constant a_0, which depends on the surface area of the lake ($A_{Fohnsee} = 0.2119\ \mathrm{km}^2$) was calculated for lake Fohnsee using the empirical approximation proposed by Hondzo and Stefan (1993) as follows:

$$a_0 = 8.17 * 10^{-4} * {A_{Fohnsee}}^{0.56} \qquad (5)$$

For lake Fohnsee a_0 was calculated to be 0.000343 $cm^2 s^{-2}$, similar to values reported in other field- studies for stratified lakes (Gargett A.E., 1984; Lewis and Landing, 1991; Blees et al., 2014).

Calculated K_z for lake Fohnsee was on average $1.3*10^6$, $m^2\ s^{-1}$ and was kept constant throughout the water column. This value is in agreement with typical values found for the hypolimnion in stratified lakes (Wenk et al., 2014; Salas De León et al., 2016), and it fits precisely to a K_z-value found for lake Fohnsee in an earlier study (Einsiedl et al., 2020).

Oxygen fluxes from the epilimnion to the hypolimnion were calculated in order to account for possible trace amounts of oxygen present in the anoxic-oxic boundary throughout the year. Subsequently, methane fluxes were balanced with the oxygen fluxes considering CO_2 and H_2O as final reactions products (Caldwell et al., 2008).

4.6.2 Diffusion-reaction model for aerobic and anaerobic oxidation of methane

Net rates of in-situ chemical consumption and production can be fitted by applying a diffusion-reaction model for simulating measured concentration profiles by inverse modelling (Bungay et al., 1969; Deutzmann et al., 2014). Previous studies at Lake Fohnsee showed that the transport of dissolved chemical species in the hypolimnion during summer stratification is not affected by mixing and wind convection (Braig et al., 2010). Resistance to mechanical mixing during the stratification period in our study area is very strong (Schmidt Stability Index *St* of 502 g cm cm^{-2}), and mean water residence times are high (Braig et al., 2010). Thus, it is reasonable to consider transport

in hypolimnion under the following assumptions: a) molecular diffusion is the dominant transport process for methane in the water column, b) vertical concentration gradients of methane are larger than horizontal concentration gradients, and c) during stratification, the hypolimnion remains stable and, therefore, the model assumes static conditions (no advective mixing) in the anoxic water column for the considered time period (May to December).

Consequently, one-dimensional transient modelling was applied for vertical reactive methane transport in lake water, using a diffusion-reaction equation for the anaerobic and aerobic zone, respectively:

$$\frac{\partial C}{\partial t} = K_z \frac{\partial^2 C}{\partial z^2} - R_{an} \quad (23)$$

$$\frac{\partial C}{\partial t} = K_z \frac{\partial^2 C}{\partial z^2} - R_{ae} \quad (24)$$

where t is time, z is the water depth, C is the concentration of methane, and R_{an} and R_{ae} represent the rate of the anaerobic and aerobic methane oxidation, respectively. R can be described as the product between the degradation rate constant (k) of first-order and the concentration of the substrate (C). As the reaction rate of methane oxidation depends on the specific microbial process, we have coupled two equations for modelling: one for diffusion and anaerobic methane oxidation (R_{an}) and another one for diffusion and aerobic methane oxidation (R_{ae}) (Eq. 23 and Eq. 24). The depth of the boundary separating the anaerobic and the aerobic parts of the water column was calculated using both the methane and oxygen fluxes, as calculated above from the flux balance. Temporally varying boundary depths were considered, where boundary depths were defined for each month. The use of calculated fluxes enabled a

realistic distinction between aerobic and truly anoxic conditions, compared to relying on oxygen concentrations measured in-situ during the sampling campaign.

Equations 23 and 24 were solved numerically using the pdepe solver within Matlab R2019b. The following boundary conditions were set: a constant methane concentration at the lower boundary and no fluxes of methane (no-flux boundary) at the upper boundary. Methane concentrations measured at the bottom of the lake (at depths z between 21 and 22 m) were used as initial concentration C_o. Values for k_{ae} and k_{an} were fitted by inverse modelling. Model calibration was achieved by using depth profiles of methane concentrations in the lake water. The standard error of the mean and the normalized mean error was used for evaluating the goodness of model fit.

4.6.3 Development of a diffusion-reaction model coupling methane consumptions rates and carbon isotope enrichment factors to describe $\delta^{13}C$ values of methane

Isotope models based on the Rayleigh distillation often allow only a rough approximation of the isotope enrichment factors in the field (Lehmann et al., 2003; Einsiedl et al., 2015). This closed-system model does not consider turbulent diffusion and substrate utilization and therefore it may significantly underestimate the extent of stable isotope fractionation during microbial processes in comparison with systems where the substrate is not limited (Thunell et al., 2004). Therefore, the above described diffusion-reaction model (Eq. 23 and 24) has been modified to consider the isotopic species $^{13}CH_4$ and $^{12}CH_4$ separately and assess the extent of carbon isotope fractionation:

$$\frac{\partial C^{12}CH_4}{\partial t} = K_{^{12}CH_4}\,\frac{\partial^2 C}{\partial z^2} - k_{ae}\,C^{12}CH^4 - k_{an}\,C^{12}CH_4 \qquad (25)$$

$$\frac{\partial C^{13}CH_4}{\partial t} = K_{^{13}CH_4}\,\frac{\partial^2 C}{\partial z^2} - \left(1 - \frac{\varepsilon_{ae}}{1000}\right) k_{ae}\,C^{13}CH^4 - \left(1 - \frac{\varepsilon_{an}}{1000}\right) k_{an}\,C^{13}CH_4 \qquad (26)$$

where $C^{12}CH_4$ and $C^{13}CH_4$ are the concentrations and $K_{^{12}CH_4}$ and $K_{^{13}CH_4}$ the diffusion coefficients of $^{12}CH_4$ and $^{13}CH_4$ respectively. k_{ae} and k_{an} are the degradation rate constants for aerobic and anaerobic methane oxidation, respectively, as described above (fitted from solving Eq. 23 and 24). Both the anaerobic and aerobic degradation terms are considered in Eq. (25) and (26), respectively. Under oxic conditions, k_{an} is set to zero (thus skipping anaerobic degradation) and under anoxic conditions, k_{ae} is set to zero (thus skipping aerobic degradation). ε_{ae} and ε_{an} are the carbon isotope enrichment factors associated with aerobic and anaerobic methane oxidation, respectively.

The first term on the right side of equations 25 and 26 represents diffusive transport in the water column specific to the isotope species $^{12}CH_4$ and $^{13}CH_4$, following e.g. de Visscher et al., (2004). Thus, stable isotope fractionation by diffusion is considered by using corrected diffusion coefficients $K^{12}CH_4$ and $K^{13}CH_4$ for the isotopic species, which account for the influence of the molar mass in the aqueous medium (Marrero and Mason, 1972; Mahieu et al., 2008):

$$K_{^{13}CH_4} = K_{^{12}CH_4}\sqrt{\frac{M_i\,(M_j + M_o)}{M_j(M_i + M_o)}} \qquad (27)$$

where M_i and M_j are the molar masses of $^{12}CH_4$ and $^{13}CH_4$ respectively, and M_o is the molar mass of water. $K^{12}CH_4$ relates to the more frequent isotope species and thus was set to the K_Z -value obtained above ($1.3*10^6$ m² s^{-1}). From modelled concentrations of the isotope species ($C^{12}CH_4$ and $C^{13}CH_4$, solution of Eq. 25 and 26), delta values ($\delta^{13}C$) were obtained by using Eq. (1), with R_{sample} = $C^{13}CH_4$ / $C^{12}CH_4$ and a value for $R_{standard}$ of 0.0112372 (International Atomic Energy Agency (IAEA), 1993).

4.7 DEVELOPMENT OF A TRANSIENT DIFFUSION MODEL FOR CONCENTRATIONS AND STABLE ISOTOPES OF AMMONIUM

4.7.1 Transient diffusion model for concentrations of ammonium in the water column

Ammonium is released from the anoxic sediments as a result of the mineralization of organic matter (Morin and Morse, 1999; Beutel, 2006; Wang et al., 2008). Fohnsee water is assumed to prevail (no advective mixing) so that ammonium is transported within the water column only by diffusion. Thus, vertical transport of NH_4^+ from the lake sediment-water interface along the anoxic water column can as well be described by equation 17.

K_z was calculated independently for each month using density profiles, that were derived from the temperature profiles measured at Fohnsee from May to September as described elsewhere (Wenk et al. 2013; Blees et al. 2014).

4.7.2 Transient diffusion model for stable isotopes of ammonium in the water column

The model described by equation 17, can be modified to consider both the isotopic species $^{14}NH_4^+$ and $^{15}NH_4^+$ separately in order to assess the extent of stable isotope fractionation due to diffusion as follows:

$$\frac{\partial C^{14}NH_4{}^+}{\partial t} = K_{^{14}NH_4{}^+} \frac{\partial^2 C}{\partial z^2} \qquad (28)$$

$$\frac{\partial C^{15}NH_4{}^+}{\partial t} = K_{^{15}NH_4{}^+} \frac{\partial^2 C}{\partial z^2} \qquad (29)$$

The final $^{15}N/^{14}N$ isotope ratio of NH_4^+ can be calculated incorporating both resulting partial differential equations for ^{15}N and ^{14}N into the general formula for stable isotope notation, using N_2 as reference material as follows:

$$\delta N^{15}NH^{4+} = \left[\frac{\left(\frac{\frac{\partial C^{15}N}{\partial t}}{\frac{\partial C^{14}N}{\partial t}} \right)}{\left(\frac{C^{15}N}{C^{14}N} \right)_{N_2}} - 1 \right] * 1000 \qquad (30)$$

Where the term $\left(\frac{C^{15}N}{C^{14}N}\right)_{N^2}$ is the isotope ratio reference of N_2 in air ($^{15}R_{air} = 0.003676$) (Mariotti, 1983), and the term above represents the changes of the concentrations of both isotopic species ^{15}N and ^{14}N in-depth and time, which are calculated solving the differential equations 28 and 29.

Equations 28 and 29 were solved numerically using the pdepe solver within Matlab R2019b and successively incorporated in equation 30.

Temporally varying boundary condition depths were considered to represent the vertical movement of the oxycline observed at lake Fohnsee throughout

the observation period. Depth boundaries were defined for each month depending on the depth where dissolved oxygen (DO) was no longer detected. The ammonium concentrations that were measured at the lake bottom in a water depth of 22 and 23 m depending on the sampled month was set as the lower boundary condition. No additional fluxes at the upper boundary were considered.

Initial $\delta^{15}N\text{-}NH_4^+$ in t_0 was assumed to be 28‰, which corresponds to the average signature of the remaining ammonium in the water column in May, and thus, it considers the rest enriched NH_4^+ in the water column from the previous months.

For the 1D diffusion model, a constant ammonium input (C_o= 0.12 $mmolL^{-1}$) corresponding to the NH_4^+ concentration measured at the lake bottom (Z=23) was assumed as the lower boundary, no-flux boundary conditions were implemented at the upper boundary and the initial ammonium concentration throughout the system is zero. The final time for each simulation (t_{end}) was set to the date of the sampling campaign, where $t_0 = 0$ corresponds to the time where we observed anaerobic conditions in the water column and a well-defined thermocline as it has been previously documented (15 of March; Pena et al, pers. comm), and assumed, therefore, that the anaerobic water column from this point was not affected by advective mixing.

None of the described parameters were used for fitting the model results with the observed data. This was done with the intention to evaluate, if the observed stable isotopes and concentrations of ammonium could be explained theoretically only by diffusive transport without microbial degradation (anammox), the movement of the oxycline and the mixing of the previously available ammonium in the water column with the newly formed ammonium in the sediment.

The model considers a source of ammonium in the anoxic zone the NH_4^+ released from the lake sediments with a constant isotopic signature for $\delta^{15}N$-NH_4^+ of 11‰, and initial $\delta^{15}N$-NH_4^+ of 28‰, which corresponds to the average signature of the ammonium in the water column in May, and thus, it considers mixing with the rest enriched NH_4^+ in the water column from the previous months.

4.8 DNA EXTRACTION AND PCR AMPLIFICATION

The filters obtained after filtering the lake water from the different layers, which were stored at – 20C°, were cut for DNA extraction on a sterile petri dish into 2 mm pieces before adding it to a lysing matrix screw cap tube. The protocol was based on phenol/chloroform/isoamyl alcohol mixture as described in Lueders et al. (2004) and Töwe et al. (2011) using PEG8000 instead of PEG6000. The concentration of the DNA was measured fluorometrically and the quality was determined by spectrophotometry. Some samples had to be excluded due to low quality or low DNA concentration (June: 20 m depth, August: 8 m depth, September: 10 and 6 m depth).

quantitative PCR (qPCR) was used to measure the overall bacterial abundance based on the copy numbers obtained for the 16S rRNA gene according to Gschwendtner et al (2011), the abundances of the hydrazine synthase β-subunit (hzsB) to determine the abundance of anammox bacteria (Wang et al. 2012) as well as marker genes for nitrite reducers (nirK, and nirS; Töwe et al. 2010). Primers, standards and PCR conditions were used as described in the original publications.

qPCR reactions were performed on a 7300 Real-Time PCR System (Applied Biosystems, USA) with the Power Sybr Green Master Mix (Applied

Biosystems, USA). A dilution series confirmed that there was no inhibition of the PCR reaction for the undiluted samples (data not shown). The R2 of all standard curves was above 0.99, and the efficiencies of the amplification were as follows: 99.21% 16S rRNA gene, 75.55% *hzsB*, 94.33% *nirK,* and 117.51% *nirS*.

Chapter 5: ANALYSING SEASONAL VARIATIONS OF METHANE OXIDATION PROCESSES COUPLED WITH DENITRIFICATION IN A STRATIFIED LAKE USING STABLE ISOTOPES AND NUMERICAL MODELLING

5.1 RESULTS

5.1.1 Depth profiles of dissolved oxygen (DO) concentrations, dissolved organic carbon (DOC) and water temperature

During the field campaign in April 2018, we observed a decrease in the concentrations of dissolved oxygen (DO), with values changing from 0.41 mmol L^{-1} near the lake surface to 0.06 mmol L^{-1} close to the lake sediments at a water depth of 21 m (Fig. 1a). DO concentrations below the detection limit (< 0.3 μmol L^{-1}) were observed starting from May at a water depth of 19 m towards the lake sediments indicating the establishment of a reducing zone. During June to December, DO concentrations continued to be negligible in the hypolimnion, and anoxic conditions (DO < 0.3 μmol L^{-1}) were observed below a water depth of ~10 m from August until the end of October. The lake water surface temperature was highest (24°C) during the summer period and decreased considerably in October (12.6°C), but temperatures remained rather

constant at 5.2°C in the hypolimnion (Fig. 5.1). With the disappearance of the thermocline in October, oxygen progressively intruded from the epilimnion towards the lake sediments. As a result, during the last sampling campaign in December, anaerobic conditions occurred at a lower water depth between 16 m and the lake bottom at 23 m, indicating the displacement of the transition zone between oxic and the strongly reducing redox zones of the water column towards the lake sediments. DOC concentrations varied vertically between 2.5 and 4.0 mg L^{-1} throughout the water column. Between June and September, DOC concentrations were highest at the lake surface and lowest in the hypolimnion, while in October and December the highest DOC concentrations were found at the lake bottom (Fig. 5.1).

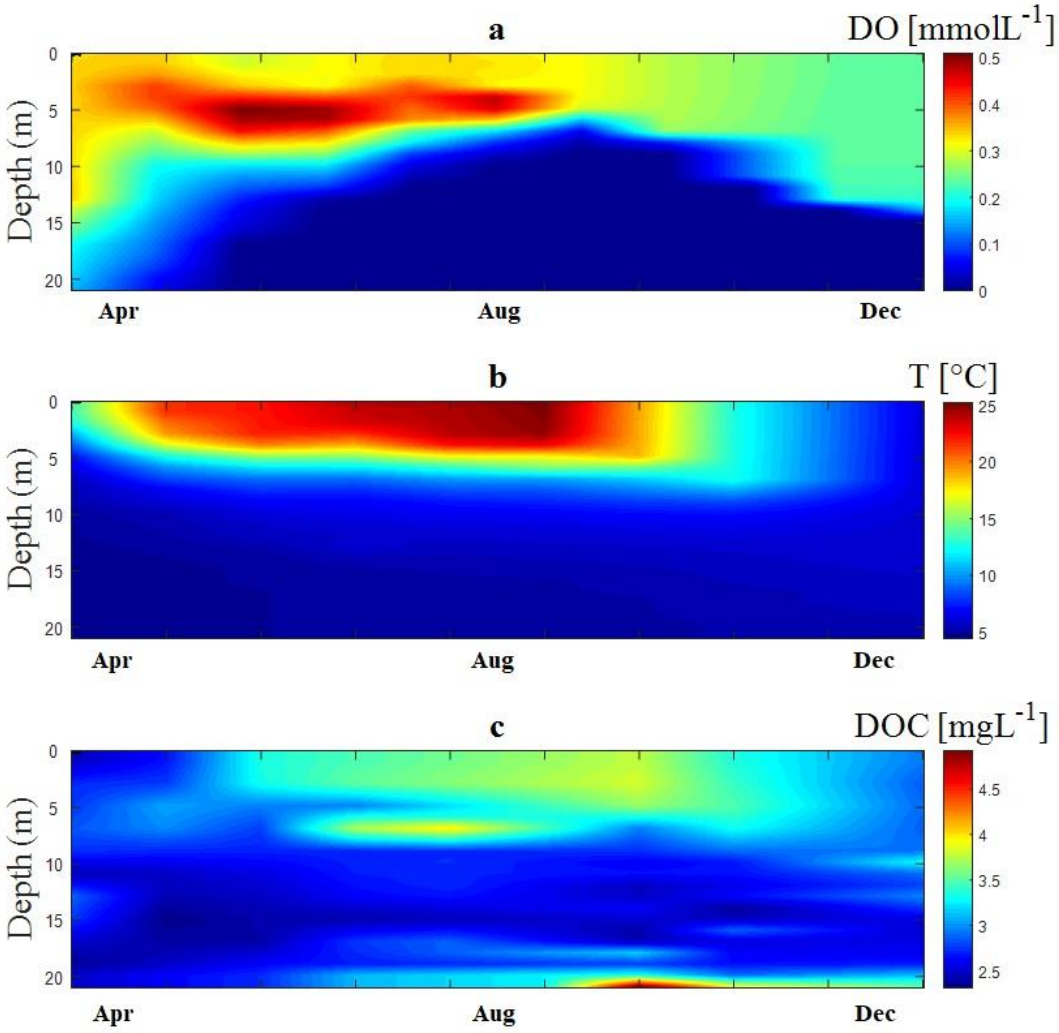

Figure 5. 1 Seasonal variations of physico-chemical parameters and DOC contents at Lake Fohnsee. a) dissolved oxygen, b) temperature, c) dissolved organic carbon (DOC). Measurements were taken once a month with a depth-resolution of 1 m. Data for the month of November were calculated by linear interpolation

5.1.2 Depth profiles of concentrations and isotopic composition of nitrate and methane

At the beginning of the sampling campaign in April 2018, methane concentrations were below the detection limit (< 0.3 µmol L^{-1}). From May to December 2018, methane was detected in the anoxic part of the lake water

column with the highest concentrations of up to 0.22 mmol L^{-1} consistently being observed at the bottom of the lake, while methane concentrations decreased towards the oxycline (Fig. 5.2). The steepest methane concentration gradients were observed between July and October, where methane concentrations were up to 0.21 mmol L^{-1} at the lake bottom and decreased to around 0.01 mmol L^{-1} close to the oxycline, indicating a decline in methane concentrations of more than 90% within the anoxic water column.

Within the anoxic zone of the water column, the decrease of methane concentrations from the bottom of the lake towards the oxycline was accompanied by increasing $\delta^{13}C$ values of methane ($\delta^{13}C$-CH_4) from around -81‰ near the water-sediment interface to up to -68‰ near the oxycline (see Fig. 5.3). In contrast, during the last sampling campaign in December, $\delta^{13}C$ values were constant through the whole anoxic water column (-79.8 ± 0.5‰) and shifts to less negative values of $\delta^{13}C$ in methane were only detected in the oxic water column, above a water depth of 17 m.

During oxic conditions throughout the lake in April, nitrate concentrations did not show any significant changes with water depth (0.125-0.137 mmolL^{-1}), and an average nitrate concentration of 0.13 mmol L^{-1} was observed (Fig. 5.2). The isotopic composition of NO_3^- was also relatively constant ($\delta^{15}N$: 5.8-6.8‰, $\delta^{18}O$: 0.8-2.4‰) with an average of 6.3‰ for $\delta^{15}N$ and 1.5‰ for $\delta^{18}O$ in April of 2018 (Fig. 5.3).

In the following months in the anoxic zone of the water column, nitrate concentrations declined from near the oxycline to the lake bottom. In samples obtained in August, nitrate concentrations were below detection at a water depth below 18 m, whereas from August to December the "nitrate-free zone" in the water column increased from the lake bottom to a water depth near 14 m. Nitrite concentrations slightly above the detection limit of 6 µmol L^{-1} were

observed between August and October at a lake water depth between 10 m and 13 m.

As nitrate concentrations decreased with increasing water depth, ^{15}N and ^{18}O became progressively enriched in the remaining nitrate in samples collected between May and July. $\delta^{15}N$ of nitrate increased from on average 6.3‰ to 18.7‰ and $\delta^{18}O$ of nitrate increased from 1.5‰ to 8.4‰ providing evidence of denitrification.

Therefore, the anoxic zone below the oxycline was characterized by a decrease in methane concentrations coupled with an increase in $\delta^{13}C\text{-}CH_4$ from the lake bottom upwards, whereas nitrate concentrations simultaneously decreased from the oxycline downwards towards the lake sediments while $\delta^{15}N\text{-}NO_3^-$ and $\delta^{18}O\text{-}NO_3^-$ increased across this nitrate-methane transition zone (NMTZ).

At the beginning of the stratification period in May, the NMTZ was located close to the lake bottom between a water depth of 18 and 21 m. Following the displacement of the thermocline (highlighted red in Fig. 5.2) in the following months, the NMTZ moved upwards and was located between 14 and 18 m depth in July. At the end of the stratification period in October, the NMTZ was located between 12 and 15 m depth. At that time, nitrate concentrations in the oxic water column were significantly lower than in spring (0.043 versus 0.15 mmol L^{-1}).

5.1.3 Depth-profiles of concentrations and isotopic compositions of sulfate and hydrogen sulfide

Following the sequence of redox reactions with respect to expected free-energy yields in the water column, bacterial sulfate reduction (BSR) usually occurs after oxygen, nitrate, and microbial iron reduction. Once nitrate was removed completely from the water column near the lake sediments in July, a decrease in sulfate concentrations from 0.10 to 0.06 mmol L^{-1} at 18 to 21 m depth was observed (Fig. 5.2). In October and December, we detected hydrogen sulfide (H_2S) in the water column with concentrations decreasing from the lake sediments toward the oxycline, while sulfate concentrations were decreasing with increasing depth. From 17 to 22 m we observed a decrease in SO_4^{2-}concentrations from 0.10 to 0.03 mmol L^{-1} and simultaneously hydrogen sulfide concentrations up to 0.07 mmol L^{-1} were detected near the lake bottom. These concentrations are consistent with the expected amount of hydrogen sulfide to be produced by BSR in the water column of lake Fohnsee based on the complete reduction of SO_4^{2-} to H_2S. Further evidence of BSR was provided by a trend of increasing $\delta^{34}S$ values of sulfate accompanied by decreasing sulfate concentrations. The $\delta^{34}S$ value of sulfate in the oxic water column was ~2.7‰ at a water depth of 4 m and increased to ~48‰ in the water column near the lake sediments (Fig. 5.3), suggesting the existence of a bacterial sulfate reduction zone (BSRZ) below the NMTZ from July to December 2018.

Between July and October 2018 we observed above the BSRZ the development of a redox zone where the decrease in nitrate concentrations was accompanied with a marked increase of $\delta^{15}N$ and $\delta^{18}O$ values of nitrate, while $\delta^{13}C$ of methane and DOC concentrations remained constant. We postulate that this

redox zone may be a chemolithotrophic denitrification zone (CDZ) where H_2S potentially acts as an electron donor for the reduction of nitrate.

5.1.4 Redox zonation in the lake water column

Analysis of geochemical and isotopic parameters revealed the development of four distinctive redox zones within the water column of lake Fohnsee between July and October. The presence and vertical extension of these zones varied seasonally and showed the following sequence, from lake surface to the bottom as shown in Figs. 5.2 and 5.3:

1. An oxic zone with constant nitrate and sulfate concentrations and constant $\delta^{15}N$ and $\delta^{18}O$ of nitrate and $\delta^{34}S$ and $\delta^{18}O$ of sulfate;
2. A nitrate-methane transition zone (NMTZ), i.e. an anoxic zone characterized by a trend of decreasing methane concentrations coupled with an increase in $\delta^{13}C\text{-}CH_4$ upwards towards the oxycline, whereas nitrate concentrations simultaneously decreased from the oxycline downwards while $\delta^{15}N\text{-}NO_3^-$ and $\delta^{18}O\text{-}NO_3^-$ increased;
3. A potential denitrification zone with a different electron donor than methane (DZ), i.e. an anoxic zone with decreasing nitrate concentrations and increasing $\delta^{15}N$ and $\delta^{18}O$ of nitrate while $\delta^{13}C$ values of methane remained constant;
4. A bacterial sulfate reduction zone (BSRZ), i.e. an anoxic zone with nitrate concentrations below the detection limit, constant $\delta^{13}C$ of methane, decreasing sulfate concentrations and increasing $\delta^{34}S$ and $\delta^{18}O$ values of sulfate with depth, accompanied by occurrence of sulfide in low concentrations.

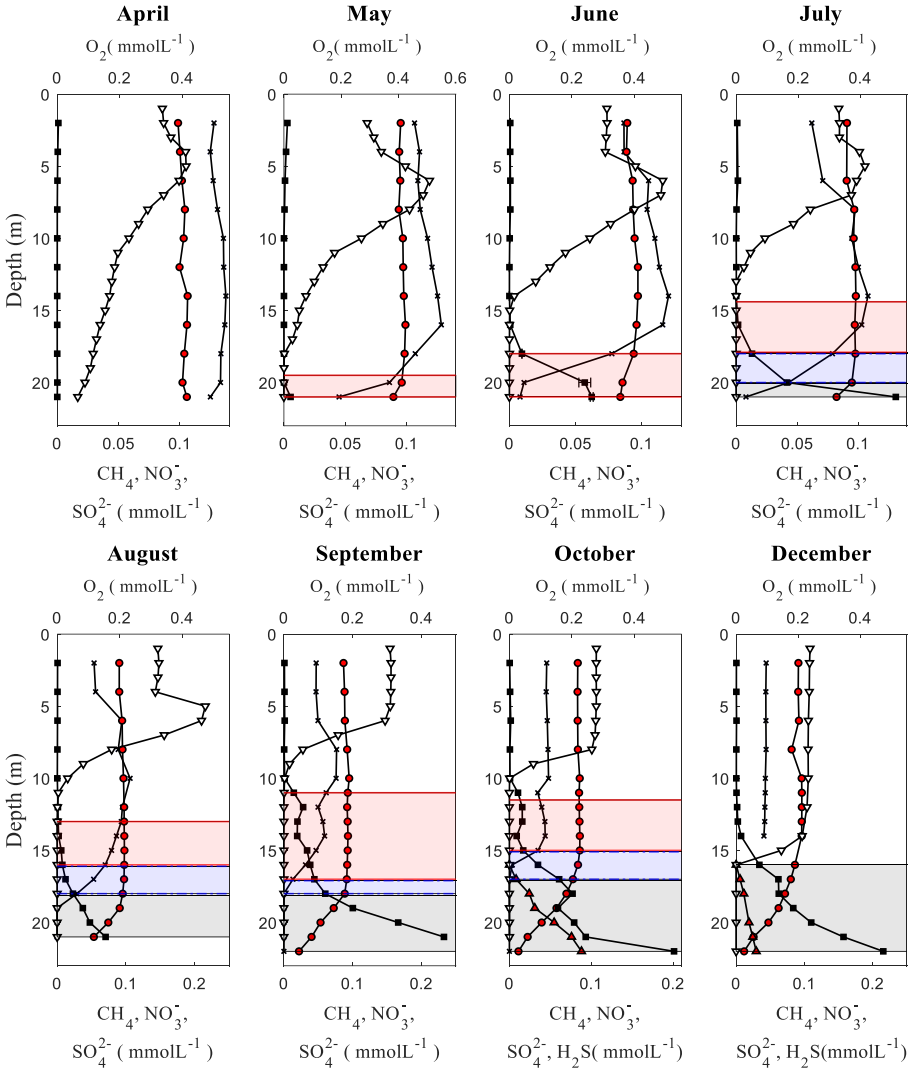

Figure 5. 2 Depth profiles of oxygen (downward-pointing triangles), nitrate (crosses), sulfate (circles), methane (squares) and hydrogen sulfide (upward-pointing triangles) concentration in lake water, measured from April to December 2018. Red areas: nitrate-methane transition zone (NMTZ), blue areas: denitrification zone (CZ), grey areas: bacterial sulphate reduction zone (BSRZ).

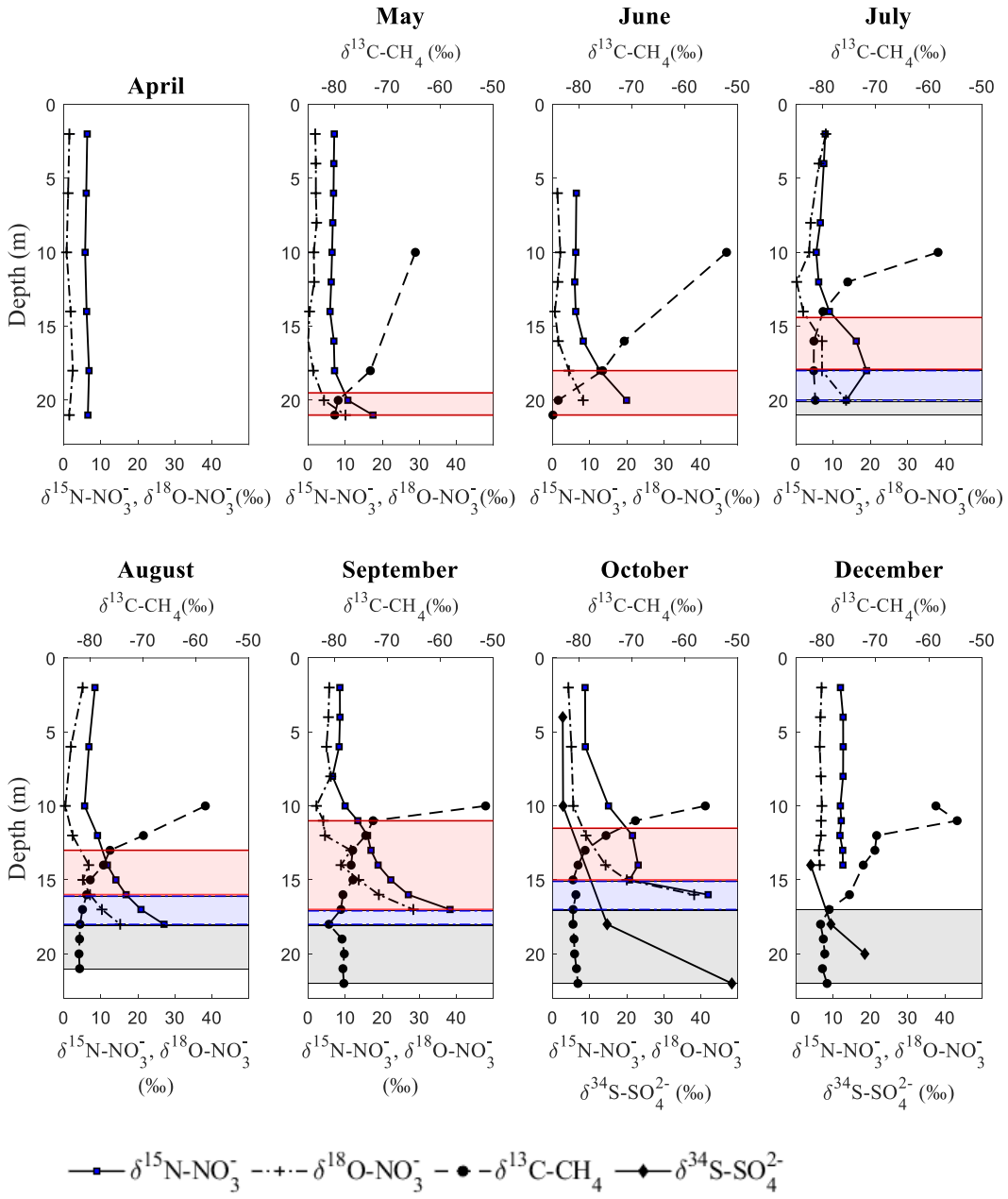

Figure 5. 3 Depth profiles of δ¹³C-CH₄ (circles), δ¹⁵N-NO₃⁻ (plus signs), and δ¹⁸O-NO₃⁻ (squares). Red areas: nitrate-methane transition zone (NMTZ), blue areas: denitrification zone (DZ), gray areas: bacterial sulfate reduction zone (BSRZ).

5.2 DISCUSSION

5.2.1 Aerobic methane oxidation and anaerobic oxidation of methane coupled to denitrification

During stratified conditions at lake Fohnsee, the flux of dissolved oxygen across the density gradient in the water column was limited. Thus, the oxygen consumed below the thermocline cannot be replenished and consequently, dissolved oxygen decreased below detection in the hypolimnion from May to September 2018.

Very low $\delta^{13}C$ values of methane around -81‰ were observed in the water column near the lake sediments from May to December 2018. This provides evidence that methane is formed by methanogenesis (Conrad, 2005) in the anoxic lake sediments of lake Fohnsee, from where it diffuses upwards towards the chemocline.

The decrease of dissolved oxygen contents below the chemocline in the hypolimnion, thermodynamically favors the microbial reduction of nitrate. Therefore, the presence of both methane and nitrate under anoxic conditions suggests favorable conditions for anaerobic oxidation of methane linked with denitrification (Deutzmann et al., 2014), as also suggested in other studies performed in stratified lakes and freshwater reservoirs (Roland et al., 2017; Naqvi et al., 2018; Einsiedl et al., 2020).

Lake water samples collected from May to October with a 1 m depth-resolution revealed a nitrate-methane transition zone (NMTZ) in the anoxic water column. In the NMTZ concentrations of methane decreased from the lake sediments to the chemocline, while the $\delta^{13}C$ values of methane increased providing evidence for microbial methane oxidation. During this process, 12C is preferentially converted to CO_2 causing a progressive enrichment of ^{13}C in

the remaining methane (Segarra et al., 2015). Therefore, the observed vertical depth-profiles of $\delta^{13}C$ and CH_4 concentrations in the absence of dissolved O_2 strongly suggest microbially driven methane oxidation under anoxic conditions within a zone located 2 to 4 m below the oxycline (Fig. 2) between May and October.

The calculation of one single apparent carbon isotope enrichment factor (ε_{app}) for methane oxidation in the entire water column using the Rayleigh equation (closed-system approach) did not yield a satisfactory results ($R^2 < 0.4$). Therefore, we pursued these calculations for three separate zones: (i) methane oxidation under aerobic conditions, (ii) methane oxidation under anaerobic conditions and where denitrification occurs simultaneously, and (iii) a third zone at a lake water depth where nitrate was no longer detected (below 17 m). The results yielded a better correlation ($R^2 > 0.6$, Fig. 4), providing further evidence for methane oxidation that proceeded in the aerobic zone with an apparent carbon isotope enrichment factor of -6.8‰, while methane oxidation in the NMTZ occurred with a lower apparent carbon isotope enrichment factor of -4.3‰ (Fig. 5.4). There was no evidence for methane oxidation in the redox zone below the NMTZ.

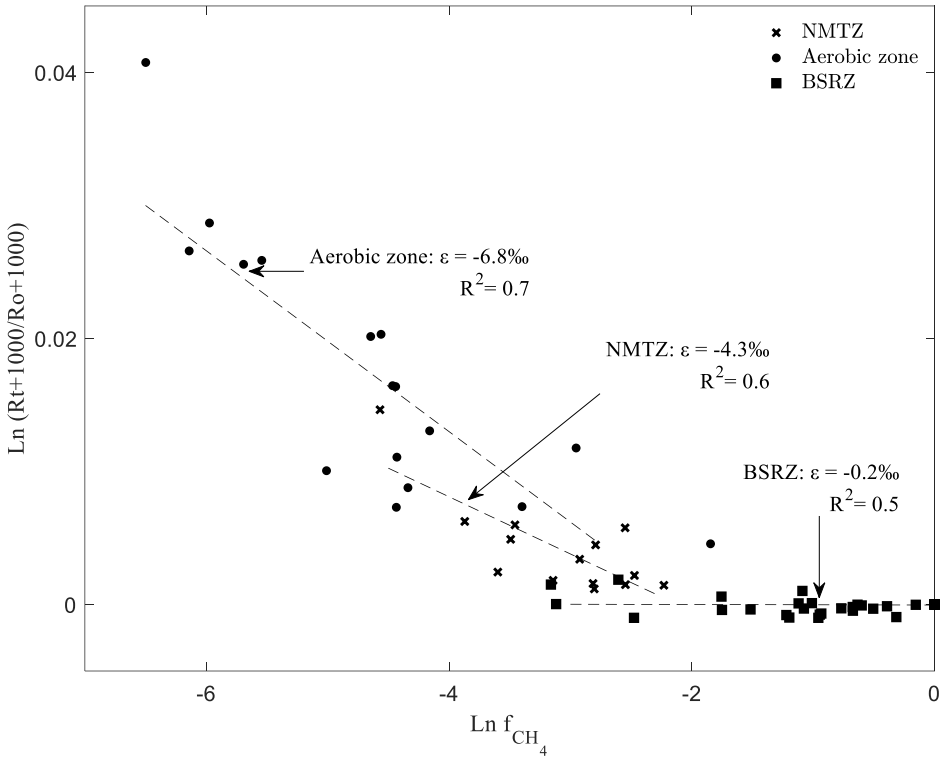

Figure 5. 4 Calculation of apparent carbon isotope enrichment factors ε for methane (closed-system approach) observed in three different zones between May and October 2018. Linear regressions (slope ε) were determined independently for three different redox zones, i.e. the aerobic zone, the Nitrate-Methane Transition Zone (NMTZ), and the Bacterial Sulfate Reduction Zone (BSRZ).

The dual isotope plot (2D plot) of $\delta^{18}O$ vs. $\delta^{15}N$ of nitrate with a slope of 0.89 (see supplementary material Fig.A1) revealed the occurrence of denitrification in the NMTZ where anaerobic oxidation of methane was observed. It is, however, difficult to quantitatively distinguish AOM coupled with denitrification from aerobic methane oxidation based solely on aqueous chemistry and stable isotope data, since it may be possible that denitrification is coupled to common heterotrophic nitrate reduction, while methane oxidation may be caused by trace amounts of oxygen in suboxic waters, as reported for lake Lugano (Blees et al., 2014). Therefore, inverse numerical modeling of reactive transport was pursued to obtain flux estimates for

dissolved oxygen and assess methane oxidation rates under oxic and anoxic conditions for the water column of lake Fohnsee.

5.2.2 Fluxes of oxygen and inverse modeling of methane concentration profiles to evaluate anaerobic and aerobic oxidation of methane rates at the chemocline

We simulated oxygen fluxes from the lake water surface through the oxycline towards the lake bottom, together with methane fluxes. The zone directly below the oxycline represents the consumption zone of methane, oxygen and nitrate, where trace amounts of dissolved oxygen below the detection limit (< 0.3 μmol L^{-1}) may occur. Figures 5.5a, b show the simulated fluxes of oxygen and methane determined by the model. Modeled DO concentrations show a zone below the oxycline where oxygen was still present at concentrations below the detection limit in the water column of lake Fohnsee (Fig. 5.5a). These trace amounts of DO were not detected in-situ during the sampling campaigns as a result of the detection limit of the utilized oxygen sensor.

As a result of these observations, the transition from aerobic to anaerobic oxidation of methane in the model was assumed to occur at <10% contribution of oxygen flux to the observed methane oxidation with the remainder of the CH_4 oxidation being caused by AOM. Figure 5c shows the electron balance for aerobic methane oxidation assuming complete oxidation of CH_4 to CO_2, and reveals that the boundary between oxic and anoxic conditions based on the modeling calculations has shifted deeper in the water column by on average 1.81 m.

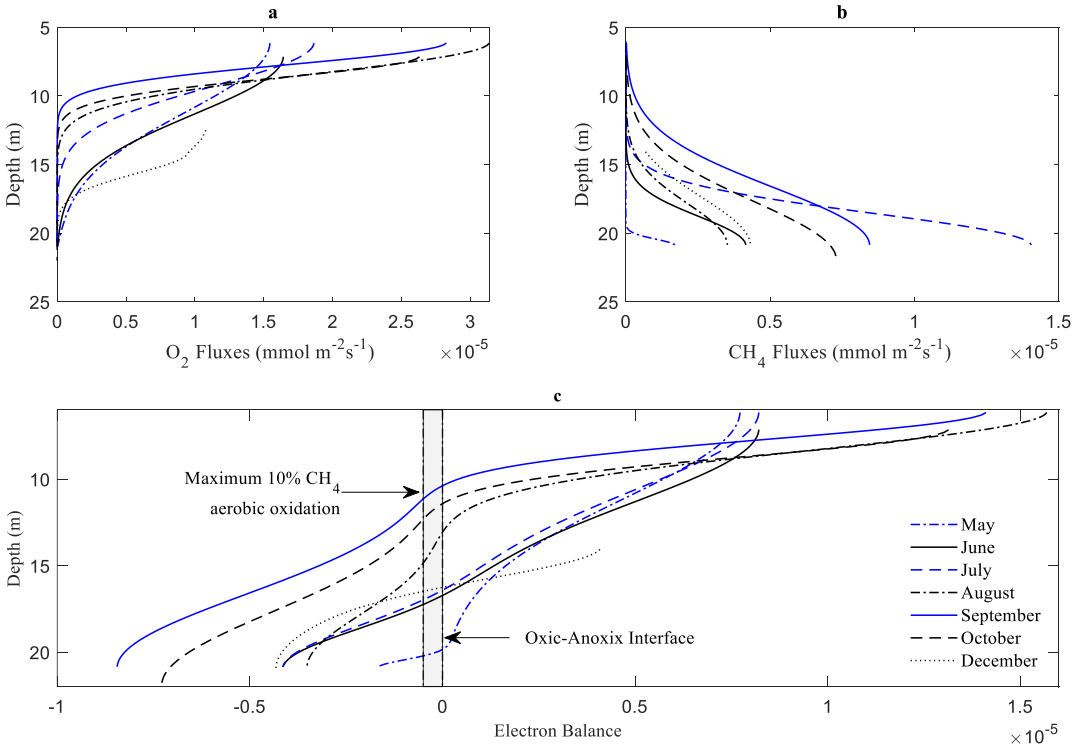

Figure 5. 5 Simulated fluxes of dissolved oxygen (a), fluxes of methane (b) and resulting electron balance assuming complete oxidation of CH_4 to CO_2 using O_2 as electron acceptor (c) in the water column of lake Fohnsee (May to December 2018). The shadowed area in panel (c) represents the oxic-anoxic interface; left of this area, anoxic conditions prevail if "anoxic" is defined as <10% contribution of oxygen fluxes to methane oxidation.

Simulation results shown in Fig. 5 indicate that oxygen influx from the top through the oxycline cannot account for all the oxidation of methane so that non-zero methane fluxes occur above the oxycline in the oxic zone. Therefore, depths where the electron balance is lower than zero (0) in Fig. 5.5c represent the zone where oxidation of methane observed in the water column must be controlled by an electron acceptor different from oxygen. The potential AOM zone is located during May very close to the lake sediments from 20 to 21 m depth, while in September the zone where AOM may occur extends from around 10 to 21 m depth.

To further investigate the occurrence of AOM, we developed a more realistic model that considers diffusive transport, and both aerobic and anaerobic oxidation of methane for ^{12}C and ^{13}C. The model was calibrated against observed methane concentrations using the first-order rate constants (k_{ae} and k_{an}) as fitting parameter. Modeling results are shown in Fig. 5.6. Fitted first order degradation constants and statistical evaluation of the model curve fits for methane concentrations vs. depth shown in Fig. 5.6 and are provided in supplementary materials Table A2.

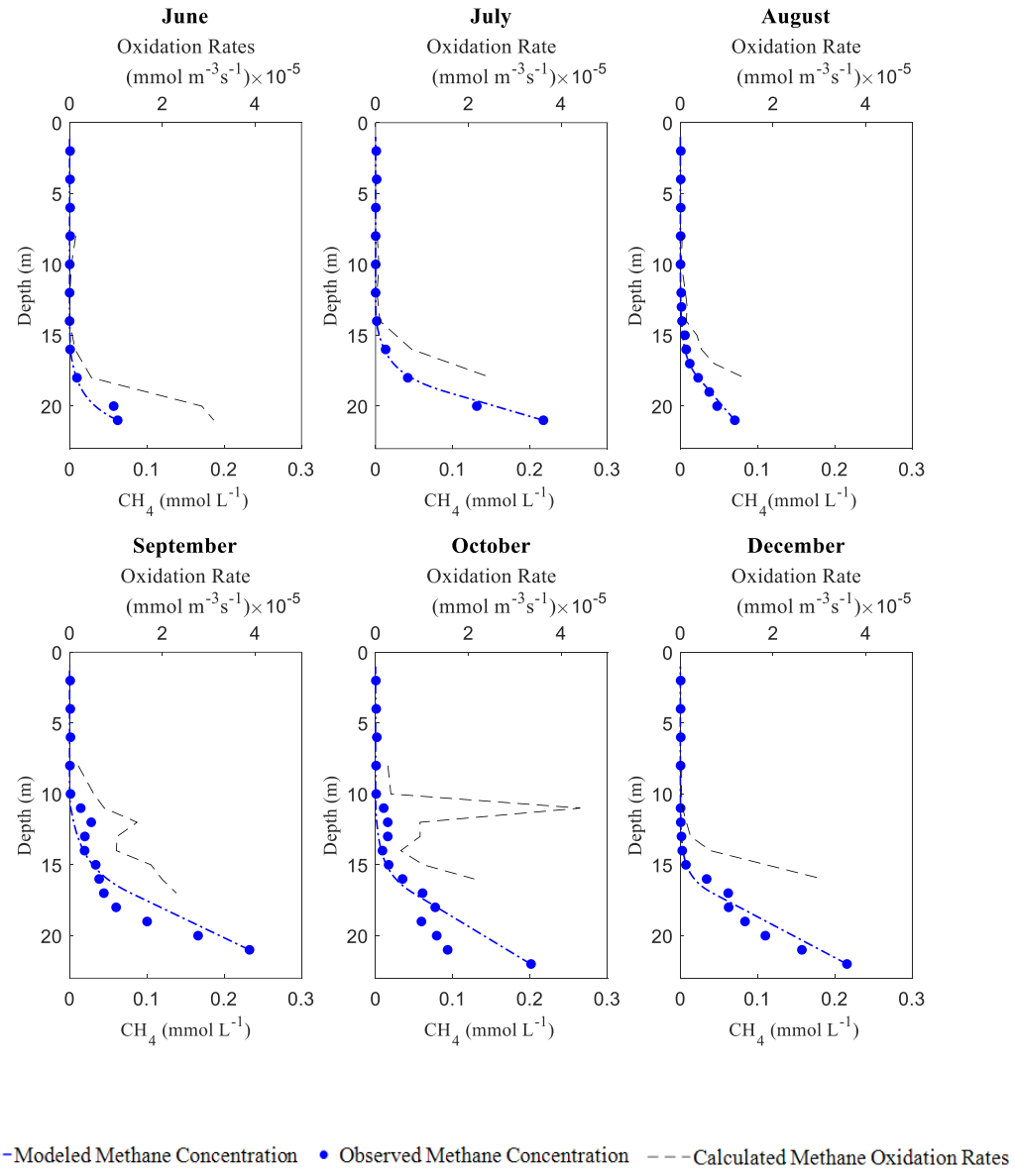

Figure 5. 6 Measured blue dots) versus simulated (blue lines) methane concentrations (CH_4) and methane oxidation rates versus depth. The oxidation rate was calculated as measured methane concentration multiplied by first-order degradation constant.

Initial numerical simulations that were performed assuming only aerobic methane oxidation did not describe satisfactorily the observed vertical variations of methane concentrations except for December 2018. In December 2018, there was no isotopic evidence of microbial nitrate reduction or microbial methane oxidation in the anoxic water column. Therefore, it appears that only aerobic methane oxidation occurred, and no anaerobic oxidation of methane

was observed as confirmed by the numerical simulations (k_{ae} of 1.9 x 10^{-6} s^{-1} and k_{an} of zero for December 2018 (supplementary materials Tab. A2). Only models including microbial oxidation of CH_4 in the oxic and anoxic water column describe satisfactorily the methane concentration profiles (Fig.5.6). Therefore, anaerobic oxidation of methane linked with denitrification must have taken place and is revealed as a key process removing methane, consistent with the chemical and isotopic data presented in Figs. 5.7 and 5.8.

5.2.3 Seasonal dynamics of aerobic and anaerobic methane oxidation in the water column

By multiplying with methane concentrations, degradation rate constants k_{an} and k_{ae} were converted into in-situ methane oxidation rates. These rates were on average, $2.1*10^{-6}$ mmol m^{-3} s^{-1} and $1.2*10^{-5}$ mmol m^{-3} s^{-1} for aerobic and anaerobic oxidation of methane, respectively. Highest AOM rates were observed in June 2018 ($3.1*10^{-5}$ mmol $m^{-3}s^{-1}$), while the highest rates of aerobic methane oxidation were observed in October 2018 ($4.4*10^{-5}$ mmol $m^{-3}s^{-1}$). It was found that the oxygen flux diffusing through the oxycline was insufficient to explain the methane oxidation rates observed in the anoxic water column, thereby providing further evidence of anaerobic oxidation of methane. Nitrate availability in the water column was sufficient to maintain AOM. The AOM rate of $1.2*10^{-5}$ mmol $m^{-3}s^{-1}$ translates into an average nitrate consumption rate in the water column of $2.2*10^{-5}$ mmol $m^{-3}s^{-1}$, or a total consumption of 0.056 mmol L^{-1} during a 30-day period assuming complete denitrification ($5CH_4 + 8NO_3^- + 8H^+ \rightarrow 5CO_2 + 4N_2 + 14H_2O$) and insignificant diffusive exchange with surrounding waters. Fluxes calculated for nitrate are sufficient for sustaining AOM in the nitrate-methane transition zone (NMTZ) as it is shown in Fig A2.

Seasonal changes of the redox potential in the water column had an effect on the vertical location of the nitrate-methane transition zone and, therefore, on the methane oxidation rates (Fig. 5.6). Aerobic and anaerobic microbial oxidation of methane rates in the water column vary during the year (Fig. 5.7) and thus their relative contributions as a methane sink also varies seasonally. Using the aerobic and anaerobic microbial oxidation of methane rates, the monthly total methane consumption was calculated from consumption rates integrated over the whole depth of the water column. Figure 5.7 reveals the relative consumption of methane due to aerobic and anaerobic oxidation of methane for April to December 2018. In April and December, we found exclusively aerobic methane oxidation in the water column. In May and October, we observed some AOM although aerobic methane oxidation still dominated. Between June and September, however, isotopic, chemical, and modeling results suggest that AOM is the major sink of methane in the water column of lake Fohnsee.

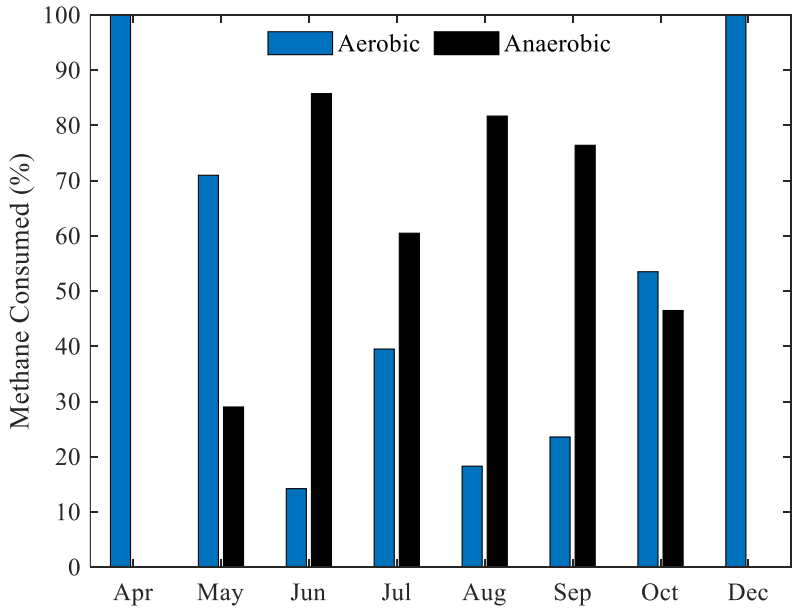

Figure 5. 7 Seasonal changes on the consumption of methane in the water column

5.2.4 Modeling of stable isotope ratios of methane ($\delta^{13}C$) to determine intrinsic carbon isotope enrichment factors for aerobic and anaerobic methane oxidation

Enrichment factors calculated with a closed-system model do not necessary exemplify the intrinsic isotope fractionation generated by microbial processes at field conditions. Therefore, we applied the carbon isotope specific diffusion-reaction model to determine apparent carbon isotope enrichment factors for aerobic (ε_{ae}) and anaerobic (ε_{an}) oxidation of methane described by Eqs. 25 and 26, and used the calibrated degradation rate constants (k_{ae} and k_{an}). Modeled $\delta^{13}C$ of methane is compared to measured values in Fig. 5.8 Data on the statistical evaluation of curve fits and fitted carbon isotope enrichment factors are presented in Table 2. Simulations combining aerobic and anaerobic oxidation of methane near the oxycline were able to explain the $\delta^{13}C$ observations with good to satisfactory curve fits. Additional simulations were performed using the assumptions (i) that only diffusion of methane through

the water column controls methane concentrations (absence of methane oxidation (Fig. 5.8c) and (ii) that only aerobic methane oxidation occurred (Fig. 5.8b). Most of these additional simulations were not capable of describing the observed $\delta^{13}C$ values for methane, except for December 2018, where no anaerobic oxidation of methane was observed (Fig. 8b).

Table 2 Fitted carbon isotope enrichment factors for aerobic (εae) and anaerobic (εan) methane oxidation (obtained from inverse modeling, solving Eq. 8 and 9) and statistical evaluation of the model curve fits for $\delta^{13}C$ of methane vs. depth presented in Fig. 5.9. MSE: standard error of the mean

Month	ε_{ae} **(‰)**	ε_{an} **(‰)**	***Normalized MSE (-)***	***MSE (‰)***
May				
	-18	-22	0.95	0.10
June	-22	-22	0.97	0.30
July	-22	-17	0.94	0.57
August	-26	-18	0.92	0.17
September	-26	-18	0.82	0.32
October	-24	-17	0.94	0.14
December	-22	none	0.82	0.90

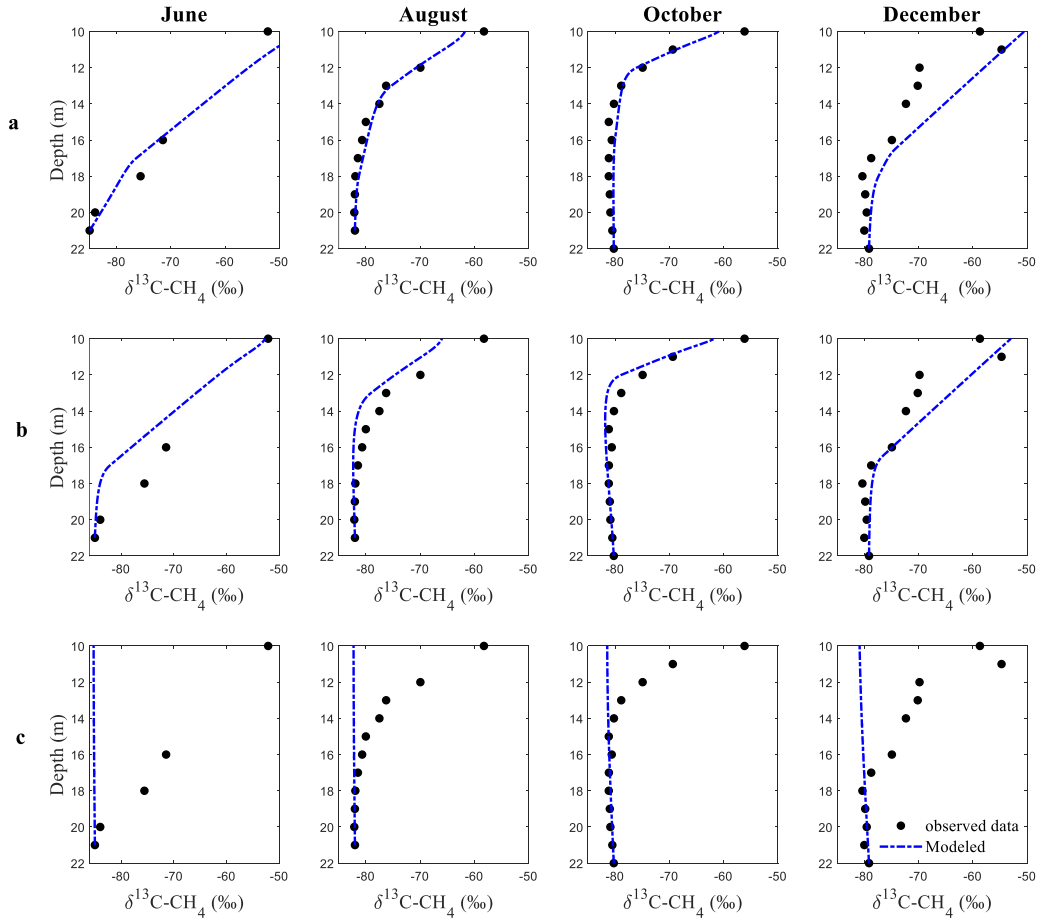

Figure 5. 8 Measured (dots) versus modeled (lines) δ¹³C of methane as a function of water column depth for selected observation months. a) Aerobic and anaerobic methane oxidation, b) aerobic methane oxidation, c) no methane oxidation (diffusion-controlled methane transport, only were considered in the model calculations. Results for May, July, and September 2018 can be found in Supplementary Information Table. A4.

Diffusion-reaction modeling of δ¹³C of methane in lake Fohnsee resulted in carbon isotope enrichment factors of -18‰ to -26‰ (mean: -22.8‰) for aerobic methane oxidation and -18‰ to -22 ‰ (mean: -19.3‰) for anaerobic oxidation of methane (Tab. 2). Although these values are within the range found for AOM in enrichment cultures (ranging from -12‰ to -39‰) (Holler et al., 2009; Feisthauer et al., 2011), they are markedly more negative than the calculated apparent enrichment factors shown in Fig. 5.4. Modeling results of other

studies suggest that diffusion can significantly mask stable isotope effects generated by microbial activity in diffusion-dominated systems, as observed in experiments performed by De Visscher (2004) and modeling studies of Mahieu et al., (2008) and Lehmann et al., (2003). Thus, apparent enrichment factors calculated using a Rayleigh equation are considerable lower than ε_{an} and ε_{ae} determined by the diffusion-reaction model.

Finally, we carried out additional numerical simulations with a wide range of reported literature values (Rudd et al., 1974; Harrits and Hanson, 1980; Rudd, 1980; Griffiths et al., 1982; Iversen et al., 1987; Carini et al., 2005; Schubert et al., 2010; Lopes et al., 2011; Blees et al., 2014) for carbon isotope enrichment factors for aerobic microbial methane oxidation, in order to test whether the $\delta^{13}C$ of methane observed in the anoxic water column can be explained by carbon isotope fractionation solely induced by aerobic methane oxidation in the oxic water column. Our modeling results showed that none of these simulations could satisfactorily reproduce $\delta^{13}C$ of methane in the anaerobic water column (see supplementary materials Fig A5). Therefore, anaerobic oxidation of methane coupled with denitrification is the most plausible explanation for the measured $\delta^{13}C$ values of methane in the water column of lake Fohnsee.

5.2.5 Bacterial sulfate reduction and chemolithotrophic denitrification

Following redox reactions in the water column based on the order of decreasing free-energy, bacterial sulfate reduction (BSR) is expected to occur after oxygen, nitrate and Fe(III) have been completely reduced. BSR occurred below the NMTZ at lake Fohnsee as evidenced by a decrease in SO_4^{2-} concentrations from 0.09 $mmolL^{-1}$ to 0.01$mmolL^{-1}$ accompanied by a significant ^{34}S enrichment in the remaining sulfate (Fig. 5.3) and the detection of H_2S (Fig. 5.2). Between the bacterial sulfate reduction (BSR) zone and the

NMTZ, a decrease in nitrate concentrations was observed accompanied by a marked increase in $\delta^{15}N$ and $\delta^{18}O$ in the remaining nitrate. Here we speculate that H_2S diffuses from the BSR zone toward the oxycline and acts as an electron donor for the reduction of nitrate by chemolithotrophic denitrification. H_2S has been shown to act as electron acceptor for the reduction of NO_3^- in several water column studies (Brettar and Rheinheimer, 1991; Jensen et al., 2009; Lavik et al., 2009; Canfield et al., 2010). Sulfide-dependent denitrification has also been proven to co-occur with heterotrophic denitrification in stratified lakes (Zhu et al., 2018) and in some cases, it has been determined to be a dominant fixed-N elimination pathway (Wenk et al., 2013).

5.2.6 Short summary

While aerobic methane oxidation in seasonally stratified lakes is well documented in the literature, knowledge about AOM linked with denitrification and its relevance in methane removal in aquatic ecosystems on the continents is sparse. Chemical and isotopic data from seasonally stratified lake Fohnsee located in Southern Germany indicate a zone within the water column where both denitrification and methane oxidation have occurred simultaneously. A newly developed diffusion-reaction model provided evidence that both aerobic and anaerobic methane oxidation coupled with nitrate reduction occur near the chemocline of lake Fohnsee in the summer months from June to September. Aerobic oxidation of methane was the process responsible for all methane oxidation observed in the water column in April and December and was responsible for 72% of methane consumption in May. In the summer months between June and September, AOM coupled with denitrification accounted for 70% of methane consumption. Therefore, aqueous geochemistry and stable isotope data combined with modeling results revealed that AOM coupled with denitrification is an important and

previously overlooked process that contributes significantly to the removal of nitrate and methane from the seasonal stratified lake Fohnsee.

Chapter 6: SEASONAL DYNAMICS OF ANAEROBIC OXIDATION OF AMMONIUM AND DENITRIFICATION IN A DIMICTIC LAKE DURING THE STRATIFIED SPRING-SUMMER PERIOD

6.1 RESULTS

6.1.1 Water column stratification and its influence on the redox zonation

Previous field investigations using stable water isotope compositions have shown that Fohnsee is almost exclusively fed by groundwater, which has a strong effect on its mixing type (Braig et al., 2010). Renewal of DO in the water column is therefore accomplished due to wind-induced mixing and diffusion. However, marked increases in the temperatures of the near-surface layers during spring result in a sharp density gradient between the warm epilimnion and the cold hypolimnion, which acts as a barrier against wind-mixing between April and the end of September. As a result, oxygen replenishment from the atmosphere depends almost exclusively on diffusion of DO across the thermocline (Fig. 6.1).

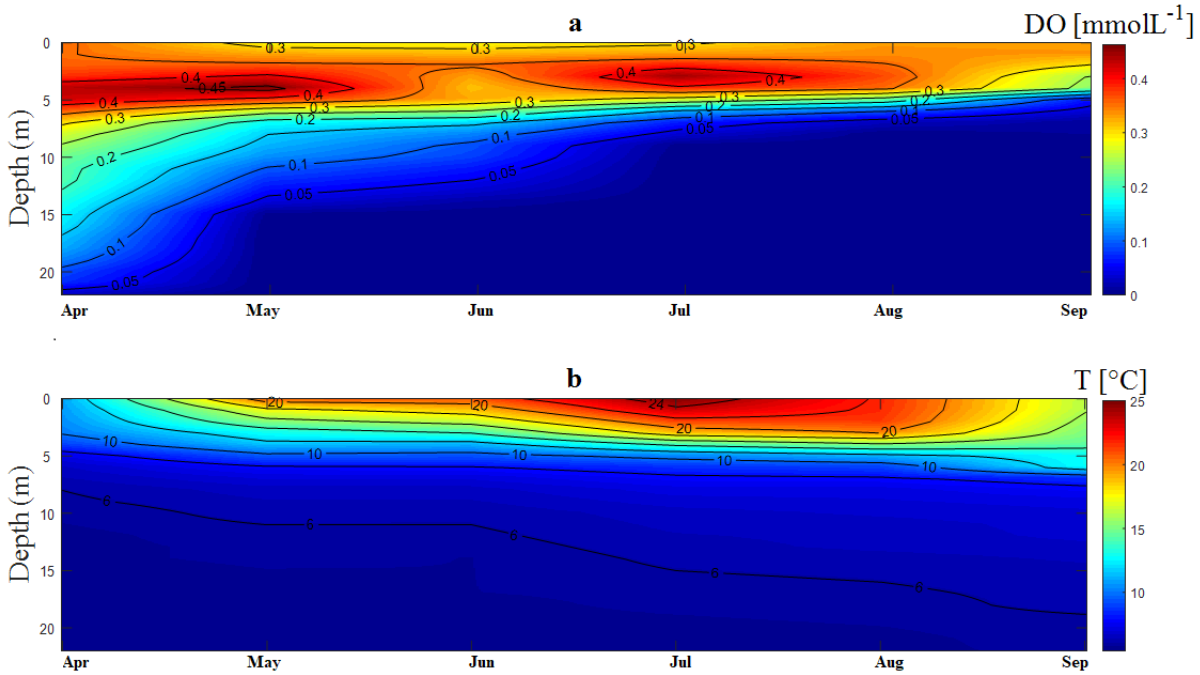

Figure 6. 1 Temperature and dissolved oxygen development from April to September in the water column of Fohnsee

In addition, a vertical downwards flux of organic matter due to spring algal blooms further increases the dissolved oxygen demand in the hypolimnion and may facilitate elevated rates of benthic bacterial sulfate reduction causing a release of sulfide to the overlying water column in late summer (Callbeck et al., 2021). The DO consumption rate in deeper layers of the lake is higher than the rate at which oxygen is renewed in the hypolimnion by diffusion, thus, significant depletion of DO occurs during the summer period. In May, strictly anoxic conditions (DO < 0.3 µmolL^{-1}) were observed below 19 m depth with a constant water temperature of 5.5°C (Fig. 6.1). Subsequently, the strictly anoxic zone expanded upwards in the water column increasing towards a depth of 9.5 m in September. DO concentrations at the lake surface were constantly around 0.3 mmol L^{-1} with maximum concentrations of 0.42 mmol L^{-1} found immediately below the thermocline indicating that the epilimnion remained oxic throughout the observation period.

6.1.2 Depths-profiles of NO_3^-, $SO42^-$ and stable isotope ratios of NO_3^-

At the beginning of the stratification period in April, constant concentrations of SO_4^{2-} and NO_3^- of ~0.1 mmol L^{-1} were observed throughout the entire water column, with the exception of the anoxic zone between 21 and 23 m depth, where nitrate concentrations decreased to around 0.06 mmol L^{-1} (Fig. 6.2a). $\delta^{15}N\text{-}NO_3^-$ and $\delta^{18}O\text{-}NO_3^-$ did not show any significant changes throughout the water column with average values of 7.0‰ and 2.6‰, respectively (Fig. 6.2a).

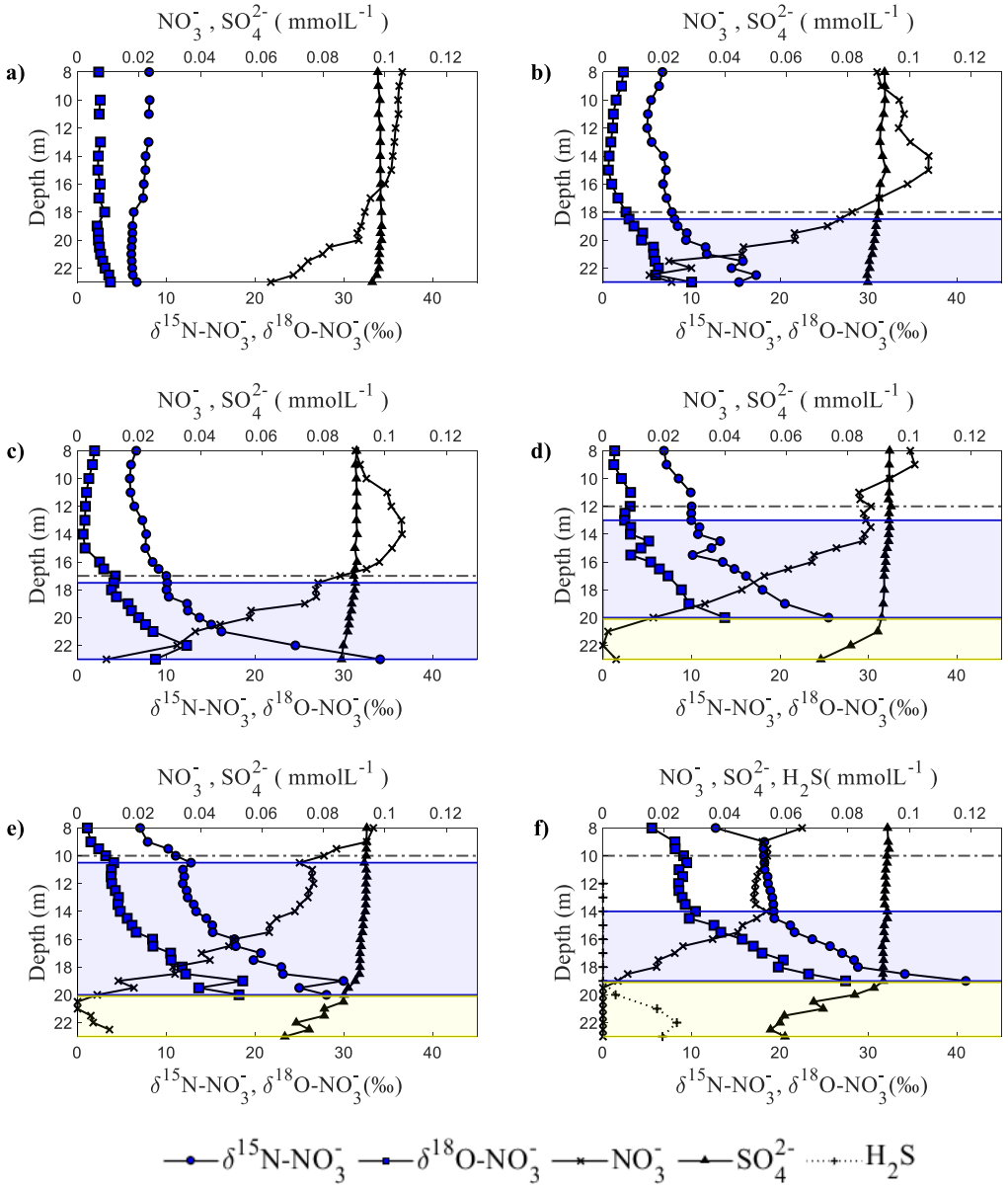

Figure 6. 2 Depth profiles of nitrate (crosses) and sulfate (triangles) concentrations, and δ¹⁵N (filled circles) and δ¹⁸O values (filled squares) of nitrate for April (a), June 5th (b), June 18th (c), July (d), August (e), September (f) 2019 at Fohnsee. Horizontal dashed lines represent the depth below which dissolved oxygen was below detection (< 0.3 µmol L⁻¹) and blue boxes highlight the potential denitrification zone below the oxycline based on isotope and chemical profiles. Light yellow boxes highlight the potential bacterial sulfate reduction

At the beginning of June, nitrate concentrations significantly decreased from 0.1 mmol L^{-1} at 17 m depth to 0.02 mmol L^{-1} at 23 m depth, while in the same zone $\delta^{15}N$ and $\delta^{18}O$ values increased from 7.2‰ to 15.4‰ and from 1.7‰ to 10.0‰, respectively (Fig. 6.2b). At the end of June, NO_3^- concentrations at 23 m depth declined to 0.01 mmol L^{-1}, while at the same time $\delta^{15}N$ and $\delta^{18}O$ values increased to 34.0‰ and 12.3‰ (22m), respectively (Fig. 6.2c). Sulfate concentrations during these months remained relatively constant.

In July, anoxic conditions were observed below 12m depth and nitrate concentrations decreased from 0.1 mmol L^{-1} at 12 m depth to concentrations below the detection limit at 21 m depth. The $\delta^{15}N$ value of NO_3^- at 21 m was 25.5‰ and the $\delta^{18}O$ value of NO_3^- was 13.8‰ (Fig. 6.2d). Measurement of the isotopic composition of nitrate below this depth was not possible due to the low NO_3^- concentrations. In July, sulfate concentrations remained constant around 0.1 mmol L^{-1} in the water column from the lake water surface to 21 m depth.

At the depths from 21 to 23 m where nitrate was completely reduced, and a decrease of SO_4^{2-} concentrations from 0.1 mmol L^{-1} to 0.071 mmol L^{-1} was observed (Fig. 6.2d).

During the following two months of August and September, NO_3^- concentrations continuously decreased in the hypolimnion while both $\delta^{15}N$-NO_3^- and $\delta^{18}O$-NO_3^- of the remaining nitrate progressively increased (Fig. 6.2e, f). During the final sampling campaign in September, a nitrate free zone was observed below 19 m depth. This depth coincided with the maximum $\delta^{15}N$-NO_3^- and $\delta^{18}O$-NO_3^- values of 41.0‰ and 27.4‰ respectively (Fig 6.2f). In the nitrate-free zone from 19 to 23m depth, sulfate concentrations decreased significantly from 0.09 mmol L^{-1} to 0.05 mmol L^{-1} at the lake bottom and H_2S was detected with a maximum concentration of 0.02 mmol L^{-1} observed at 23m depth (Fig 6.2f). This reveals that towards the end of the observation period, a

zone with bacterial (dissimilatory) sulfate reduction had been established in the lowest section of the water column, representing a different redox zonation pattern compared to spring.

At the beginning of the lake stratification period in June, the nitrate reduction zone was located close to the lake bottom between a water depth of 18 and 22 m. Following the upwards movement of the oxycline indicated by the dashed line in Fig. 6.2 in subsequent months, the zone where nitrate was reduced moved upwards reaching a depth between 13 and 20 m in July. At the end of the sampling period in September, the NO_3^- reduction zone was located between 14 and 19 m depth.

6.1.3 Concentrations and stable isotope composition of ammonium

At the beginning of the observation period in April, ammonium concentrations were highest near the lake bottom with 0.038 mmol L^{-1} accompanied by a $\delta^{15}N\text{-}NH_4^+$ value near 14‰. NH_4^+ concentrations decreased towards the lake surface to 0.012 mmolL^{-1} at 8m, while $\delta^{15}N\text{-}NH_4^+$ increased to 18‰ at a water depth of 20 m (Fig. 6.3a). Ammonium was below detection from 0 to 8 m depth.

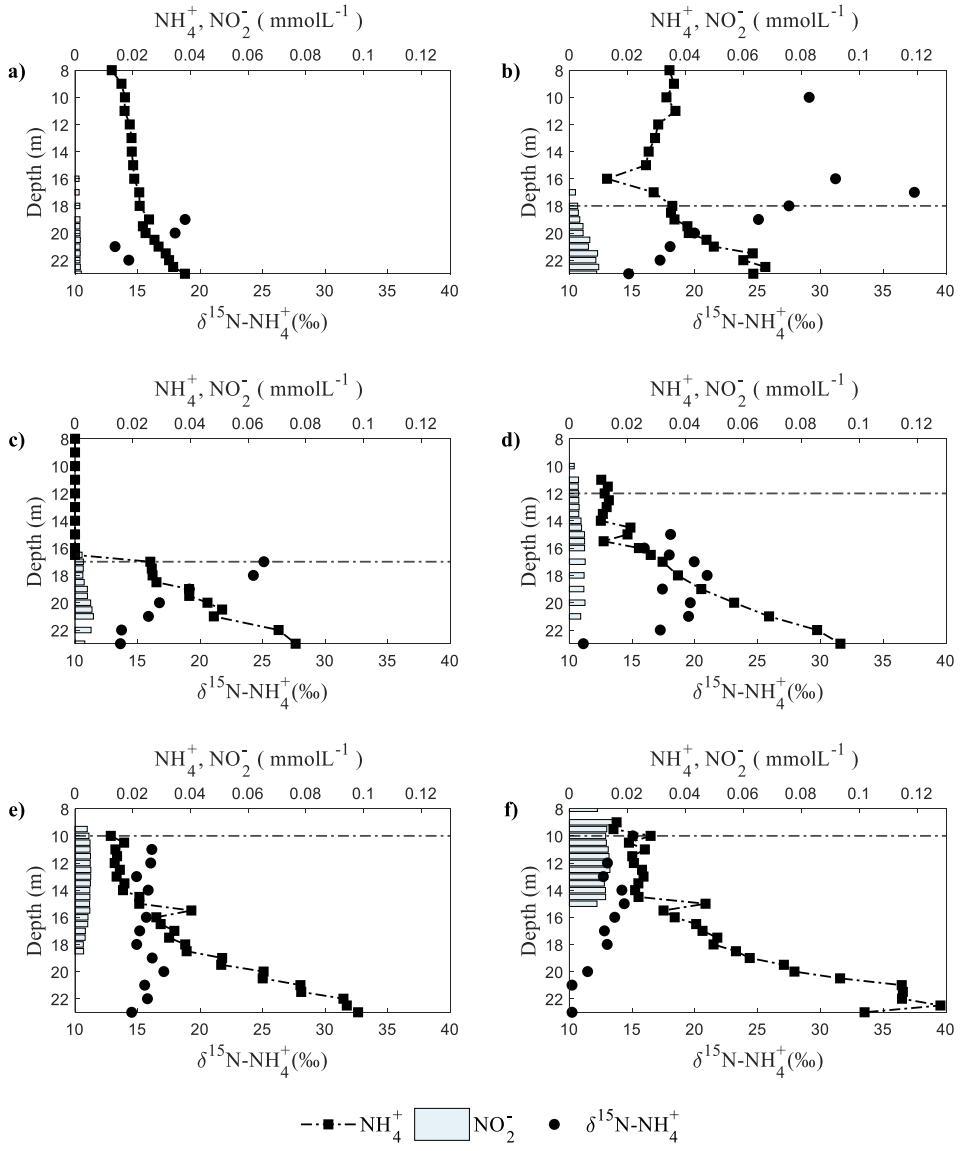

Figure 6. 3 *Depth profiles of ammonium (squares) and nitrite concentrations (bars), and δ¹⁵N values of ammonium (circles) for April (a), beginning of June (b), end of June (c), July (d), August (e), September (f) 2019 at Lake Fohnsee. The horizontal dashed line represents the depth below which dissolved oxygen was below detection (< 0.3 µmol L⁻¹)*

Figures 6.3b,c reveal that ammonium concentrations in June decreased from 0.063 mmol L^{-1} at the lake bottom (23m) to 0.035 mmol L^{-1} at the oxycline (18m). Simultaneously, $\delta^{15}N\text{-}NH_4^+$ increased from 14.7‰ at the lake bottom to 27.5‰ below the oxycline (18 m). $\delta^{15}N\text{-}NH_4^+$ values indicated that NH_4^+ in the

oxic zone was markedly enriched in ^{15}N with an average $\delta^{15}N\text{-}NH_4^+$ value of 37.3‰ (Fig. 6.3b) compared to ammonium found in the anoxic zone. From the end of June to September 2019, maximum ammonium concentrations at the lake bottom of around 0.085 $mmolL^{-1}$ were observed, which decreased towards the oxycline to concentrations below the detection limit (Fig. 6.3c-f). The decrease in ammonium concentrations from the lake bottom towards the oxic zone was accompanied by an increase in $\delta^{15}N\text{-}NH_4^+$ values of up to 12‰. The increase in $\delta^{15}N\text{-}NH_4^+$ that was observed in the anoxic zone of the water column was most pronounced at the end of June (13.6‰ at 23 m to 25.1 ‰ at 17 m depth) and least pronounced in September (10.2‰ at 23m to 15.1‰ at 10 m depth). In August, $\delta^{15}N\text{-}NH_4^+$ values remained constant throughout the hypolimnion with an average of 15.6‰, except for the water depth from 23m to 20m depth where ^{15}N of NH_4^+ varied by 3‰ (Fig. 6.3e). From June to September, the NH_4^+ concentration in the oxic zone was consistently below or very close to the detection limit and therefore measurement of $\delta^{15}N\text{-}NH_4^+$ values were not possible.

6.1.4 Quantitative PCR and microbial abundance for anammox and denitrifying bacteria

The number of bacterial 16S rRNA gene copies indicated that bacterial abundance in the water column remained relatively constant throughout the water column in depth and time, independent of changes in redox conditions. The copy numbers ranged in the magnitude of 10^7 copies mL^{-1}, except for some samples from 6 m, 10 m and 14 m depth, where the copy numbers were slightly reduced.

Both nitrite reductase genes, *nirK* and *nirS*, were identified in the water column (Fig. 6.4). In the oxic zones, bacteria harboring the *nirS* gene were less abundant than their counterpart carrying the *nirK* gene (Fig. 6.4a). In the

anoxic zones, both groups contributed equally to the overall abundance of nitrite reducers, which was mostly related to a significant increase of bacteria harboring the *nirS* gene. In the anoxic zone the abundance for *nirK* and *nirS* genes was for both genes in the range of 10^5 copies ml^{-1}. Overall the dynamics of nitrite reducers followed the dynamics of the oxycline over the season, resulting in an increase in the upper water layers from April to August. In August a significant increase of nitrite reducers was observed in 10 m depth whereas in April this increase was only detectable in 18 m. We did not observe any significant temporal or spatial changes in the number *hzsB* genes i.e. changes between the anoxic and oxic water column. Furthermore, the number of *hzsB gene* copies was considerably lower than *nirK* copies. In most of the analyzed samples, we observed only around 10^1 copies ml^{-1} or less of *hzsB* genes with exception of a sample taken in 14 m depth in September, and 14 m and 17 m in June, where the magnitude of number of gene copies was close to 10^2 copies ml^{-1}. Overall, anammox communities were in average 10^4 times less abundant than denitrifying communities.

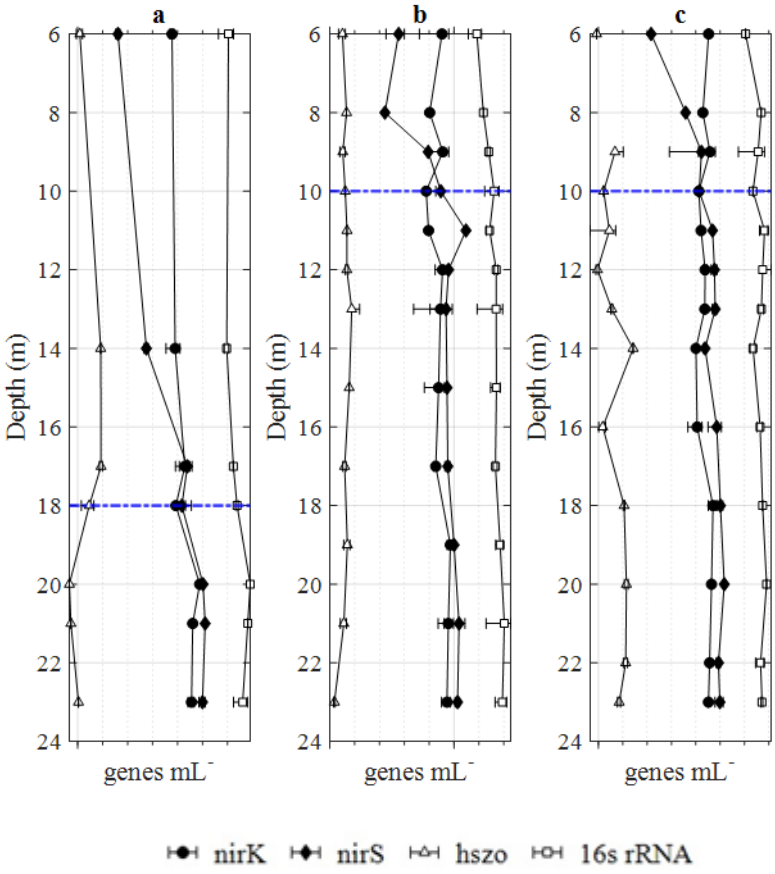

Figure 6. 4 *Depth profile of number of gene copies hszB, nirK, nirS and 16S rRNA for a. June, b. August, c. September, the dotted blue line shows the depth at where anoxic conditions were observed (DO < 0.3 µmol L⁻¹)*

6.2 DISCUSSION

6.2.1 Nitrogen transformation processes revealed by shifts in $\delta^{15}N$ and $\delta^{18}O$ of nitrate

During predominantly oxic conditions in April, concentrations and $\delta^{15}N$ and $\delta^{18}O$ values (~7 and 5‰, respectively) of nitrate were relatively constant throughout the entire water depth at Fohnsee as a result of mixing following the spring overturn event. Nitrate reduction during this month occurs predominantly via by benthic denitrification due to elevated O_2 concentrations in the water column. In subsequent months, the depletion of oxygen in the

water column observed during the stratification of the lake from June to September resulted in conditions that are thermodynamically favorable for the microbial reduction of nitrate. In the absence of molecular oxygen (DO < 0.3 μmol L^{-1}), concentrations of nitrate decreased from the oxycline toward the bottom of the lake throughout June to September, while $\delta^{15}N$ values of nitrate NO_3^- increased from 7.0‰ to 42.2‰ and $\delta^{18}O$ increased from 5 to 28‰ (Fig. 6.2).

During nitrate reduction, molecules containing the lighter isotopes (^{14}N and ^{16}O) are generally consumed by microorganisms at higher rates than those containing the heavier isotopes (^{15}N and ^{18}O), leaving the remaining nitrate in water enriched in ^{15}N and ^{18}O (Blackmer and Bremner, 1977; Böttcher et al., 1990). In addition, nitrite concentrations peaked (up to 0.017 mmol) in the anoxic zone near the lake bottom where the highest $\delta^{15}N$ values of nitrate were observed, suggesting that nitrate is reduced to nitrite (Ge et al., 2012; Wang and Li, 2014; Chen et al., 2017).Therefore, the observed chemical and isotopic data in the anoxic zone near the lake bottom suggest that some nitrate is reduced to nitrite in lake water column. This interpretation is supported by two previous studies (Einsiedl et al., 2020; Peña Sanchez et al., 2022) at Fohnsee that demonstrated using isotopic fingerprinting of NO_3^-, NO_2^-, and methane combined with modelling that denitrification occurred within the water column coupled with methane oxidation as electron donor.

The data patterns showed that the nitrate reduction zone was located near the lake bottom at the beginning of the stratification period and moved upwards following the seasonal vertical displacement of the oxycline.

Additional insights on nitrogen transformations processes can be derived from a dual isotope plot of $\delta^{18}O$ versus $\delta^{15}N$ of nitrate. Figure 6.5 reveals that increasing $d^{15}N$ and $d^{18}O$ values with decreasing nitrate concentrations plot on straight lines with slopes between 0.66 and 0.96 in all 5 months with an anoxic

water column which is indicative of denitrification (Böttcher et al., 1990; Aravena and Robertson, 1998); Wunderlich et al. 2012). However, it is known that isotope exchange processes between water oxygen and nitrite-oxygen (Carolyn Buchwald and Casciotti, 2010; Wunderlich et al., 2012), and inverse isotope effects of N during anammox (Brunner et al., 2013) can occur and it cannot be exclude that the isotopic composition of nitrate is additionally affected by other N transformations such as nitrate reduction to nitrite coupled to anammox and DNRA. Nonetheless, the presented chemical and isotopic data strongly suggest that nitrate reduction to nitrite and subsequently to NO and N_2 is a key N removal process at lake Fohnsee once reducing conditions are established starting at the beginning of June, similar to many other studies that have identified denitrification as the dominant N removal process (i.e. Bulow et al. 2010).

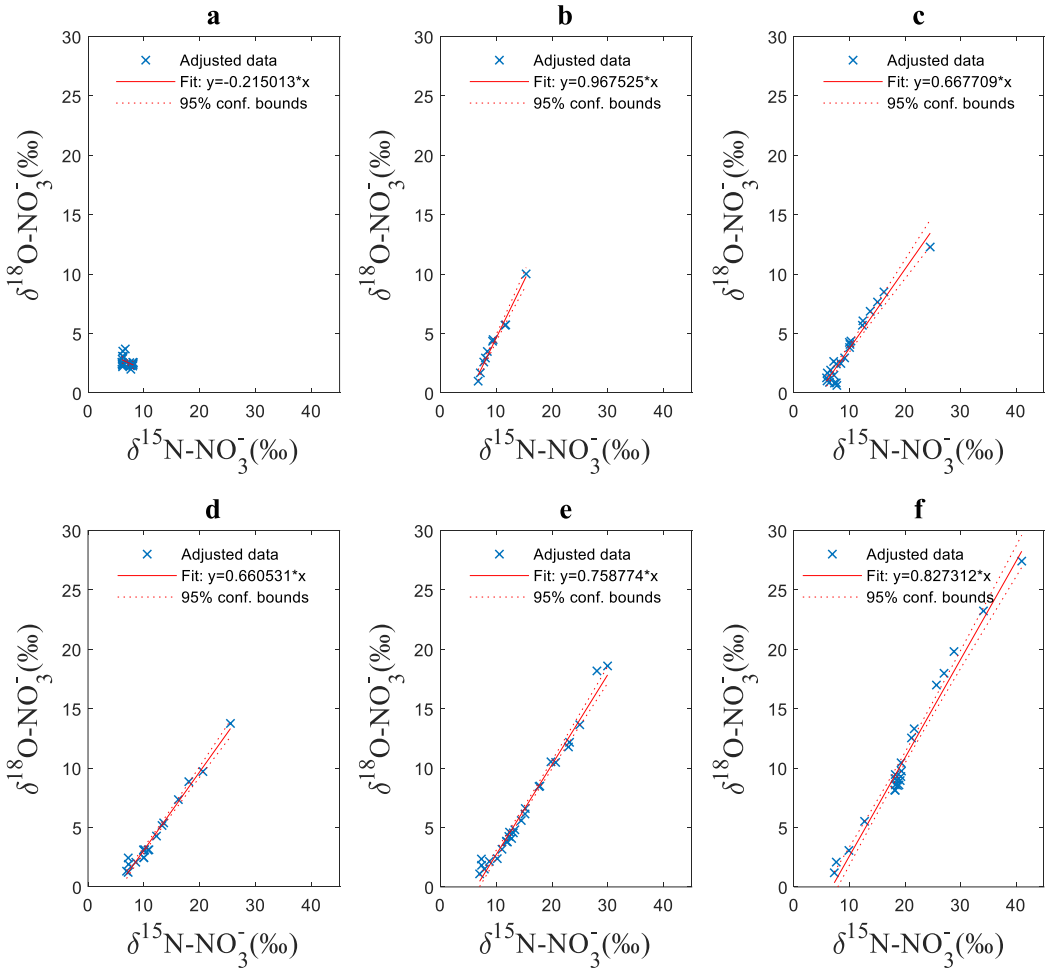

Figure 6. 5 *Linear trajectories of δ¹⁵N vs δ¹⁸O of nitrate for a) April, b) beginning of June, c) end of June, d) July, e) August, f) September. Adjusted data refers to the data points included in the fit and the 95% confidence bounds.*

6.2.2 Nitrogen transformation processes revealed by shifts in δ¹⁵N of ammonium

Ammonium is frequently formed as a result of microbial degradation of nitrogen-containing organic matter in lake sediments (Robertson and Groffman, 2007). The observed elevated ammonium concentrations within the oxic water column of Fohnsee in April (Fig. 6.3a) are likely the result of entrainment of the benthic ammonium into the lake water during the lake turnover in spring and the limited aerobic ammonium oxidation as result of

the low temperatures in the water column. Also, the dilution of the ammonium oxidizing organisms delaying nitrification in the water column for weeks to months has been reported as a cause of limited rates of nitrification in stratified lakes (Haas et al., 2021). Several field studies have shown that nitrification rates drop with the decrease in water temperature (Quinlan, 1986; Shammas, 1986; Holloway and Lyberatos, 1990; Saad and Conrad, 1993; Grundmann et al., 1995), where growth of nitrifying bacteria is strongly inhibited at temperatures < 10°C. Temperatures in the water column of lake Fohnsee throughout April range between 5.4°C at the bottom and 10.8°C at the lake surface, thus, nitrification might have been limited during this month, contributing to ammonium accumulation in April. During the sampling campaigns from June to September, the highest ammonium concentrations of ~0.09 mmol L^{-1} were always observed near the lake bottom close to the sediment-water interface, while ammonium concentrations decreased towards the oxycline to < 0.02 mmol L^{-1}. This suggests that ammonium is released from the lake sediments at Fohnsee with $\delta^{15}N$ values between 11‰ and 14‰.

Ammonium diffusing from the lake sediment into the water column can be consumed by nitrification, ammonium assimilation and/or by anammox bacteria with NO_2^- as electron acceptor (Schubert et al., 2006; Roland et al., 2018). Microorganisms performing aerobic and anaerobic oxidation of ammonium preferentially metabolize ^{14}N resulting in an enrichment of ^{15}N in the remaining ammonium as concentrations decrease (Granger et al., 2008; Karsh et al., 2012; Kritee et al., 2012). Thus, the observed trend of $\delta^{15}N\text{-}NH_4^+$ increasing from 5 to 15‰ in the anaerobic water column from the lake bottom to the oxycline between June and September (Fig. 6.3b,c,f) is consistent with microbially driven anaerobic ammonium oxidation. However, some nitrification might also occur at very low rates in anoxic waters due to O_2

production by phototrophic organisms, a process that could also contribute to the observed ^{15}N enrichment in ammonium (Callbeck et al., 2021). In the oxic zone, decomposition of N containing organic matter and ammonification produce NH_4^+ that is usually rapidly converted to nitrate due to nitrification (Casciotti et al., 2011). Since both processes preferentially metabolize ^{14}N to ammonium and subsequently to nitrate (Mariotti et al., 1981), the remaining ammonium and nitrate become progressively enriched in ^{15}N as observed in our study (Fig. 3a-b). Nitrogen isotope enrichment factors for nitrification in aquatic systems have been reported in the range of 17 to 19‰ (Lehmann et al., 2004). Such marked N isotope enrichment is very similar to the $\varepsilon_{NH_4^+}$ observed for aerobic conditions in our study for samples obtained in April.

Ammonium in the water column of Fohnsee can also be produced by decomposition of plankton in the lake or can stem from vertical fluxes of suspended inorganic particles coated with N sinking through the water column (Wakeham and Lee, 1993; Smemo and Yavitt, 2007). N coated on organic carbon or inorganic particles may also lead to the observed high shift of $\delta^{15}N$ values of ammonium (15‰ to 37‰) at Fohnsee. The NH_4^+ remaining in the oxic zone with elevated $d^{15}N$ will mix with newly formed NH_4^+ released from the sediments in the anoxic zone below the oxycline with much lower $d^{15}N$ values resulting in a mixing trend that could also be interpreted as an isotope enrichment of ^{15}N in remaining NH_4 from the bottom to the top of the anoxic lake water column that could be interpreted as anaerobic ammonium oxidation. Thus, although hydrochemical and stabile isotope profiles suggest that oxidation of ammonium under anaerobic conditions is taking place, the data are ambiguous regarding possible processes that could also lead to the observed trends in $\delta^{15}N\text{-}NH_4^+$ throughout the water column. For example, the increase in $\delta^{15}N\text{-}NH_4$ might be also the result of mixing between the

ammonium formed by organic matter decomposition in the lake sediments of the anoxic hypolimnion with a $\delta^{15}N\text{-}NH_4^+$ value of ~11‰, and the ^{15}N enriched ammonium remaining from ammonification and nitrification in the oxic zone with a $\delta^{15}N\text{-}NH_4^+$ value of up to 37‰. To test if this mixing hypothesis and only physical transport could theoretically describe the observed trends in $\delta^{15}N$ of ammonium and the concentration depth-profiles in the water column respectively, a numerical model was developed for $\delta^{15}N\text{-}NH_4$ values and ammonium concentrations.

6.2.3 Modeling of diffusion-controlled transport of ammonium and $\delta^{15}N$ values of NH_4^+

Ammonium concentrations simulated across the water column of Fohnsee using the diffusion model (Eq. 28) with the initial ammonium concentration and calculated *Kz* values showed a very good fit between the measured and observed NH_4^+ concentration depth profiles. The numerical simulations based on upward diffusion of sediment-derived ammonium explain more than 90% of the observations made in the field during the months of June, July, August, and September (Fig. 6.6).

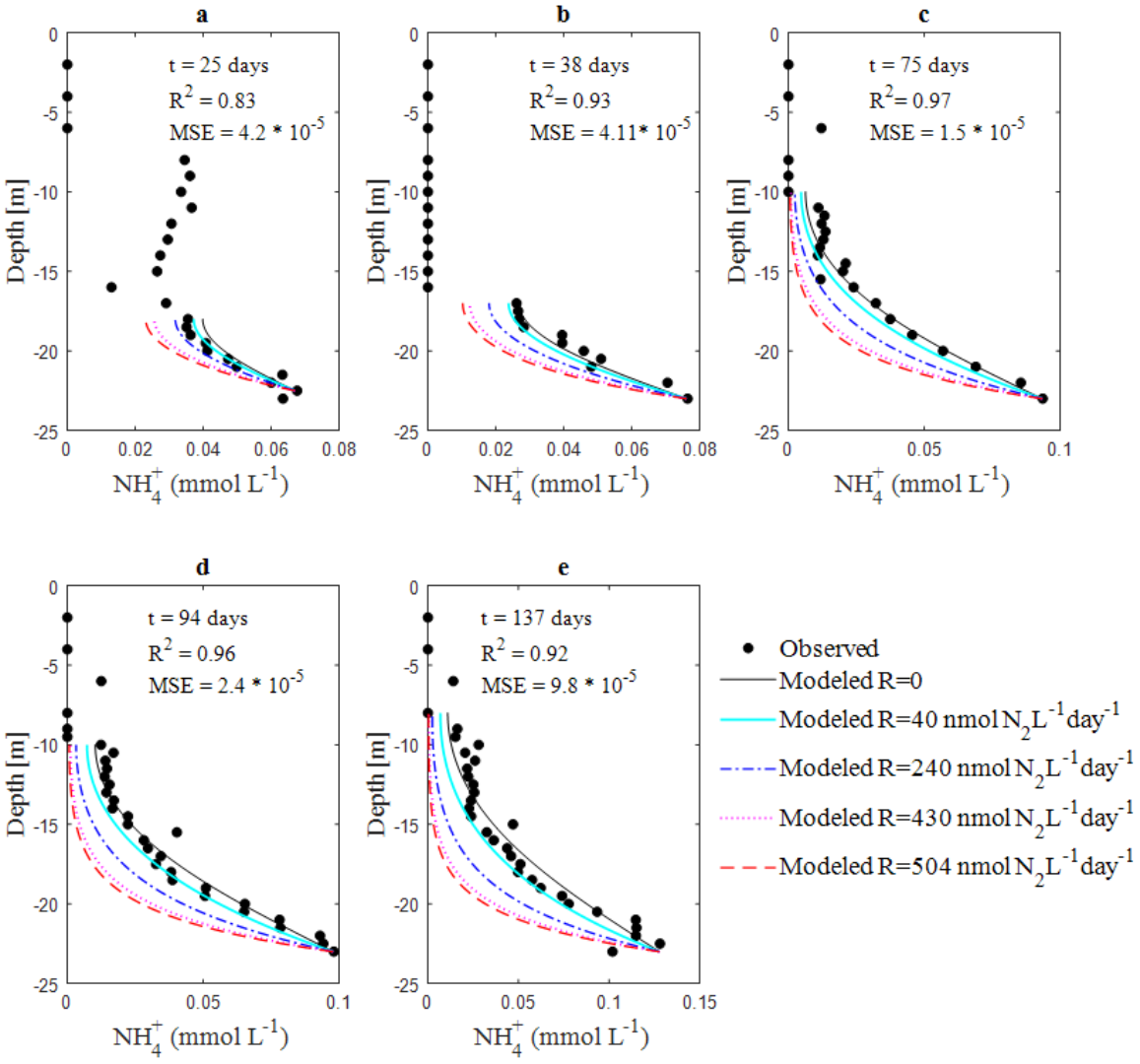

Figure 6. 6 Simulated and measured ammonium concentrations vs. depth for a. June first sampling, b. June second sampling, c. July, d. August, e. September. Statistics presented in the figure correspond to fit for this study.

Diffusion-reaction models have been used in other studies to explain concentrations of N-containing dissolved species throughout the water column (Lehmann et al. 2003) and to calculate reaction rates by inverse modeling using the consumption rate (R) or the decay constant (k) as fitting parameters (Wenk et al., 2014). Our results revealed, however, that the observed decrease in the ammonium concentrations from the sediment-water interface in the hypolimnion to the oxycline at Fohnsee can be mostly

explained by diffusive transport alone (R^2>0.9), requiring only minor contributions from ammonium consumption processes such as anammox.

Additional simulations performed with ammonium consumptions rates observed for anammox in other studies in lake water columns (Lake Tanganyika: 240 nmol N_2 $L^{-1}day^{-1}$ (Schubert et al., 2006), Lake Rassnitzer: 504 nmol N_2 $L^{-1}day^{-1}$ (Robert Hamersley et al., 2009)) and water columns in marine environments (430 nmol N_2 $L^{-1}day^{-1}$ (Dalsgaard et al., 2003; Kuypers et al., 2005; Thamdrup et al., 2006)), resulted in concentration profiles which did not match our observed data (Fig. 6.6). In contrast, simulations performed with anammox rates similar to the ones observed for lake Lugano (~40 nmol N_2 $L^{-1}day^{-1}$ (Wenk et al., 2014)) resulted in plausible NH_4^+ concentration profiles matching the observed data, but with a lower fit than simulations performed without anammox (R^2> 0.9 for anammox rates = 0 nmol N_2 $L^{-1}day^{-1}$, in comparison with R^2>0.8 for simulations with anammox rates of ~40 nmol N_2 $L^{-1}day^{-1}$). The exception was the month of June (see Fig.6. 6a and 6b) where the model fit was slightly better or similar for simulations with low anammox rates (R^2= 0.83 and R^2= 0.93 for rates = 0 nmol N_2 $L^{-1}day^{-1}$, and R^2= 0.89 and R^2= 0.93 for simulations with anammox rates of ~40 nmol N_2 $L^{-1}day^{-1}$). Thus, although NH_4^+ concentrations in the anoxic part of the water column are predominantly caused by diffusion, modeling results suggest that anaerobic oxidation of NH_4^+ likely also occurs especially in June at rates of ~40 nmol N_2 $L^{-1}day^{-1}$. This interpretation is consistent with previous isotope study and microbiological investigations at Fohnsee that revealed the occurrence of anammox within the water column in the summer period (Einsiedl et al., 2020).

6.2.4 Effect of mixing processes and movement of the oxycline on $\delta^{15}N$-NH_4^+ values

Interpretation of stable isotope data requires a thorough understanding of all biotic and hydrodynamic (mixing, advection, diffusion) processes influencing the $\delta^{15}N\text{-}NH_4^+$ pool in the water column. We have expanded the diffusion-model shown in Eq. 28, 29 to account for both isotope species of ammonium, ^{14}N and ^{15}N. The simulated scenario considers the $\delta^{15}N\text{-}NH_4^+$ in the oxic water column in April, a constant NH_4^+ influx from the sediment, and the upwards movement of the oxycline toward the lake surface throughout the spring and summer observation period. The model was able to simulate the $\delta^{15}N\text{-}NH_4^+$ values measured in the water column with a very good fit with the measured data for June and September ($R^2>0.8$) and a satisfactory fit for August ($R^2>0.6$)(Fig. 6.6).

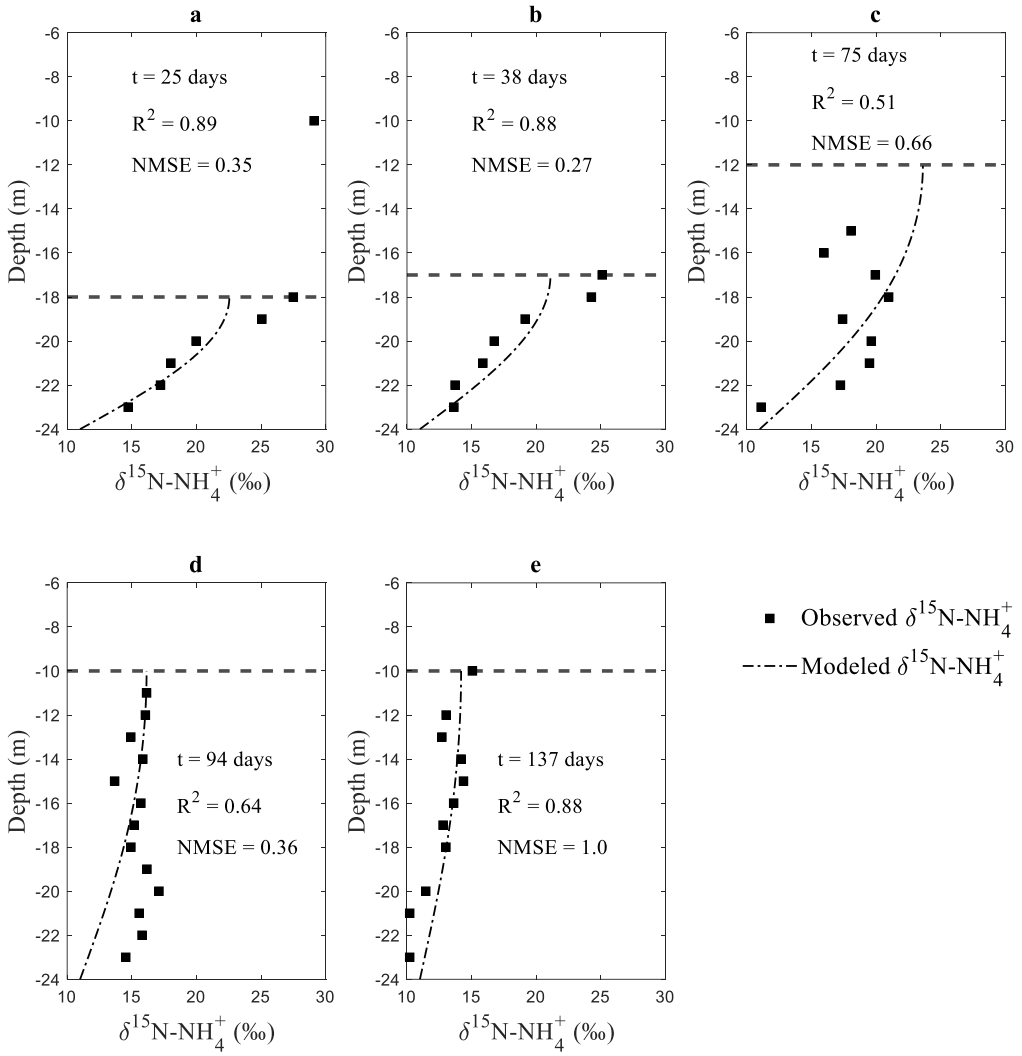

Figure 6. 7 Simulated and measured δ¹⁵N of ammonium versus depth for a. June first sampling, b. June second sampling, c. July, d. August, e. September. Normalized Mean Square Error (NMSE).

At the beginning of the stratification period in April, the oxycline was located close to the lake bottom (Fig. 6.3a). Ammonium diffusing from the lake sediment into the overlying oxic water column in April was likely mostly oxidized by nitrifying bacteria to dissolved nitrate. Nitrifying bacteria consume ^{14}N at a higher rate than ^{15}N with a kinetic N isotope effect between 14.2‰ and 38.2‰ (Mariotti et al., 1981; Casciotti et al., 2003), leaving the remaining NH_4^+ enriched in ^{15}N resulting in progressively increasing δ¹⁵N-

NH_4^+ values. This is consistent with the observed high $\delta^{15}N\text{-}NH_4^+$ values of ~+20 ‰ at 20 m depth (Fig. 6.3a) resulting from aerobic oxidation of ammonium to nitrate in the water column under oxic conditions in April.

At the beginning of June, anoxic conditions were observed below 18m depth (Fig. 6.6a). $\delta^{15}N\text{-}NH_4^+$ values near the lake water sediment interface were ~15‰ and trended to higher values of up to 27‰ below the oxycline. A strong increase of $\delta^{15}N\text{-}NH_4^+$ of ammonium was also observed at the end of June in the anoxic water column from 14‰ near the lake bottom towards 26‰ at the oxycline (Fig. 6.6b). Our model reveals that the N isotope shift of ammonium observed in the anaerobic water column appears to be result of mixing between the previously ^{15}N enriched NH_4^+ in the oxic water column resulting from nitrification when oxic conditions prevailed, and the newly formed NH_4^+ in the anoxic sediments ($\delta^{15}N\text{-}NH_4^+$ of ~11‰) induced by the upwards displacement of the oxycline.

As the oxycline moved upwards during the observation period throughout the summer, nitrification became progressively limited in the upper 10 m depth of the water column and the remaining NH_4^+ enriched in ^{15}N became a less dominant end member for mixing. Consequently, influx of ammonium with $\delta^{15}N\text{-}NH_4^+$ values near +11‰ from the anoxic lake sediments into the overlying water column resulted in a shift to less positive $\delta^{15}N\text{-}NH_4^+$ values during August and September (Fig. 6.6d,e).

Since ammonium from different sources with distinct $\delta^{15}N$ values appears to mix within the water column of Fohnsee, the model results suggest that the trends of increasing $\delta^{15}N\text{-}NH_4^+$ values with decreasing ammonium concentrations observed in the anoxic water column can be predominantly explained by mixing and diffusion, although anaerobic oxidation of NH_4^+ can also play a minor role.

It is interesting to note that the $\delta^{15}N\text{-}NH_4^+$ values predicted by our model for the anoxic water column between 23 and 20 m in August are lower than the $\delta^{15}N\text{-}NH_4^+$ values that were observed in the water column in July and August (Fig. 6.6c,d). In these months, we observed a significant decrease of sulfate concentrations in lower part of the hypolimnion (Fig. 6.2d,e) and the occurrence of H_2S providing evidence that bacterial sulfate reduction has occurred in the deepest section of the water column after nitrate was completely consumed. The H_2S produced by bacterial sulfate reduction near the sediment-water interface at Fohnsee may serve as an electron donor for chemolithotrophic denitrification (Brunet and Garcia-Gil, 1996) in the water column layers above the sulfate reducing zone. Therefore, it is possible that ammonium could be formed as product during the oxidation of H_2S using nitrate as electron acceptor during dissimilatory nitrate reduction to ammonium (DNRA). During this process, NO_3^- is reduced to NO_2^-, and subsequently converted to NH_4^+ (Tiedje, 1988). The formed NO_2^-, and thus, the subsequently produced NH_4^+ are both enriched in ^{14}N in comparison with the source of NO_3^-. However, if the initial NO_3^- is highly enriched in ^{15}N as observed in the water column of Fohnsee in August ($\delta^{15}N\text{-}NO_3^-$ 20‰, Fig. 6.2e), the newly formed NH_4^+ resulting from DNRA may have higher ^{15}N values than the NH_4^+ released from the sediments (11‰). Thus, the $\delta^{15}N\text{-}NH_4^+$ that is formed by DNRA might have the potential to shift the $\delta^{15}N$ of ammonium to values between +11 and + 20 ‰, as observed near the lake bottom in August (Fig. 6.6d).

6.2.5 Denitrifying and anammox bacteria abundances in the water column

Gene abundances of *nirK, and nirS* of up to $1*10^5$ copies ml^{-1} in the denitrification zone strongly suggested the presence of denitrifying bacteria in

the water column of Fohnsee. *Nirk* and *nirS* are responsible for the catalysis of nitric oxide from nitrite, which is a key step during denitrification (Jones et al., 2008). Thus, primers targeting these specific genes provide a quantitative measure for the abundance of denitrifying communities in the water column (Wei et al., 2015). Denitrification genes abundance of the same magnitude have been reported for other permanently and seasonally stratified lakes were denitrification has occurred (Wenk et al., 2013; Pajares et al., 2017).

In June, *nirK* and *nirS* peaked at a water depth of 17 to 18m and remained constant towards the lake bottom. This zone also coincided with the zone where we observed strong ^{15}N and ^{18}O enrichment in the remaining nitrate (Fig. 6.5) suggesting microbially driven NO_3^- reduction to NO_2^-. In addition, we observed an increase in the denitrifying bacterial abundance in the water layers when aerobic conditions changed to anaerobic conditions (Fig. 6.4a1 in 14m to Fig. 6.4b1 in 14m), strongly indicating the growth of bacterial species carrying *nirK* and *nirS* genes. Although abundance of the genes *nirK* and *nirS* alone demonstrate only the potential for denitrification, several lines of complementary qualitative and quantitative evidence from chemical and isotopic data indicates that denitrification is taking place in the anoxic water column.

The abundance of the *hzsB* gene characteristic for anammox bacteria (Harhangi et al., 2012) reached values of 10^2 copies per mL^{-1} in the oxic-suboxic zone during the month of June (Fig. 6.4) where isotopic and water chemistry data also suggested that anammox might have occurred. In contrast, gene abundance for anammox was markedly lower (mostly ~10^1 copies per mL^{-1}) in samples collected in August. For comparison, the anammox bacteria abundance reported in the water column where anammox was inferred in the permanently stratified lakes Lugano, Tanganyika and Lake Rassnitzer were as

high as 10^4 copies per mL^{-1} (Schubert et al., 2006; Robert Hamersley et al., 2009; Wenk et al., 2013), which is up to 4 orders of magnitude higher compared to our study. The moderate (June) to low numbers of *hzsB* genes (August) observed are consistent with the modelled low anammox rates in June but would require further in-situ measurements. Starting in late July, Fohnsee developed a sulfidic zone near the lake bottom where nitrate had been completely reduced and bacterial sulfate reduction had taken place producing H_2S (Fig. 6.2d-f). Thus, the presence of H_2S in the water column at Fohnsee might have inhibited the growth of anammox bacteria directly above the bacterial sulfate reduction zone after the end of July. A decline in anammox activity in sulfidic waters has been previously observed in the anoxic basin of Golfo Dulce and in the central Baltic Sea (Dalsgaard et al., 2003; Hannig et al., 2007) and laboratory experiments performed in bioreactors also showed a decrease in anammox rates in the presence of H_2S (Russ et al., 2014). Anammox bacteria have very low doubling times (Kuenen, 2008), and thus, they may be unable to adapt to fast changing environmental conditions. Changes in the redox conditions during stratification periods at Fohnsee and during turnover periods may limit microbial growth of anammox bacteria with more favorable conditions in June and July prior to onset of eth occurrence of H_2S in the deeper portions of the water column.

In September, anammox gene copies peaked at a water column depth of 14 m, 6 meters above the sulfidic zone. This suggests that anammox might occur in the anoxic water column where sulfide is not present and fluxes of NH_4^+ and NO_2^- are sufficient to maintain anammox activity. This observation is comparable to a study conducted by Wenk et al. (2013) that observed that anammox bacteria peaked under non-sulfidic and suboxic conditions, above the sulfate reduction zone in lake Lugano.

6.2.6 Short summary

Water chemistry data, the isotopic composition of nitrate, and qPCR data that nitrate reduction to nitrite and NO and subsequently N_2 was a dominant N removal process once a sub-oxic zone developed below the oxycline. Concentration and isotope trends for NH_4^+ were dominated by mixing and diffusive processes in the water column. Additional isotope effects likely occurred due to the activity of anammox bacteria, the consumption of NH_4^+due to nitrification at nanomolar O_2 levels and ammonium assimilation, and the occurrence of ammonium production during DNRA, however, these effects were most likely masked by the dominant mixing and diffusion processes in the water column. Modeling and qPCR results suggested that nitrate reduction to nitrite and NO and anammox have the potential to co-occur in the water column after thermal stratification during June.

Bacterial sulfate reduction was observed from the end of July to September in the water column near the lake sediment. The presence of sulfide might have inhibited the activity of anammox bacteria in the water column immediately above the sulfate reduction zone. But an increase in the gene number of anammox bacteria from August to September suggested that anammox bacteria may have been active in a limited zone below the oxycline where sulfide was not present.

Chapter 7: Synaptic discussion and conclusions

The objective of this thesis was to investigate the seasonal dynamics of aerobic and anaerobic methane oxidation processes and the potential coupling of DAMO and anammox in the water column of the seasonally stratified lake Fohnsee. We collected monthly water samples for measurement of isotope values of methane (δ^{13}C-CH4), ammonium (δ^{15}N-NH_4^+), and nitrate (δ^{15}N and δ^{18}O-NO_3^-), water chemistry data, and samples for microbiological testing from April to December in 2018 and from May to September in 2019.

This thesis presents a combined approach of the isotope and water chemistry data, and Quantitative PCR (qPCR) results for the functional genes for anammox (hszB) and denitrification (*nirK, nirS*) together with modeling of the transport and consumption of CH_4, O_2, NO_3^- , and NH_4^+ using the partial differential equation of reaction-diffusion, to improve our understanding of the biochemical processes taking place in the water column of lake Fohnsee.

It has been shown with high certainty that anaerobic oxidation of methane is taking place in the water column of lake Fohnsee with nitrate as an electron acceptor (DAMO) in a zone located below the oxycline during the stratification period.

Our data set together with the results of the numerical model revealed a redox zone within the water column where both denitrification and anaerobic oxidation of methane are linked, contributing to approximately 70% of methane removal between June and September. Therefore, DAMO represents the dominant methane sink in the water column of lake Fohnsee during summer stratification.

The data patterns also showed that the anaerobic oxidation of methane zone was located near the lake bottom in May and moved upwards following the seasonal vertical displacement of the oxycline and the availability of nitrate. This redox dynamic within the water column of lake Fohnsee also influenced the relevance of aerobic and anaerobic oxidation of methane removing methane from the water column during the year.

Subsequently, in 2019, we investigated the anaerobic transformations of nitrogen with a focus on anaerobic ammonium oxidation and denitrification. The water chemistry data, the isotopic composition of nitrate, and qPCR results showed that nitrate reduction was a dominant N removal process once a sub-oxic zone developed below the oxycline. Water chemistry data, qPCR analysis, and increases of $\delta^{15}N$ and $\delta^{18}O$ values of nitrate from 7.0 to 41.0‰ and 2.0 to 28.0‰, respectively, showed that nitrate reduction to nitrite and NO occurs in an upward moving zone of the water column from June to September following the displacement of the oxycline caused by thermal stratification. We also observed an increase in $\delta^{15}N$ of ammonium from 15‰ to 28‰ in the anoxic water column. Modeling results suggest that this shift in $\delta^{15}N\text{-}NH_4^+$ is predominantly controlled by mixing between ammonium stemming from the oxic water column with $\delta^{15}N$ values of 25‰ and ammonium that is likely formed in the lake sediments by oxidation of organic matter with $\delta^{15}N$ values of 11‰. Observed gene abundances (*hzsB*, *nirK,* and *nirS*) in lake water samples collected in June and July indicated the co-occurrence of nitrate reduction and low rates of anammox, while the presence of sulfide in August and September may have inhibited the activity of anammox bacteria near the sulfate reduction zone at the lake bottom.

Therefore, it is concluded that anammox bacteria may have been active only for a short period, and in a limited zone below the oxycline at lake Fohnsee. We suggest that highly dynamic redox conditions similar to the ones observed in the water column of Fohnsee might not be the optimal environment for the development of anammox bacteria communities.

Oxygen and H_2S can be toxic for anammox bacteria thus, seasonally stratified lakes might not represent an optimum growing environment for anaerobic ammonium oxidizers due to the following reasons: first, water columns in temperate lakes are subject to complete mixing at least twice per year, resulting in the intrusion of DO into the deeper layers and thus, affecting further growth of anammox communities. Second, the presence of hydrogen sulfide due to bacterial sulfate reduction activity at the end of the summer period might also result in the inhibition of the anammox bacteria population.

This work shows that anaerobic oxidation of methane coupled with nitrate reduction is an overlooked process in the seasonally stratified lake leading to reduced emissions of methane to the atmosphere, and suggested that anammox has the potential to co-occur in the water column with DAMO after thermal stratification, most likely during June.

7.1 Denitrifying Ammonium Oxidation

I believe that we have not fully encrypted all biochemical processes taking place at lake Fohnsee. The following section discusses the Denitrifying ammonium oxidation (DEAMOX) process. DEAMOX combines anaerobic ammonium oxidation with chemolithotrophic denitrification using

sulfide as an electron donor to produce nitrite from nitrate (Kalyuzhnyi et al., 2006). In this section, I would like to highlight that there are some indications that the novel process of Denitrifying Ammonium Oxidation (DEAMOX) might be taking place at lake Fohnsee.

In the first step of DEAMOX, nitrate is reduced to nitrite using sulfide as an electron donor by chemolithotrophic denitrifiers, and consequently, nitrite will oxidize ammonium by anammox bacteria. Water chemistry data collected in 2018 and 2019 suggests that at the end of the summer period, NO_3^- reduction is carried out with H_2S as the electron donor. H_2S in the water column of Fohnsee is the result of bacterial sulfate reduction taking place in the water layers near the sediments. Additionally, the study published in 2020 by Einsiedl et al, identified a potential OTU (operational taxonomic units sharing 97% sequence identity) affiliated with 'Candidatus Anammoximicrobium'. The Candidatus anammoximicrobium was first identified in a waste water fermented sludge bioreactor in 2013 by Khramenkov et al (2013). Although the literature about this string of anammox bacteria is very limited, a study published in 2020 by Zhang et al, identified anammoximicrobium as one of the predominant communities in a reactor where DEAMOX was taking place.

As observed in other bioreactors studies, anammoximicrobium could be more resistant to H_2S in comparison with other anammox bacteria (Liu et al., 2015), and thus, they are a good candidate for surviving in environments with sulfidic bottoms like is the case of lake Fohnsee during summer stratification. From the data collected in 2016 (Einsiedl et al., 2020), 2018 (Peña Sanchez et al., 2022), and 2019 (Peña Sanchez et al., 2022), I consider that is worth further research, as the DEAMOX process has not been so far observed in nature.

7.2 Implications of using numerical models for supporting isotope interpretation in seasonal studies

This study demonstrates that the combination of chemical, isotopic, and hydrochemical modeling approaches is suitable for revealing novel insights into biochemical processes in aquatic ecosystems such as seasonally stratified lakes.

Parameters used for describing isotope behavior during microbial-driven processes in nature have been mostly derived using closed-system models. These models have limitations representing natural conditions in ecosystems, principally because intrinsic characteristics of open-systems, such as external interactions of matter and energy exchanges with the surroundings and inside itself are difficult to integrate and simulate using closed-systems.

It has been observed that using the numerical modeling approach presented in this thesis to investigate isotope data bring two principal advantages:

1. Consideration of the effect of diffusive transport on dissolved compounds entering the water column from one single source as is the case of methane produced in sediments.

2. Representation of continuous data in seasonal studies and the consideration of initial conditions in the system that might differ from the time-frame of interest, such as fully aerobic conditions observed in April at lake Fohnsee in contrast with anaerobic conditions during the summer time.

The following section will focus on point 1.

7.2.1 Carbon isotope effects of diffusion transport

Although stable isotope fractionation parameters derived from the closed system model are in many cases a pertinent approximation of the isotope fractionation taking place in natural ecosystems (open system), they fell very short when applied to more complex systems. Physical effects such as molecular diffusion might have a significant effect on the isotope fractionation patterns, in comparison with laboratory set ups where usually diffusion can be neglected.

In the case of open systems such as water columns, it has been observed that closed systems models continuously underestimate the intrinsic isotope fractionation (εcell) of microbiological-driven processes (Thunell et al., 2004; Wenk et al., 2013). We were able to observe this same phenomenon after calculating the isotope fractionation for $\delta^{13}C\text{-}CH_4$ using both a closed-system and an open-system approach, the second one implemented as a numerical model. In the case of our data set for $\delta^{13}C$, it can be inferred that one of the reasons for the discrepancy between the two models might be related to how the methane molecules move in a stagnant water column.

Methane entering the water column will mostly move through the water column due to diffusive transport. In systems where transport is dominated by diffusion, mass differences between the heavier and the lighter isotopes might lead to slightly different diffusion rates. In other words, the heavier molecules of methane (i.e $^{13}C\text{-}CH_4^+$) will move slower in comparison with the lighter molecules (i.e $^{12}C\text{-}CH_4^+$), changing the initial isotope $^{13}C/^{12}C$ relationship in methane and thus, its isotope signature (i.e $\delta^{13}C$). This seems to be of particular importance while modeling relatively short periods of time as it is necessary to study dynamic environments such as seasonally stratified lakes.

The use of models differentiating between diffusion-controlled, and reaction-controlled isotopic fractionation processes might help us to better understand the development of isotope signatures in a system due to a physical phenomenon. This is important in enabling the estimation of more realistic isotope enrichment factors that could be used in the elucidation of possible biochemical reaction mechanisms observed in nature.

Bibliography

Andersson P., Torssander P. and Ingri J. (1992) Sulphur isotope ratios in sulphate and oxygen isotopes in water from a small watershed in Central Sweden. *Hydrobiologia* **235–236**, 205–217.

Anthony C. (1983) The Biochemistry of Methylotrophs. **160**, 1983.

Aravena R. O. and Robertson W. (1998) Use of multiple isotope tracers to evaluate denitrification in ground water: Study of nitrate from a large-flux septic system plume. *Groundwater* **36,** 975-982.

Barker J. F. and Fritz P. (1981) Carbon isotope fractionation during microbial methane oxidation James. **293**, 289–291.

Barnes R. O. and Goldberg E. D. (1976) Methane production and consumption in anoxic marine sediments. *Geology* **4**, 297–300.

Bastviken D. (2009) Methane. Encyclopedia of inland water, Oxford: Elsevier, 1, 783-805.

Bastviken D., Cole J. J., Pace M. L. and Van de-Bogert M. C. (2008) Fates of methane from different lake habitats: Connecting whole-lake budgets and CH4 emissions. *J. Geophys. Res. Biogeosciences* **113**, 1–13.

Bastviken D., Ejlertsson J. and Tranvik L. (2002) Measurement of methane oxidation in lakes: A comparison of methods. *Environ. Sci. Technol.* **36**, 3354–3361.

Bastviken D., Tranvik L. J., Downing J., Crill J. a, M P. and Enrich-prast A. (2011) the Continental Carbon Sink. *Science (80-.).* **331**, 50.

van den Berg E. M., Elisário M. P., Kuenen J. G., Kleerebezem R. and van Loosdrecht M. C. M. (2017) Fermentative bacteria influence the competition between denitrifiers and DNRA bacteria. *Front. Microbiol.* **8**,

1–13.

Beutel M. W. (2006) Inhibition of ammonia release from anoxic profundal sediments in lakes using hypolimnetic oxygenation. *Ecol. Eng.* **28**, 271–279.

Blackmer A. M. and Bremner J. M. (1977) Nitrogen isotope discrimination in denitrification of nitrate in soils. *Soil Biol. Biochem.* **9**, 73–77.

Blees J., Niemann H., Wenk C. B., Zopfi J., Schubert C. J., Kirf M. K., Veronesi M. L., Hitz C. and Lehmann M. F. (2014) Micro-aerobic bacterial methane oxidation in the chemocline and anoxic water column of deep south-Alpine Lake Lugano (Switzerland). *Limnol. Oceanogr.* **59**, 311–324.

Bodelier P. L. E., Pérez G., Veraart A. J., Krause and B. S. M. (2019) Methanotroph Ecology, Environmental Distribution and Functioning. In Springer. pp. 205–229.

Bonaglia S., Klawonn I., Brabandere L. De, Deutsch B. and Thamdrup B. (2016) Denitrification and DNRA at the Baltic Sea oxic – anoxic interface : Substrate spectrum and kinetics. , 1900–1915.

Borrel G., Jézéquel D., Biderre-Petit C., Morel-Desrosiers N., Morel J. P., Peyret P., Fonty G. and Lehours A. C. (2011) Production and consumption of methane in freshwater lake ecosystems. *Res. Microbiol.* **162**, 833–847.

Böttcher J., Strebel O., Voerkelius S. and Schmidt H. L. (1990) Using isotope fractionation of nitrate-nitrogen and nitrate-oxygen for evaluation of microbial denitrification in a sandy aquifer. *J. Hydrol.* **114**, 413–424.

Braig E. L. (2015) Stable isotopes of bioelements for tracing limnological key processes in the Osterseen lake district , Upper Bavaria. .

Braig E., Welzl G., Stichler W., Raeder U. and Melzer A. (2010) Entrainment,

annual circulation and groundwater inflow in a chain of lakes as inferred by stable 18O isotopic signatures in the water column. *J. Limnol.* **69**, 278–286.

Brettar I. and Rheinheimer G. (1991) Denitrification in the central Baltic: evidence for H2S-oxidation as motor of denitrification at the oxic-anoxic interface. *Mar. Ecol. Prog. Ser.* **77**, 157–169.

Brunet R. C. and Garcia-Gil L. J. (1996) Sulfide-induced dissimilatory nitrate reduction to ammonia in anaerobic freshwater sediments. *FEMS Microbiol. Ecol.* **21**, 131–138.

Brunner B., Contreras S., Lehmann M. F., Matantseva O., Rollog M., Kalvelage T., Klockgether G., Lavik G., Jetten M. S. M., Kartal B. and Kuypers M. M. M. (2013) Nitrogen isotope effects induced by anammox bacteria. *Proc. Natl. Acad. Sci.* **110**, 18994–18999.

Buchwald C and Casciotti K. L. (2010) Oxygen isotopic exchange and fractionation during bacterial nitrite oxidation. *Limnol. Oceanogr.* **55**, 1064–1074.

Buchwald Carolyn and Casciotti K. L. (2010) Oxygen isotopic fractionation and exchange during bacterial nitrite oxidation. *Limnol. Oceanogr.* **55**, 1064–1074.

Bulow S. E., Rich J. J., Naik H. S., Pratihary A. K. and Ward B. B. (2010) Denitrification exceeds anammox as a nitrogen loss pathway in the Arabian Sea oxygen minimum zone. *Deep. Res. Part I Oceanogr. Res. Pap.* **57**, 384–393.

Bungay H. R., Whalen W. J. and Sanders W. M. (1969) Microprobe techniques for determining diffusivities and respiration rates in microbial slime systems. *Biotechnol. Bioeng.* **11**, 765–772.

Burgin A. J. and Hamilton S. K. (2007) Have we over emphasized the role of

denitrification in aquatic ecosystems? A review of nitrate removal pathways. *Front. Ecol. Environ.* **5**, 89–96.

Burgin A. J., Yang W. H., Hamilton S. K. and Silver W. L. (2011) Beyond carbon and nitrogen: How the microbial energy economy couples elemental cycles in diverse ecosystems. *Front. Ecol. Environ.* **9**, 44–52.

Caldwell S., Laidler J., Brewer E. A., Eberly J. O., Sandborgh S. C. and Colwell F. S. (2008) Anaerobic oxidation of methane- mechanisms, bioenergetics, and the Ecology of associated microorganisms. *Environ. Sci. Technol.* **42**, 6791–6799.

Callbeck C. M., Ehrenfels B. and Schubert C. J. (2021) Anoxic chlorophyll maximum enhances local organic matter remineralization and nitrogen loss in Lake Tanganyika. *Nat. Commun.*, 1–11.

Canfield D. E., Stewart F. J., Thamdrup B., De Brabandere L., Dalsgaard T., Delong E. F., Revsbech N. P. and Ulloa O. (2010) A cryptic sulfur cycle in oxygen-minimum-zone waters off the Chilean coast. *Science (80-.).* **330**, 1375–1378.

Carini S., Bano N., LeCleir G. and Joye S. B. (2005) Aerobic methane oxidation and methanotroph community composition during seasonal stratification in Mono Lake, California (USA). *Environ. Microbiol.* **7**, 1127–1138.

Carlson H. K., Lui L. M., Price M. N., Kazakov A. E., Carr A. V., Kuehl J. V., Owens T. K., Nielsen T., Arkin A. P. and Deutschbauer A. M. (2020) Selective carbon sources influence the end products of microbial nitrate respiration. *ISME J.* **14**, 2034–2045.

Casciotti K. L., Buchwald C., Santoro A. E. and Frame C. (2011) *Assessment of nitrogen and oxygen isotopic fractionation during nitrification and its expression in the marine environment*. 1st ed., Elsevier Inc.

Casciotti K. L., McIlvin M. and Buchwald C. (2010) Oxygen isotopic exchange and fractionation during bacterial ammonia oxidation. *Limnol. Oceanogr.* **55**, 1805.

Casciotti K. L., Sigman D. M., Hastings M. G., Bo J. K. and Hilkert A. (2002) Measurement of the Oxygen Isotopic Composition of Nitrate in Seawater and Freshwater Using the Denitrifier Method. *Anal. Chem.* **74**, 4905–4912.

Casciotti K. L., Sigman D. M. and Ward B. B. (2003) Linking diversity and stable isotope fractionation in ammonia-oxidizing bacteria. *Geomicrobiol. J.* **20**, 335–353.

Chen D., Chen X., Huang X., He S. and Huang J. (2017) Controlling denitrification accompanied with nitrite accumulation at the sediment-water interface. *Ecol. Eng.* **100**, 194–198.

Cline J. D. and Kaplan I. (1975) Isotopic fractionation of dissolved nitrate during denitrification in the eastern tropical north pacific ocean. *Mar. Chem.* **3**, 271–299.

Cojean A. N. Y., Lehmann M. F., Robertson E. K., Thamdrup B. and Zopfi J. (2020) Controls of H2S, Fe2 +, and Mn2 + on Microbial NO3−-Reducing Processes in Sediments of an Eutrophic Lake. *Front. Microbiol.* **11**, 1–17.

Conrad R. (2020) Importance of hydrogenotrophic, aceticlastic and methylotrophic methanogenesis for methane production in terrestrial, aquatic and other anoxic environments: A mini review. *Pedosphere* **30**, 25–39.

Conrad R. (2009) Minireview The global methane cycle : recent advances in understanding the microbial processes involved. **1**, 285–292.

Conrad R. (2005) Quantification of methanogenic pathways using stable carbon isotopic signatures: A review and a proposal. *Org. Geochem.* **36**,

739–752.

Conrad R., Claus P. and Casper P. (2009) Characterization of methanogenic Archaea and stable isotope fractionation during methane production in the profundal sediment of an oligotrophic lake (Lake Stechlin, Germany). *Limnol. Oceanogr.* **54**, 457–471.

Crowe S. A., Katsev S., Leslie K., Sturm A., Magen C., Nomosatryo S., Douglas G., Pack M. A., Kessler J. D., Reeburgh W. S., Roberts J. A. and Gonza L. (2011) The methane cycle in ferruginous Lake Matano. , 61–78.

Crowe S. A., Treusch A. H., Forth M., Li J., Magen C., Canfield D. E., Thamdrup B. and Katsev S. (2017) Novel anammox bacteria and nitrogen loss from Lake Superior. *Sci. Rep.* **7**, 1–7.

Cui M., Ma A., Qi H., Zhuang X. and Zhuang G. (2015) Anaerobic oxidation of methane: An "active" microbial process. *Microbiologyopen* **4**, 1–11.

Daims H., Lebedeva E. V., Pjevac P., Han P., Herbold C., Albertsen M., Jehmlich N., Palatinszky M., Vierheilig J., Bulaev A., Kirkegaard R. H., Von Bergen M., Rattei T., Bendinger B., Nielsen P. H. and Wagner M. (2015) Complete nitrification by Nitrospira bacteria. *Nature* **528**, 504–509.

Dake J. M. K. and Harleman D. R. F. (1969) Thermal stratification in lakes: Analytical and laboratory studies. *Water Resour. Res.* **5**, 484–495.

Dalsgaard T., Canfield D.E., Peterson J., Thamdrup B. and Acuna-Gonzales J. (2003) N production by anamox in the anoxic water column of Golfo Dulce, Costa Rica. *Nature* **422**, 606–608.

Dalton H. (1992) Methane Oxidation by Methanotrophs.

Delwiche C. and Bryan B. A. (1976) Denitrification. *Annu. Rev. Microbiol.*

Deutzmann J. S. (2020) Anaerobic Methane Oxidation in Freshwater Environments. In *Anaerobic Utilization of Hydrocarbons, Oils, and Lipids*

Deutzmann J. S., Stief P., Brandes J. and Schink B. (2014) Anaerobic methane oxidation coupled to denitrification is the dominant methane sink in a deep lake. *Proc. Natl. Acad. Sci.* **111**, 18273–18278.

Ding J., Fu L., Ding Z., Lu Y., Cheng S. H. and Zeng R. J. (2015) Environmental evaluation of coexistence of denitrifying anaerobic methane-oxidizing archaea and bacteria in a paddy field.

Downing J. A., Cole J. J., Prairie Y. T., Duarte C. M., Tranvik L. J., Striegl R. G., McDowell W. H., Kortelainen P., Caraco N. F., Melack J. M. and Middelburg J. J. (2006) The global abundance and size distribution of lakes , ponds , and impoundments. *Limnol. Oceanogr.* **51**, 2388–2397.

Drake HL, Küsel K and Matthies C (2006) *Acetogenic Prokaryotes*. 3rd edn, v.,

Duc N. T., Crill P. and Bastviken D. (2010) Implications of temperature and sediment characteristics on methane formation and oxidation in lake sediments. *Biogeochemistry* **100**, 185–196.

Einsiedl F., Pilloni G., Ruth-Anneser B., Lueders T. and Griebler C. (2015) Spatial distributions of sulphur species and sulphate-reducing bacteria provide insights into sulphur redox cycling and biodegradation hot-spots in a hydrocarbon-contaminated aquifer. *Geochim. Cosmochim. Acta* **156**, 207–221.

Einsiedl F., Wunderlich A., Sebilo M., Coskun Ö., Orsi W. and Mayer B. (2020) Biogeochemical evidence of anaerobic methane oxidation and anaerobic ammonium oxidation in a stratified lake using stable isotopes. *Biogeosciences Discuss.* **30**, 1–21.

Elçi Ş. (2008) Effects of thermal stratification and mixing on reservoir water quality. *Limnology* **9**, 135–142.

Elsner M. (2010) Stable isotope fractionation to investigate natural transformation mechanisms of organic contaminants: Principles,

prospects and limitations. *J. Environ. Monit.* **12**, 2005–2031.

Engström P., Dalsgaard T., Hulth S. and Aller R. C. (2005) Anaerobic ammonium oxidation by nitrite (anammox): Implications for N2 production in coastal marine sediments. *Geochim. Cosmochim. Acta* **69**, 2057–2065.

Ettwig K. F., Alen T. Van, Pas-schoonen K. T. Van De, Jetten M. S. M. and Strous M. (2009) Enrichment and Molecular Detection of Denitrifying Methanotrophic Bacteria of the NC10 Phylum . **75**, 3656–3662.

Ettwig K. F., Butler M. K., Le Paslier D., Pelletier E., Mangenot S., Kuypers M. M. M., Schreiber F., Dutilh B. E., Zedelius J., De Beer D., Gloerich J., Wessels H. J. C. T., Van Alen T., Luesken F., Wu M. L., Van De Pas-Schoonen K. T., Op Den Camp H. J. M., Janssen-Megens E. M., Francoijs K. J., Stunnenberg H., Weissenbach J., Jetten M. S. M. and Strous M. (2010) Nitrite-driven anaerobic methane oxidation by oxygenic bacteria. *Nature* **464**, 543–548.

Ettwig K. F., Zhu B., Speth D., Keltjens J. T., Jetten M. S. M. and Kartal B. (2016) Archaea catalyze iron-dependent anaerobic oxidation of methane. *Proc. Natl. Acad. Sci. U. S. A.* **113**, 12792–12796.

Fan S. Q., Xie G. J., Lu Y., Liu B. F., Xing D. F., Ding J., Han H. J. and Ren N. Q. (2021) Nitrate/nitrite dependent anaerobic methane oxidation coupling with anammox in membrane biotrickling filter for nitrogen removal. *Environ. Res.* **193**, 110533.

Feisthauer S., Vogt C., Modrzynski J., Szlenkier M., Krüger M., Siegert M. and Richnow H. H. (2011) Different types of methane monooxygenases produce similar carbon and hydrogen isotope fractionation patterns during methane oxidation. *Geochim. Cosmochim. Acta* **75**, 1173–1184.

Fenchel T., King G. . and Blackburn T. . (1999) *Bacterial biogeochemistry: The*

ecophysiology of mineral cycling. third., Elsevier.

Frenzel P., Thebrath B. and Conrad R. (1990) Oxidation of methane in the oxic surface layer of a deep lake sediment (Lake Constance). *FEMS Microbiol. Lett.* **73**, 149–158.

Gao D., Wang X., Liang H., Wei Q., Dou Y. and Li L. (2018) Anaerobic ammonia oxidizing bacteria: ecological distribution, metabolism, and microbial interactions. *Front. Environ. Sci. Eng.* **12**, 1–15.

Gargett A.E. (1984) Vertical eddy diffusivity in the ocean interior. *J. Mar. Res.* **42**, 359–393.

Ge S., Peng Y., Wang S., Lu C., Cao X. and Zhu Y. (2012) Bioresource Technology Nitrite accumulation under constant temperature in anoxic denitrification process : The effects of carbon sources and COD / NO 3 - N. *Bioresour. Technol.* **114**, 137–143.

Giblin A. E., Tobias C. R., Song B., Weston N., Banta G. T. and Rivera-Monroy V. H. (2013) The importance of dissimilatory nitrate reduction to ammonium (DNRA) in the nitrogen cycle of coastal ecosystems. *Oceanography* **26**, 124–131.

Van De Graaf A. A., De Bruijn P., Robertson L. A., Jetten M. S. M. and Kuenen J. G. (1997) Metabolic pathway of anaerobic ammonium oxidation on the basis of 15N studies in a fluidized bed reactor. *Microbiology* **143**, 2415–2421.

Granger J., Sigman D. M., Lehmann M. F. and Tortell P. D. (2008) Nitrogen and oxygen isotope fractionation during dissimilatory nitrate reduction by denitrifying bacteria. *Limnol. Oceanogr.* **53**, 2533–2545.

Granger J. and Wankel S. D. (2016) Isotopic overprinting of nitrification on denitrification as a ubiquitous and unifying feature of environmental nitrogen cycling. *Proc. Natl. Acad. Sci.* **113**, E6391–E6400.

Grasshoff K., Kremling K. and Ehrhardt M. (1978) *Methods of seawater analysis*.,

Griffiths R. P., Caldwell B. A., Cline J. D., Broich W. A. and Morita R. Y. (1982) Field Observations of Methane Concentrations and Oxidation Rates in the Southeastern Bering Sea. *Appl. Environ. Microbiol.* **44**, 435–446.

Grossart H.-P., Frindte K., Dziallas C., Eckert W. and Tang K. W. (2011) Microbial methane production in oxygenated water column of an oligotrophic lake. *Proc. Natl. Acad. Sci.* **108**, 19657–19661.

Grundmann G. L., Renault P., Rosso L. and Bardin R. (1995) Differential Effects of Soil Water Content and Temperature on Nitrification and Aeration. *soil Sci. Soc. Am. J.*

Haas S., Robicheau B. M., Rakshit S., Tolman J., Algar C. K., LaRoche J. and Wallace D. W. R. (2021) Physical mixing in coastal waters controls and decouples nitrification via biomass dilution. *Proc. Natl. Acad. Sci. U. S. A.* **118**.

Hamersley M. R., Lavik G., Woebken D., Rattray J. E., Lam P., Hopmans E. C., Sinninghe Damsté J. S., Krüger S., Graco M., Gutiérrez D. and Kuypers M. M. M. (2007) Anaerobic ammonium oxidation in the Peruvian oxygen minimum zone. *Limnol. Oceanogr.* **52**, 923–933.

Hannig M., Lavik G., Kuypers M. M. M., Woebken D., Martens-Habbena W. and Jürgens K. (2007) Shift from denitrification to anammox after inflow events in the central Baltic Sea. *Limnol. Oceanogr.* **52**, 1336–1345.

Hanson R. S. and Hanson T. E. (1996) Methanotrophic bacteria. *Microbiol. Rev.* **60**, 439–471.

Harhangi H. R., Le Roy M., van Alen T., Hu B. lan, Groen J., Kartal B., Tringe S. G., Quan Z. X., Jetten M. S. M. and Op den Camp H. J. M. (2012)

Hydrazine synthase, a unique phylomarker with which to study the presence and biodiversity of anammox bacteria. *Appl. Environ. Microbiol.* **78**, 752–758.

Haroon M. F., Hu S., Shi Y., Imelfort M., Keller J., Hugenholtz P., Yuan Z. and Tyson G. W. (2013) Anaerobic oxidation of methane coupled to nitrate reduction in a novel archaeal lineage. *Nature* **500**, 567–570.

Harrison A. G. and Thode H. G. (1958) Mechanism of the bacterial reduction of sulphate from isotope fractionation studies. *Trans. Faraday Soc.* **54**, 84–92.

Harrits S. M. and Hanson R. S. (1980) Stratification of aerobic methane-oxidizing organisms in Lake Mendota, Madison, Wisconsin. *Limnol. Oceanogr.* **25**, 412–421.

Hartog N., Griffioen J. and Van der Weijden C. H. (2002) Distribution and reactivity of O2-reducing components in sediments from a layered aquifer. *Environ. Sci. Technol.* **36**, 2338–2344.

Hoehler T. M., Alperin M. J., Albert D. B., Martens S. and Field A. (1994) Field and laboratory studies of methane oxidation in an anoxic marine sediment ' Evidence for a methanogen-sulfate reducer consortium that methanogens and. **8**, 451–463.

Holler T., Wegener G., Knittel K., Boetius A., Brunner B., Kuypers M. and Widdel F. (2009) Substantial 13C/12C and D/H fractionation during anaerobic oxidation of methane by marine consortia enriched in vitro. *Environ. Microbiol. Rep.* **1**, 370–376.

Holloway B. and Lyberatos G. (1990) Effect of temperature and pH on the effective maximum specific growth rate of nitrifying bacteria. *Water Res.* **24**, 97–101.

Hondzo M. and Stefan H. G. (1993) Lake water temperature simulation

model. *J. Hydraul. Eng.* **119**, 1251–1273.

Houghton J. ., Ding Y., Griggs D. ., Noguer M., von der Linden P. ., Dai X., Maskell K. and Johnson C. . (2001) *Climate Change 2001: The Scientific Basis.*,

Imboden D. M. and Wüest A. (1995) Mixing Mechanisms in Lakes. *Phys. Chem. Lakes*, 83–138.

International Atomic Energy Agency (IAEA) (1993) *Reference and intercomparison materials for stable isotopes of light elements.*,

IPCC I. P. in C. C. (2007) *Changes in Atmospheric Constituents and in Radiative Forcing.*,

Iversen N., Oremland R. S. and Klug M. J. (1987) Big Soda Lake (Nevada). 3. Pelagic methanogenesis and anaerobic methane oxidation. *Limnol. Oceanogr.* **32**, 804–814.

Jackson R. B., Saunois M., Bousquet P., Canadell J. G., Poulter B., Stavert A. R., Bergamaschi P., Niwa Y., Segers A. and Tsuruta A. (2020) Increasing anthropogenic methane emissions arise equally from agricultural and fossil fuel sources. *Environ. Res. Lett.* **15**.

Jassby A. and Powell T. (1975) Vertical patterns of eddy diffusion during stratification in Castle Lake, California. *Limnol. Oceanogr.* **20**, 530–543.

Jensen M. M., Petersen J., Dalsgaard T. and Thamdrup B. (2009) Pathways, rates, and regulation of N2 production in the chemocline of an anoxic basin, Mariager Fjord, Denmark. *Mar. Chem.* **113**, 102–113.

Jin Q. and Bethke C. M. (2007) The thermodynamics and kinetics of microbial metabolism. *Am. J. Sci.* **307**, 643–677.

Jones C. M., Stres B., Rosenquist M. and Hallin S. (2008) Phylogenetic analysis of nitrite, nitric oxide, and nitrous oxide respiratory enzymes

reveal a complex evolutionary history for denitrification. *Mol. Biol. Evol.* **25**, 1955–1966.

Kaiserli A., Voutsa D. and Samara C. (2002) Phosphorus fractionation in lake sediments - Lakes Volvi and Koronia, N. Greece. *Chemosphere* **46**, 1147–1155.

Kalyuzhnyi S., Gladchenko M., Mulder A. and Versprille B. (2006) DEAMOX-New biological nitrogen removal process based on anaerobic ammonia oxidation coupled to sulphide-driven conversion of nitrate into nitrite. *Water Res.* **40**, 3637–3645.

Kampbell D. H., Wilson J. T. and Vandegrift S. A. (2006) Dissolved Oxygen and Methane in Water by a GC Headspace Equilibration Technique. *Int. J. Environ. Anal. Chem.* **7319**.

Karsh K. L., Granger J., Kritee K. and Sigman D. M. (2012) Eukaryotic assimilatory nitrate reductase fractionates N and O isotopes with a ratio near unity. *Environ. Sci. Technol.* **46**, 5727–5735.

Kartal B., Maalcke W. J., De Almeida N. M., Cirpus I., Gloerich J., Geerts W., Op Den Camp H. J. M., Harhangi H. R., Janssen-Megens E. M., Francoijs K. J., Stunnenberg H. G., Keltjens J. T., Jetten M. S. M. and Strous M. (2011) Molecular mechanism of anaerobic ammonium oxidation. *Nature* **479**, 127–130.

Kendall C. (1998) *Tracing Nitrogen Sources and Cycling in Catchments*., Elsevier B.V.

Kendall C., Elliott E. M. and Wankel S. D. (2008) Tracing Anthropogenic Inputs of Nitrogen to Ecosystems. *Stable Isot. Ecol. Environ. Sci. Second Ed.*, 375–449.

van Kessel M. A., Stultiens K., Kartal B., Slegers M. F., Guerrero Cruz S., Jetten M. S., Stultiens K. and Op den Camp H. J. (2018) Current

perspectives on the application of N-damo and anammox in wastewater treatment. *Curr. Opin. Biotechnol.* **50**, 222–227.

Khramenkov S. V., Kozlov M. N., Kevbrina M. V., Dorofeev A. G., Kazakova E. A., Grachev V. A., Kuznetsov B. B., Polyakov D. Y. and Nikolaev Y. A. (2013) A novel bacterium carrying out anaerobic ammonium oxidation in a reactor for biological treatment of the filtrate of wastewater fermented sludge. *Microbiol. (Russian Fed.* **82**, 628–636.

Kits K. D., Klotz M. G. and Stein L. Y. (2015) Methane oxidation coupled to nitrate reduction under hypoxia by the Gammaproteobacterium Methylomonas denitrificans , sp . nov . type strain FJG1. *Environ. Microbiol.* **17**, 3219–3232.

Knittel K. and Boetius A. (2009) Anaerobic oxidation of methane: Progress with an unknown process. *Annu. Rev. Microbiol.* **63**, 311–334.

Knöller K., Vogt C., Haupt M., Feisthauer S. and Richnow H. H. (2011) Experimental investigation of nitrogen and oxygen isotope fractionation in nitrate and nitrite during denitrification. *Biogeochemistry* **103**, 371–384.

Kobayashi K., Makabe A., Yano M., Oshiki M., Kindaichi T., Casciotti K. L. and Okabe S. (2019) Dual nitrogen and oxygen isotope fractionation during anaerobic ammonium oxidation by anammox bacteria. *ISME J.* **13**, 2426–2436.

Kritee K., Sigman D. M., Granger J., Ward B. B., Jayakumar A. and Deutsch C. (2012) Reduced isotope fractionation by denitrification under conditions relevant to the ocean. *Geochim. Cosmochim. Acta* **92**, 243–259.

Kuenen J. G. (2008) Anammox bacteria: from discovery to application. *Nat. Rev. Microbiol.* **6**, 320–326.

Kuypers M. M. M., Lavik G., Woebken D., Schmid M., Fuchs B. M., Amann R., Jørgensen B. B. and Jetten M. S. M. (2005) Massive nitrogen loss from

the Benguela upwelling system through anaerobic ammonium oxidation. *Proc. Natl. Acad. Sci.*

Kuypers M. M. M., Sliekers A. O., Lavik G. and Schmid M. (2003) Anaerobic ammonium oxidation by anammox bacteria in the Black Sea. **422**, 2–5.

Lane S. L., Flanagan S., Wilde F. D., Wilde F. D., Radtke D. B., Gibs J., Iwatsubo R. T. and Groat C. G. (2003) National Field Manual for Collection of Water-Quality Data. In *Handbooks for Water-Resources Investigations* U.S. Geological Survey.

Lavik G., Stührmann T., Brüchert V., Van Der Plas A., Mohrholz V., Lam P., Mußmann M., Fuchs B. M., Amann R., Lass U. and Kuypers M. M. M. (2009) Detoxification of sulphidic African shelf waters by blooming chemolithotrophs. *Nature* **457**, 581–584.

Lehmann M. F., Reichert P., Bernasconi S. M., Barbieri A. and McKenzie J. A. (2003) Modelling nitrogen and oxygen isotope fractionation during denitrification in a lacustrine redox-transition zone. *Geochim. Cosmochim. Acta* **67**, 2529–2542.

Lehmann M. F., Sigman D. M. and Berelson W. M. (2004) Coupling the 15N/14N and 18O/ 16O of nitrate as a constraint on benthic nitrogen cycling. *Mar. Chem.* **88**, 1–20.

Lewis B. L. and Landing W. M. (1991) The biogeochemistry of manganese and iron in the Black Sea. *Deep. Res. Part A* **38**, S773–S803.

Lieberman R. L. and Rosenzweig A. C. (2004) Biological methane oxidation: Regulation, biochemistry, and active site structure of particulate methane monooxygenase. *Crit. Rev. Biochem. Mol. Biol.* **39**, 147–164.

Lipscomb J. D. (1994) Biochemistry of the soluble methane. *Annual Review of Microbiology. **48**, 371-399.*

Lipsewers Y. A., Hopmans E. C., Meysman F. J. R., Sinninghe Damsté J. S. and Villanueva L. (2016) Abundance and diversity of denitrifying and anammox bacteria in seasonally hypoxic and sulfidic sediments of the saline lake grevelingen. *Front. Microbiol.* **7**, 1–15.

Liu C., Zhao D., Yan L., Wang A., Gu Y. and Lee D. J. (2015) Elemental sulfur formation and nitrogen removal from wastewaters by autotrophic denitrifiers and anammox bacteria. *Bioresour. Technol.* **191**, 332–336.

Lopes F., Viollier E., Thiam A., Michard G., Abril G., Groleau A., Prévot F., Carrias J., Albéric P. and Jézéquel D. (2011) Applied Geochemistry Biogeochemical modelling of anaerobic vs . aerobic methane oxidation in a meromictic crater lake (Lake Pavin , France). *Appl. Geochemistry* **26**, 1919–1932.

López-archilla A. I., Moreira D., Velasco S. and López-garcía P. (2007) Archaeal and bacterial community composition of a pristine coastal aquifer in Doñana. **47**, 123–139.

ST. Louis V., Kelly C. A., Duchemin E., Rudd J. W. M. and Rosenberg D. M. (2000) Reservoir Surfaces as Sources of Greenhouse Gases to the Atmosphere : A Global Estimate. *Bioscience* **50**.

Lueders T., Manefield M. and Friedrich M. W. (2004) Enhanced sensitivity of DNA- and rRNA-based stable isotope probing by fractionation and quantitative analysis of isopycnic centrifugation gradients. *Environ. Microbiol.* **6**, 73–78.

Luyssaert S., Abril G., Andres R., Bastviken D., Bellassen V., Bergamaschi P., Bousquet P. and Chevallier F. (2012) The European land and inland water CO2 , CO , CH4 and N2O balance between 2001 and 2005. *Biogeosciences*, 3357–3380.

Mahieu K., De Visscher A., Vanrolleghem P. A. and Van Cleemput O. (2008)

Modelling of stable isotope fractionation by methane oxidation and diffusion in landfill cover soils. *Waste Manag.* **28**, 1535–1542.

Mariotti A. (1983) Atmospheric nitrogen is a reliable standard for natural 15N abundance measurements. *Nature*, 8–10.

Mariotti A., Germon J. C., Hubert P., Kaiser P., Letolle R., Tardieux A. and Tardieux P. (1981) Experimental determination of nitrogen kinetic isotope fractionation: Some principles; illustration for the denitrification and nitrification processes. *Plant Soil* **62**, 413–430.

Marrero T. R. and Mason E. A. (1972) Gaseous Diffusion Coefficients. *J. Phys. Chem.* **1**.

Martens C. S. and Berner R. A. (1977) Interstitial water chemistry of anoxic Long Island Sound sediments. 1. Dissolved gases. *Limnol. Oceanogr.* **22**, 10–25.

McGlynn S. E. (2017) Energy metabolism during anaerobic methane oxidation in ANME archaea. *Microbes Environ.* **32**, 5–13.

Meng H., Wang Y. F., Chan H. W., Wu R. N. and Gu J. D. (2016) Co-occurrence of nitrite-dependent anaerobic ammonium and methane oxidation processes in subtropical acidic forest soils. *Appl. Microbiol. Biotechnol.* **100**, 7727–7739.

Morin J. and Morse J. W. (1999) Ammonium release from resuspended sediments in the Laguna Madre estuary. *Mar. Chem.* **65**, 97–110.

Murphy A. E., Bulseco A. N., Ackerman R., Vineis J. H. and Bowen J. L. (2020) Sulphide addition favours respiratory ammonification (DNRA) over complete denitrification and alters the active microbial community in salt marsh sediments. *Environ. Microbiol.* **22**, 2124–2139.

Naqvi S. W. A., Lam P., Narvenkar G., Sarkar A., Naik H., Pratihary A.,

Shenoy D. M., Gauns M., Kurian S., Damare S., Duret M., Lavik G. and Kuypers M. M. M. (2018) Methane stimulates massive nitrogen loss from freshwater reservoirs in India. *Nat. Commun.*

Nie S., Lei X., Zhao L., Wang Y., Wang F., Li H., Yang W. and Xing S. (2018) Response of activity, abundance, and composition of anammox bacterial community to different fertilization in a paddy soil. *Biol. Fertil. Soils* **54**, 977–984.

Nizzoli D., Carraro E., Nigro V. and Viaroli P. (2010) Effect of organic enrichment and thermal regime on denitrification and dissimilatory nitrate reduction to ammonium (DNRA) in hypolimnetic sediments of two lowland lakes. *Water Res.* **44**, 2715–2724.

Norði K. a´ and Thamdrup B. (2014) Nitrate-dependent anaerobic methane oxidation in a freshwater sediment. *Geochim. Cosmochim. Acta* **132**, 141–150.

Orphan V. J., House C. H., Hinrichs K. U., McKeegan K. D. and DeLong E. F. (2002) Multiple archaeal groups mediate methane oxidation in anoxic cold seep sediments. *Proc. Natl. Acad. Sci. U. S. A.* **99**, 7663–7668.

Oswald K., Graf J. S., Littmann S., Tienken D., Brand A., Wehrli B., Albertsen M., Daims H., Wagner M., Kuypers M. M. M., Schubert C. J. and Milucka J. (2017) Crenothrix are major methane consumers in stratified lakes. *ISME J.* **11**, 2124–2140.

Oswald K., Milucka J., Brand A., Littmann S., Wehrli B., Kuypers M. M. M. and Schubert C. J. (2015) Light-dependent aerobic methane oxidation reduces methane emissions from seasonally stratified lakes. *PLoS One* **10**, 1–22.

Padilla C. C., Bristow L. A., Sarode N., Garcia-robledo E., Ramírez E. G., Benson C. R., Bourbonnais A., Altabet M. A., Girguis P. R., Thamdrup B.

and Stewart F. J. (2016) NC10 bacteria in marine oxygen minimum zones. , 1–5.

Pajares S., Merino-Ibarra M., Macek M. and Alcocer J. (2017) Vertical and seasonal distribution of picoplankton and functional nitrogen genes in a high-altitude warm-monomictic tropical lake. *Freshw. Biol.* **62**, 1180–1193.

Peña Sanchez G. A., Mayer B., Wunderlich A., Rein A. and Einsiedl F. (2022) Analysing seasonal variations of methane oxidation processes coupled with denitrification in a stratified lake using stable isotopes and numerical modeling. *Geochim. Cosmochim. Acta*.

Peng L., Nie W. B., Ding J., Ni B. J., Liu Y., Han H. J. and Xie G. J. (2020) Denitrifying Anaerobic Methane Oxidation and Anammox Process in a Membrane Aerated Membrane Bioreactor: Kinetic Evaluation and Optimization. *Environ. Sci. Technol.* **54**, 6968–6977.

Praetzel L. S. E., Nora P., Schilling S., Marcel, Schmiedeskamp Gabriele B. and Knorr K.-H. (2020) Organic matter and sediment properties determine in-lake variability of sediment CO2 and CH4 production and emissions of a small and shallow lake. *Biogeosciences*, 5057–5078.

Qin H., Han C., Jin Z., Wu L., Deng H., Zhu G. and Zhong W. (2018) Vertical distribution and community composition of anammox bacteria in sediments of a eutrophic shallow lake. *J. Appl. Microbiol.* **125**, 121–132.

Quinlan A. V (1986) Optimum temperature shift for Nitrobacter Winogradskyi. *Water Res.* **20**.

Raghoebarsing A. A., Pol A., Van De Pas-Schoonen K. T., Smolders A. J. P., Ettwig K. F., Rijpstra W. I. C., Schouten S., Sinninghe Damsté J. S., Op Den Camp H. J. M., Jetten M. S. M. and Strous M. (2006) A microbial consortium couples anaerobic methane oxidation to denitrification. *Nature* **440**, 918–921.

Ramesh Reddy K. and DeLaune R. D. (2008) *Biogeochemistry of Wetlands: Science and Applications*., CRC Press, Taylor and Francis Group, LLC.

Reeburgh W. S. and Heggie D. T. (1977) Microbial methane consumption reactions and their effect on methane distributions in freshwater and marine environments. *Limnol. Oceanogr.* **22**, 1–9.

Robert Hamersley M., Woebken D., Boehrer B., Schultze M., Lavik G. and Kuypers M. M. M. (2009) Water column anammox and denitrification in a temperate permanently stratified lake (Lake Rassnitzer, Germany). *Syst. Appl. Microbiol.* **32**, 571–582.

Robertson G. P. and Groffman P. M. (2007) Nitrogen Transformations BT - Soil Microbiology, Ecology, and Biochemistry. *Soil Microbiol. Ecol. Biochem.*, 341–364.

Rockström J., Steffen W., K. Noone, Å. Persson, F. S. Chapin, E. F. Lambin, T. M. Lenton, M. Scheffer, C. Folke, H. J. Schellnhuber, B. Nykvist, C. A. de Wit, T. Hughes, S. van der Leeuw, H. Rodhe, S. Sörlin, P. K. Snyder, R. Costanza, U. Svedin, M. Falkenmark, L. Karlberg, R. W. Corell, V. J. Fabry, J. Hansen, B. Walker, D. Liverman, K. Richardson, P. Crutzen and J. A. Foley (2009) A safe operation space for humanity. *Nature* **461**, 472–475.

Roland F. A. E., Darchambeau F., Borges A. V., Morana C., De Brabandere L., Thamdrup B. and Crowe S. A. (2018) Denitrification, anaerobic ammonium oxidation, and dissimilatory nitrate reduction to ammonium in an East African Great Lake (Lake Kivu). *Limnol. Oceanogr.* **63**, 687–701.

Roland F. A. E., Darchambeau F., Morana C., Bouillon S. and Borges A. V. (2017) Emission and oxidation of methane in a meromictic, eutrophic and temperate lake (Dendre, Belgium). *Chemosphere* **168**, 756–764.

Roland F. A. E., Darchambeau F., Morana C., Crowe S. A. and Borges A. V

(2016) Anaerobic methane oxidation in an East African great lake (Lake Kivu). *Biogeosciences Discuss.*, 1–27.

Rudd J. W. M. (1980) Methane oxidation in Lake Tanganyika (East Africa). *Limnol. Oceanogr.* **25**, 958–963.

Rudd J. W. M., Furutani A., Flett R. J. and Hamilton R. D. (1976) Factors controlling methane oxidation in shield lakes: The role of nitrogen fixation and oxygen concentration. *Limnol. Oceanogr.* **21**, 357–364.

Rudd J. W. M., Hamilton R. D. and Campbell N. E. R. (1974) Measurement of microbial oxidation of methane in lake water. *Limnol. Oceanogr.* **19**, 519–524.

Rudy J. W. M., Furutani A., Flett R. J. and Hasmilton R. D. (1976) Factors controlling methane oxidation in shield lakes: The role of nitrogen fixation and oxygen concentration. *Limnol. Oceanogr.* **21**, 357–364.

Russ L., Speth D. R., Jetten M. S. M., Op den Camp H. J. M. and Kartal B. (2014) Interactions between anaerobic ammonium and sulfur-oxidizing bacteria in a laboratory scale model system. *Environ. Microbiol.* **16**, 3487–3498.

Saad O. A. L. O. and Conrad R. (1993) Temperature dependence of nitrification, denitrification, and turnover of nitric oxide in different soils. *Biol. Fertil. Soils*, 21–27.

Salas De León D. A., Alcocer J., Ardiles Gloria V. and Quiroz-Martínez B. (2016) Estimation of the eddy diffusivity coefficient in a warm monomictic tropical lake. *J. Limnol.* **75**, 161–168.

Schleper C. and Nicol G. W. (2010) *Ammonia-oxidising archaea - physiology, ecology and evolution*., Elsevier Ltd.

Schouten S., Strous M., Kuypers M. M. M., Rijpstra W. I. C., Baas M.,

Schubert C. J., Jetten M. S. M. and Damsté J. S. S. (2004) Stable carbon isotopic fractionations associated with inorganic carbon fixation by anaerobic ammonium-oxidizing bacteria. *Appl. Environ. Microbiol.* **70**, 3785–3788.

Schubert C. J., Durisch-Kaiser E., Wehrli B., Thamdrup B., Lam P. and Kuypers M. M. M. (2006) Anaerobic ammonium oxidation in a tropical freshwater system (Lake Tanganyika). *Environ. Microbiol.* **8**, 1857–1863.

Schubert C. J., Lucas F. S., Stierli R., Diem T., Scheidegger O., Vazquez F. and Mu B. (2010) Oxidation and emission of methane in a monomictic lake (Rotsee , Switzerland). *Aquat. Sci.*, 455–466.

Schubert C. J., Vazquez F., Lösekann-Behrens T., Knittel K., Tonolla M. and Boetius A. (2011) Evidence for anaerobic oxidation of methane in sediments of a freshwater system (Lago de Cadagno). *FEMS Microbiol. Ecol.* **76**, 26–38.

Sebilo M., Mayer B., Grably M., Billion D. and Mariotti A. (2004) The use of the "ammonium diffusion" method for δ15N-NH4+and δ15N-NO3- Measurements: Comparison with other techniques. *Environ. Chem.* **1**, 99–103.

Segarra K. E. A., Schubotz F., Samarkin V., Yoshinaga M. Y., Hinrichs K. U. and Joye S. B. (2015) High rates of anaerobic methane oxidation in freshwater wetlands reduce potential atmospheric methane emissions. *Nat. Commun.* **6**, 1–8.

Shammas N. K. (1986) Interactions of temperature, pH, and biomass on the nitrification process. *Water Pollut. Control Fed.* **58**, 52–59.

Shen L., Liu S., Zhu Q. and Li X. (2014) Distribution and Diversity of Nitrite-Dependent Anaerobic Methane-Oxidising Bacteria in the Sediments of the Qiantang River. , 341–349.

Sigman D. M., Casciotti K. L., Andreani M., Barford C., Galanter M. and Böhlke J. K. (2001) A bacterial method for the nitrogen isotopic analysis of nitrate in seawater and freshwater. *Anal. Chem.* **73**, 4145–4153.

Sigman D. M., Robinson R., Knapp A. N., Van Geen A., McCorkle D. C., Brandes J. A. and Thunell R. C. (2003) Distinguishing between water column and sedimentary denitrification in the Santa Barbara Basin using the stable isotopes of nitrate. *Geochemistry, Geophys. Geosystems* **4**, 1–20.

Smemo K. A. and Yavitt J. B. (2007) Evidence for Anaerobic CH4 Oxidation in Freshwater Peatlands. *Geomicrobiol. J.* **4**, 583–597.

Stoecker K., Nielsen P. H., Nielsen J. L., Baranyi C., Bendinger B., Toenshoff E. R., Daims H. and Wagner M. (2006) Cohn's Crenothrix is a filamentous methane oxidizer with an unusual methane monooxygenase. **103**, 2363–2367.

Stone M. and English M. C. (1993) Geochemical composition, phosphorus speciation and mass transport of fine-grained sediment in two Lake Erie tributaries. *Hydrobiologia* **253**, 17–29.

Straub K. L., Benz M., Schink B. and Widdel F. (1996) Anaerobic, nitrate-dependent microbial oxidation of ferrous iron. *Appl. Environ. Microbiol.* **62**, 1458–1460.

Strock J. S. (2008) Encyclopedia of Ecology. *Encycl. Ecol.*, 162–165.

Sundh I., Bastviken D. and Tranvik L. J. (2005) Abundance, activity, and community structure of pelagic methane-oxidizing bacteria in temperate lakes. *Appl. Environ. Microbiol.* **71**, 6746–6752.

Thamdrup B. and Dalsgaard T. (2002) Production of N2 through anaerobic ammonium oxidation coupled to nitrate reduction in marine sediments. *Appl. Environ. Microbiol.* **68**, 1312–1318.

Thamdrup B., Dalsgaard T., Jensen M. M., Ulloa O., Farías L. and Escribano R. (2006) Anaerobic ammonium oxidation in the oxygen-deficient waters off northern Chile. *Limnol. Oceanogr.* **51**, 2145–2156.

Thauer R. K. and Shima S. (2008) Methane as fuel for anaerobic microorganisms. *Ann. N. Y. Acad. Sci.* **1125**, 158–170.

Thunell R. C., Sigman D. M., Muller-Karger F., Astor Y. and Varela R. (2004) Nitrogen isotope dynamics of the Cariaco Basin, Venezuela. *Global Biogeochem. Cycles* **18**.

Tiedje J. M. (1988) Ecology of denitrification and dissimilatory nitrate reduction to ammonium. *Environ. Microbiol. Anaerobes*, 179–244.

Töwe S., Albert A., Kleineidam K., Brankatschk R., Dümig A., Welzl G., Munch J. C., Zeyer J. and Schloter M. (2010) Abundance of Microbes Involved in Nitrogen Transformation in the Rhizosphere of Leucanthemopsis alpina (L.) Heywood Grown in Soils from Different Sites of the Damma Glacier Forefield. *Microb. Ecol.* **60**, 762–770.

Töwe S., Wallisch S., Bannert A., Fischer D., Hai B., Haesler F., Kleineidam K. and Schloter M. (2011) Improved protocol for the simultaneous extraction and column-based separation of DNA and RNA from different soils. *J. Microbiol. Methods* **84**, 406–412.

Utsumi M., Nojiri Y., Nakamura T., Nozawa T., Otsuki A. and Seki H. (1998) Oxidation of dissolved methane in a eutrophic, shallow lake: Lake Kasumigaura, Japan. *Limnol. Oceanogr.* **43**, 471–480.

Valentine D. L. (2002) Biogeochemistry and microbial ecology of methane oxidation in anoxic environments: A review. *Antonie van Leeuwenhoek, Int. J. Gen. Mol. Microbiol.* **81**, 271–282.

Valentine D. L. and Reeburgh W. S. (2000) New perspectives on anaerobic methane oxidation. *Environ. Microbiol.* **2**, 477–484.

de Visscher A., de Pourcq I. and Chanton J. (2004) Isotope fractionation effects by diffusion and methane oxidation in landfill cover soils. *J. Geophys. Res. Atmos.* **109**, 1–8.

Wakeham S. G. and Lee C. (1993) Production, transport, and alteration of particulate organic matter in the marine water column. *Org. geochemistry Princ. Appl.*, 145–169.

Wang J., Wang S., Jin X., Zhu S. and Wu F. (2008) Ammonium release characteristics of the sediments from the shallow lakes in the middle and lower reaches of Yangtze River region, China. *Environ. Geol.* **55**, 37–45.

Wang L. and Li Y. (2014) Nitrite accumulation and nitrous oxide emission during denitrification processes with quinoline or indole as the sole carbon source.

Wang Y., Huang P., Ye F., Jiang Y., Song L., Op den Camp H. J. M., Zhu G. and Wu S. (2016) Nitrite-dependent anaerobic methane oxidizing bacteria along the water level fluctuation zone of the Three Gorges Reservoir. *Appl. Microbiol. Biotechnol.* **100**, 1977–1986.

Wang Y., Zhu G., Harhangi H. R., Zhu B., Jetten M. S. M., Yin C. and Op den Camp H. J. M. (2012) Co-occurrence and distribution of nitrite-dependent anaerobic ammonium and methane-oxidizing bacteria in a paddy soil. *FEMS Microbiol. Lett.*, 1–10.

Ward B. B. (2003) Significance of anaerobic ammonium oxidation in the ocean. *Trends Microbiol.* **11**, 408–410.

Weber H. S., Habicht K. S. and Thamdrup B. (2017) Anaerobic methanotrophic archaea of the ANME-2d cluster are active in a low-sulfate, iron-rich freshwater sediment. *Front. Microbiol.* **8**, 1–13.

Wei W., Isobe K., Nishizawa T., Zhu L., Shiratori Y., Ohte N., Koba K., Otsuka S. and Senoo K. (2015) Higher diversity and abundance of

denitrifying microorganisms in environments than considered previously. *ISME J.* **9**, 1954–1965.

Wenk C. B., Blees J., Zopfi J., Veronesi M., Bourbonnais A., Schubert C. J., Niemann H. and Lehmann M. F. (2013) Anaerobic ammonium oxidation (anammox) bacteria and sulfide-dependent denitrifiers coexist in the water column of a meromictic south-alpine lake. *Limnol. Oceanogr.* **58**, 1–12.

Wenk C. B., Zopfi J., Blees J., Veronesi M., Niemann H. and Lehmann M. F. (2014) Community N and O isotope fractionation by sulfide-dependent denitrification and anammox in a stratified lacustrine water column. *Geochim. Cosmochim. Acta* **125**, 551–563.

Whiticar M. J. (1999) Carbon and hydrogen isotope systematics of bacterial formation and oxidation of methane. *Chem. Geol.* **161**, 291–314.

Whiticar M. J. and Faber E. (1986) Methane oxidation in sediment and water column environments-Isotope evidence. *Org. Geochem.* **10**, 759–768.

Wild L. M., Mayer B. and Einsiedl F. (2018) Decadal Delays in Groundwater Recovery from Nitrate Contamination Caused by Low O2 Reduction Rates. *Water Resour. Res.* **54**, 9996–10,012.

Winogradsky S. (1890) Recherches sur les organismes de la nitrification. *Ann. Inst. Pasteur* **4**, 213–331.

Wunderlich A., Meckenstock R. and Einsiedl F. (2012) Effect of different carbon substrates on nitrate stable isotope fractionation during microbial denitrification. *Environ. Sci. Technol.* **46**, 4861–4868.

Wunderlich A., Meckenstock R. U. and Einsiedl F. (2013) A mixture of nitrite-oxidizing and denitrifying microorganisms affects the δ18O of dissolved nitrate during anaerobic microbial denitrification depending on the δ18O of ambient water. *Geochim. Cosmochim. Acta* **119**, 31–45.

Yan Z., Joshi P., Gorski C. A. and Ferry J. G. (2018) A biochemical framework for anaerobic oxidation of methane driven by Fe(III)-dependent respiration. *Nat. Commun.* **9**, 1–9.

Yang J., Jiang H., Wu G., Hou W., Sun Y., Lai Z. and Dong H. (2012) Co-occurrence of nitrite-dependent anaerobic methane oxidizing and anaerobic ammonia oxidizing bacteria in two Qinghai-Tibetan saline lakes. *Front. Earth Sci.* **6**, 383–391.

Zhao J., ZHU D., FAN J., HUA Y. and ZHOU W. (2015) Seasonal Variation of Anammox and Denitrification in Sediments of Two Eutrophic Urban Lakes. *Polish J. Environ. Stud.* **24**, 2779–2783.

Zhu B., Dijk G. Van, Fritz C., Smolders A. J. P., Pol A., Jetten M. S. M. and Ettwig K. F. (2012) Anaerobic Oxidization of Methane in a Minerotrophic Peatland : Enrichment of Nitrite-Dependent Methane-Oxidizing Bacteria. **78**, 8657–8665.

Zhu G., Jetten M. S. M., Kuschk P., Ettwig K. F. and Yin C. (2010) Potential roles of anaerobic ammonium and methane oxidation in the nitrogen cycle of wetland ecosystems. *Appl. Microbiol. Biotechnol.* **86**, 1043–1055.

Zhu J., He Y., Zhu Y., Huang M. and Zhang Y. (2017) Biogeochemical sulfur cycling coupling with dissimilatory nitrate reduction processes in freshwater sediments. *Environ. Rev.*, 1–12.

Zhu J., He Y., Zhu Y., Huang M. and Zhang Y. (2018) Biogeochemical sulfur cycling coupling with dissimilatory nitrate reduction processes in freshwater sediments. *Environ. Rev.* **26**, 121–132.

Appendices

A.1 DATA USED FOR THE CALCULATION K_z FOR 2018

Table A 1. Data used for the calculation K_z for the sampling campaign in 2018

Month	Depth	Temperature (C°)	ρ_z (kg m^{-3})	$d\rho$ (kg m^{-3})	dz (kg m^{-3})	K_z (m^{2}s^{-1})
May	8	6.6	999.631225	0.34328438	14	2.21*10^{-6}
	22	4.1	999.974509			
June	8	9.1	998.220775	1.73533079	14	9.83 *10^{-6}
	22	4.7	999.956106			
July	8	9	998.30507		14	1.01*10^{-6}
	22	4.9	999.942902	1.63783123		
August	8	10	997.339787		14	8.02*10^{-7}
	22	4.9	999.942902	2.60311446		
August (second campaign)	8	10.1	997.227696		14	7.85*10^{-7}
	22	4.9	999.942902	2.71520599		
September	8	11	996.081768		14	6.59*10^{-7}
	22	4.9	999.942902	3.86113408		
October	8	12.5	993.576714		14	5.14*10^{-7}
	22	5.1	999.925589	6.34887503		
December	8	6	999.787854		14	3.38*10^{-7}
	22	5	999.93478	0.14692607		
					Average	***1.29*10^{-6}**

For this study a_0 was calculated to be 0.000343 $cm^2 s^{-2}$, similar to values reported in other field- studies for stratified lakes (Gargett A.E., 1984; Lewis and Landing, 1991; Blees et al., 2014). Calculated K_z for lake Fohnsee was on average $1.3*10^6$, $m^2\ s^{-1}$.

This value is in agreement with typical values found for the hypolimnion in stratified lakes (Wenk et al., 2014; Salas De León et al., 2016), and it fits precisely to a K_z-value found for lake Fohnsee in an earlier study (Einsiedl et al., 2020). to reduce model complexity, we assumed Kz to be constant over the model domain below the thermocline (8m to 22m) where density gradients are not strong.

A.2 SIGNIFICANCE OF THE DUAL ISOTOPE PLOT (2D PLOT) OF $\Delta^{18}O$ VS. $\Delta^{15}N$ FOR THE DATA SET 2018

We interpreted the concentrations and stable isotope compositions of nitrate in the different redox zones of the lake water column. In the oxygenated portion of the lake, nitrate concentrations were elevated and $\delta^{15}N$ and $\delta^{18}O$ of nitrate remained constant at low values (Fig. A1). In the NMTZ, concentrations of nitrate decreased while $\delta^{15}N$ and $\delta^{18}O$ of NO_3^- increased markedly by up to 42.0 and 38.2‰, respectively. This provides clear evidence that denitrification was the process responsible for decreasing nitrate concentration with increasing depth in the NMTZ, where methane concentrations decreased and $\delta^{13}C$ values of methane increased.

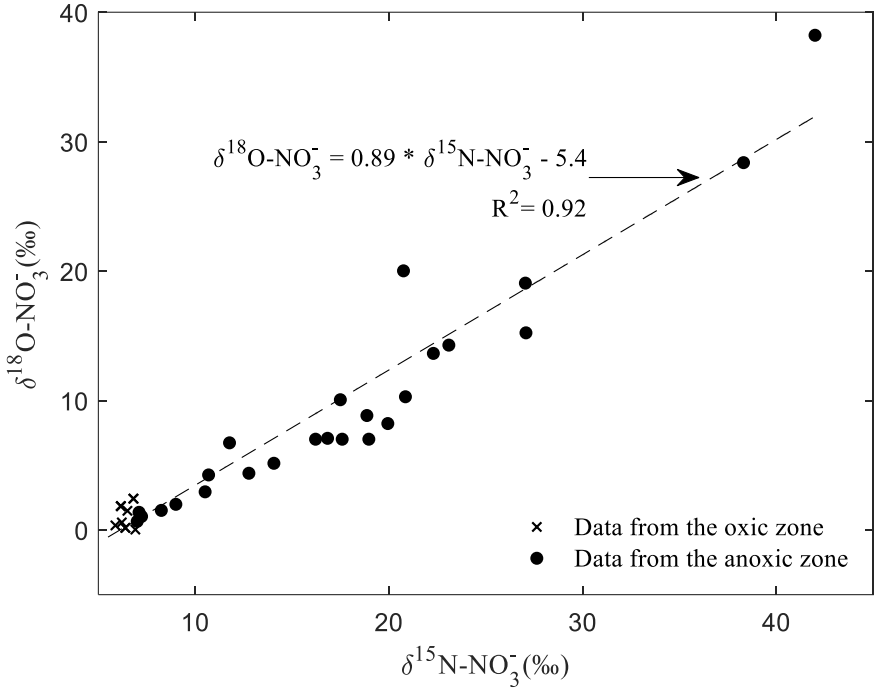

Figure A 1. $\delta^{15}N\text{-}NO_3^-$ plotted against $\delta^{18}O\text{-}NO_3^-$ values and fitted linear equation

The dual isotope plot (2D plot) of $\delta^{18}O$ vs. $\delta^{15}N$ showed a good linear correlation (R^2 = 0.92) with a slope of 0.89 (Fig. A1). Laboratory studies with pure cultures of denitrifying bacteria have consistently shown a proportional increase of $\delta^{18}O$ and $\delta^{15}N$ following linear trajectories near 1 (Casciotti et al., 2002; Sigman et al., 2003; Granger et al., 2008; Knöller et al., 2011; Wunderlich et al., 2013) as observed in our study at Lake Fohnsee.

Deviations from a slope of 1 for microbial denitrification (Knöller et al., 2011; Wunderlich et al., 2012) have been previously explained by the overlap of isotopic effects produced by oxidative NO_3^- formation (Granger and Wankel, 2016) by occasional downward intrusion of O_2 into anoxic environments (Hartog et al., 2002) and/or by anammox (Granger and Wankel, 2016). Both processes lead to a slope on the $\delta^{18}O$ vs. $\delta^{15}N$ cross plot for nitrate that is considerably lower than the expected slope for denitrification of 1. Since the slope observed in Fig. A1 is only slightly lower than 1, we conclude that neither

anammox nor downward intrusion of O_2 into anoxic environments were significant at Lake Fohnsee during our observation period.

A.3 FITTED FIRST-ORDER DEGRADATION CONSTANTS FOR AEROBIC (KAE) AND ANAEROBIC (KAN)

Table A 2 *Fitted first-order degradation constants for aerobic (k_{ae}) and anaerobic (k_{an}) methane oxidation (obtained from inverse modeling, solving Eqs. 6 and 7) and statistical evaluation of the model curve fits for methane concentration vs. depth presented in Fig. 6.6b. MSE: standard error of the mean.*

Month	***k_{ae} (s^{-1})***	***k_{an} (s^{-1})***	***Normalized MSE (-)***	**MSE (mmol L^{-1})**
May	$4.20*10^{-6}$	$5.30*10^{-7}$	0.7642	$1.40*10^{-5}$
June	$1.80*10^{-6}$	$5.00*10^{-7}$	0.8595	$8.25*10^{-4}$
July	$4.50*10^{-6}$	$6.00*10^{-7}$	0.9898	$8.38*10^{-4}$
August	$1.00*10^{-6}$	$6.00*10^{-7}$	0.9907	$6.88*10^{-5}$
September	$4.50*10^{-6}$	$5.20*10^{-7}$	0.9406	$5.18*10^{-3}$
October	$4.20*10^{-6}$	$6.10*10^{-7}$	0.7371	$1.26*10^{-2}$
December	$1.90*10^{-6}$	0.00	0.9491	$3.13*10^{-3}$

Vertical changes of the methane concentrations are controlled by both anaerobic and aerobic methane oxidation governed by different degradation constants. Table A2 reveals that k_{ae} and k_{an} fitted from inverse modeling were in a similar range for all months, but the degradation rate constants for aerobic oxidation k_{ae} were consistently about one order of magnitude higher than those for anaerobic methane oxidation k_{an}. First-order degradation rate constants for aerobic ($2.7 *10^{-6}$ s^{-1}) and anaerobic methane oxidation (7.7

*10^{-7} s^{-1}) with nitrate were measured in batch experiments in a study conducted in the water column of the temperate lake Dendre in Belgium (Roland et al., 2016). These rate constants are very similar to the first-order degradation rate constants (k_{an}) found at lake Fohnseeby applying the diffusion-reaction model approach. Our results are also in excellent agreement with the findings of Einsiedl et al., (2020) who used a simple 1D diffusion model linked with a reaction term to calculate first order rate constants for describing methane oxidation coupled with nitrate reduction at Lake Fohnsee (k_{an} = 3.5 *10^{-7} s^{-1}).

A.4 RESULTING ELECTRON BALANCE BETWEEN NITRATE AND METHANE FLUXES ASSUMING COMPLETE DENITRIFICATION

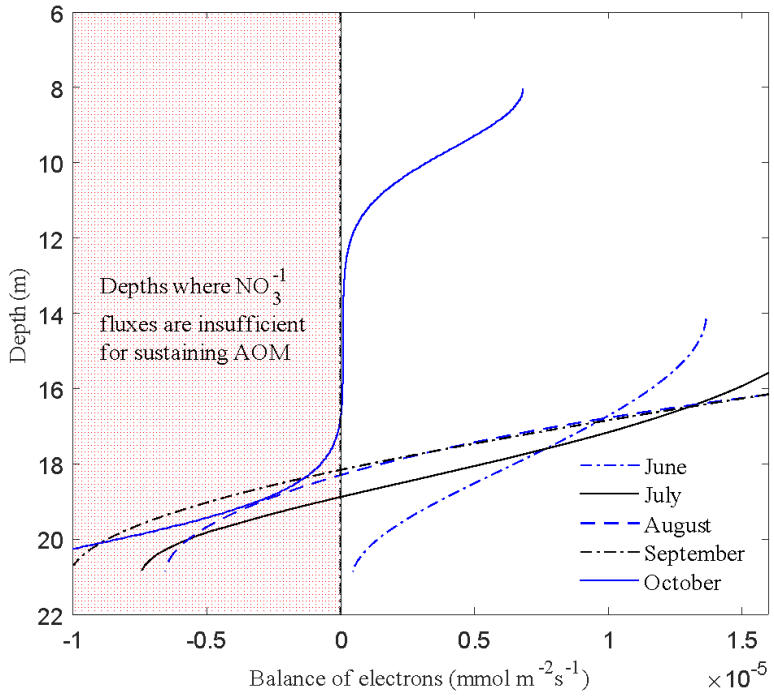

Figure A 2 Resulting electron balance between nitrate and methane fluxes assuming complete denitrification ($5CH_4 + 8NO_3^- + 8H+ \rightarrow 5CO_2 + 4N_2 + 14H_2O$) in the water column of lake

Fohnsee (June to October 2018). The curves crossing the zero line in the highlighted area correspond to the depths where nitrate fluxes would be insufficient to sustain AOM.

A.5 METHANE CONCENTRATIONS SIMULATIONS ASSUMING ONLY AEROBIC METHANE OXIDATION.

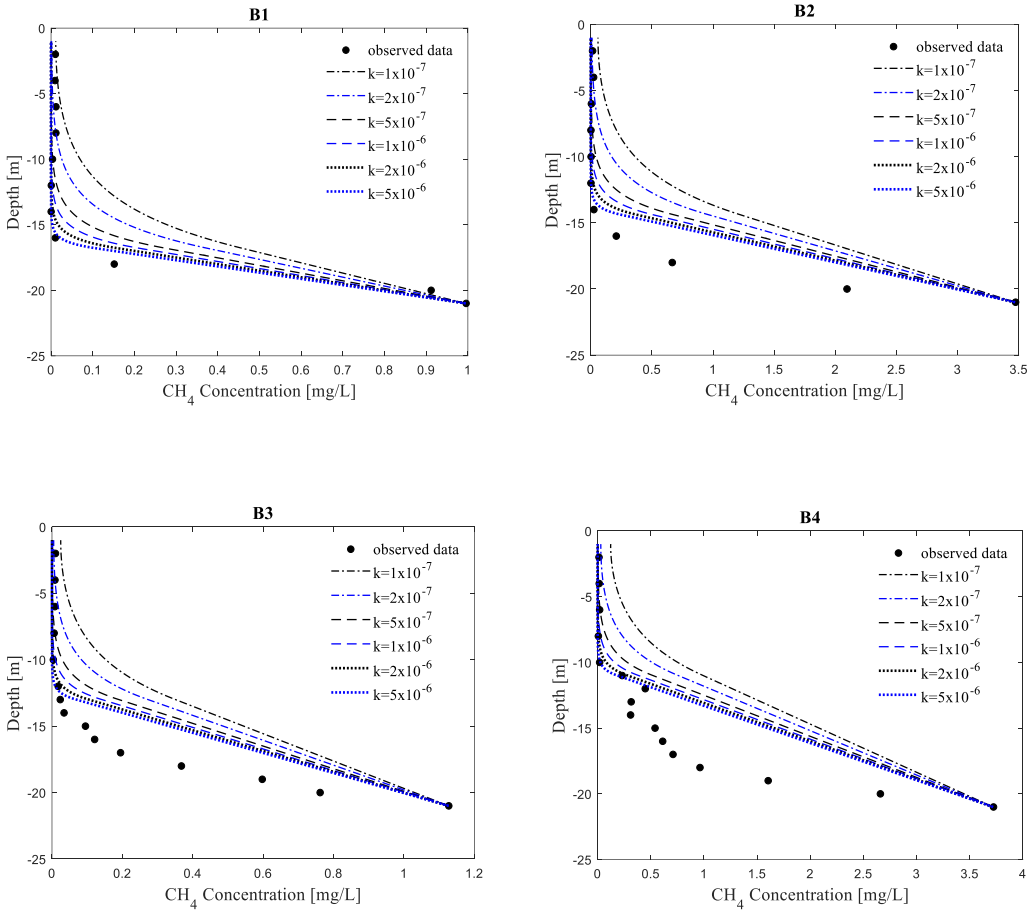

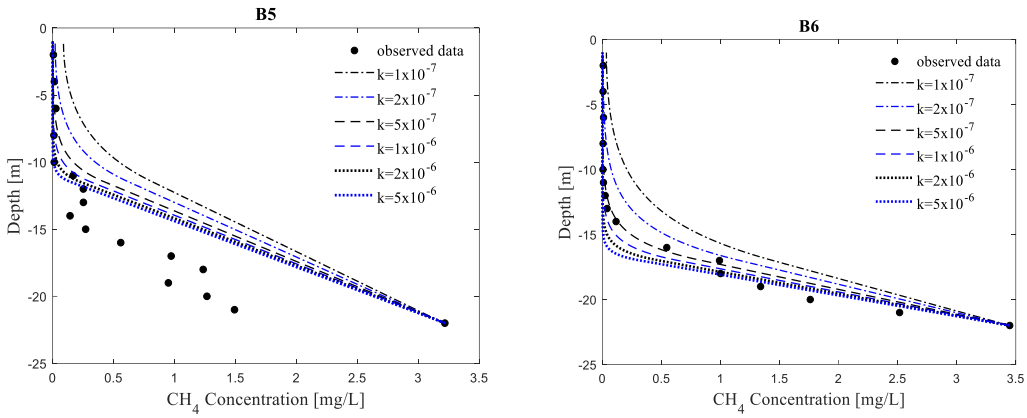

Figure A 3 Methane concentrations simulations assuming only aerobic methane oxidation for: B1. June, B2. July, B3. August, B4. September, B5. October, B6. December.

A.6. DIFFUSION-REACTION MODEL FOR Δ¹³C RESULTS ONLY CONSIDERING AEROBIC METHANE OXIDATION

Table A 3 Results and fit for the 13C-methane Diffusion-Reaction model only for aerobic methane oxidation

Month	*Enrichment factor Aerobic oxidation [‰]*	*MSE [‰]*	*Normalized MSE*	*SRMSE*
June	-10	150.12	-9.91	-2.303
	-15	23.7424	0.8384	0.598
	-20	23.31	0.8827	0.6575
	-25	34.2478	0.8679	0.6366
	-30	217.8	0.6493	0.4077
July	-10	186.2	-182.9	-12.56
	-15	42.01114	0.184	0.0967

	-20	21.58	0.7258	0.4764
	-25	18.72	0.9193	0.7159
	-30	135.84	0.7125	0.4638
	-10	56.17	-100.65	-9.08
	-15	20.3247	-0.8817	-0.3718
August	-20	14.5732	0.0308	0.0155
	-25	3.8	0.9042	0.6905
	-30	0.5605	0.99	0.9
	-10	37.6147	-82921	-2.0483
	-15	17.398	-0.1895	-0.0906
September	-20	5.9363	0.8195	0.5752
	-25	2.92	0.3758	0.2099
	-30	3.43	0.5461	0.3262
	-10	49.1195	-23.36111	-14.5
	-15	15.77	-0.0529	-0.2368
October	-20	13.7392	-0.1497	-0.0722
	-25	2.07	0.9373	0.7496
	-30	17.0142	0.8352	0.594
	-10	142.48	-81.39	-8.07
	-15	10.564	0.7189	0.4698
December	-20	8.62	0.8086	0.5626
	-25	71.5235	0.5334	0.3169
	-30	400.5024	0.1852	0.0974

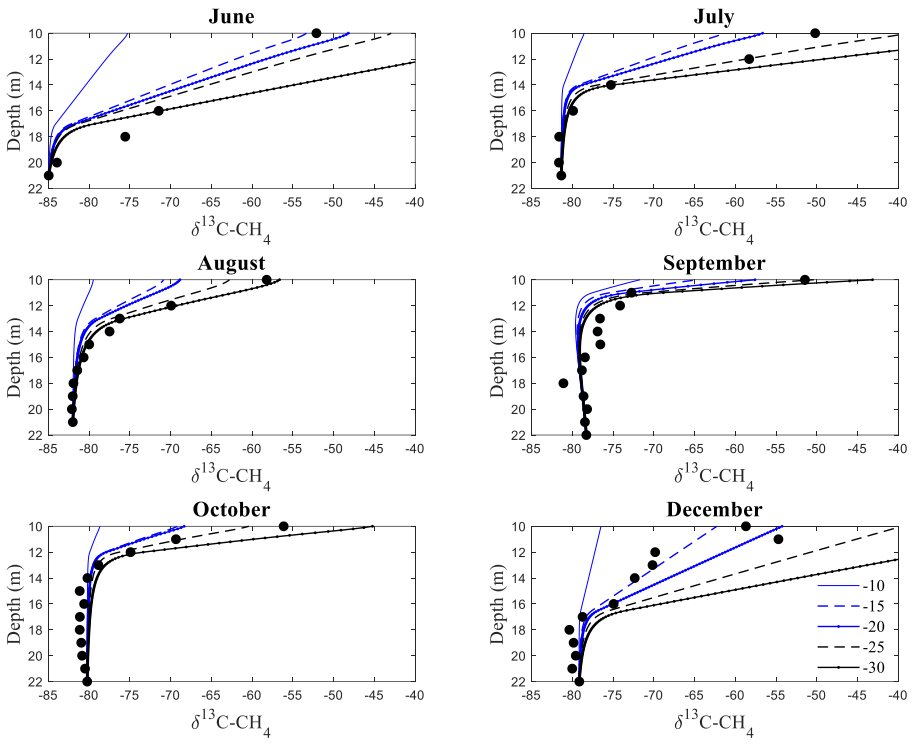

Figure A 4 Diffusion-reaction model for δ¹³C results only considering aerobic methane oxidation; enrichment factors between -10 ‰ to -30 ‰

A.7. ISOTOPE MODELING RESULTS FOR MAY, JULY AND SEPTEMBER

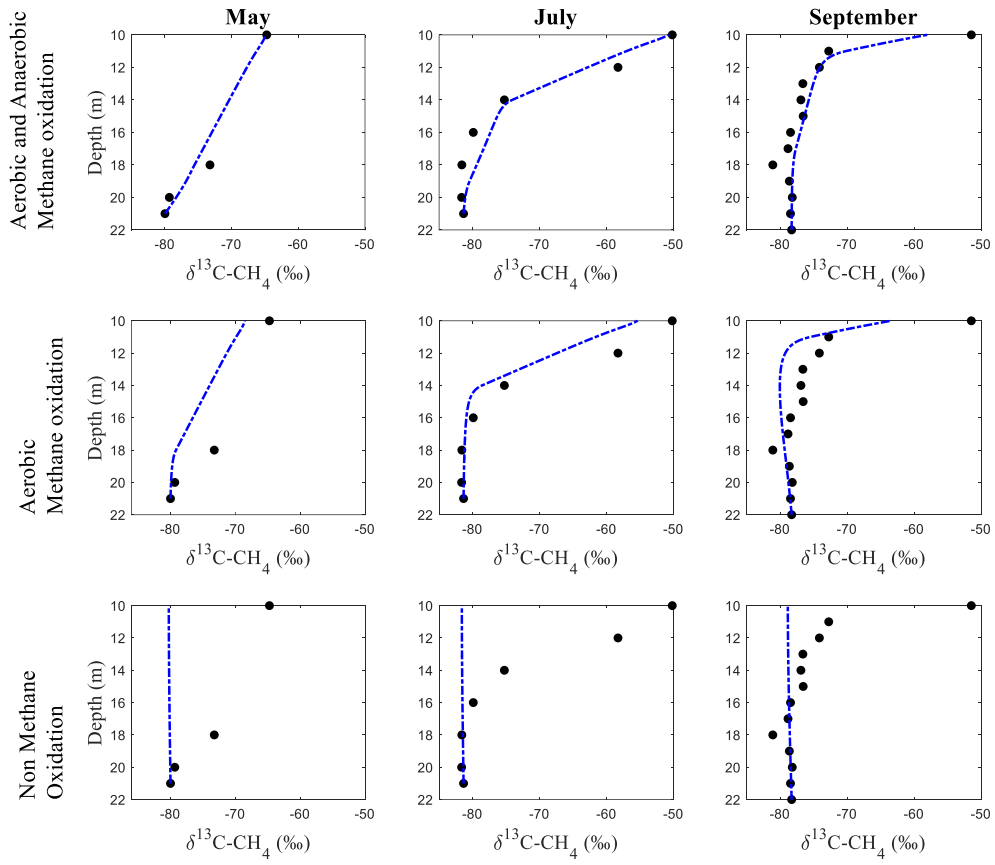

Figure A 5 Isotope Modeling results for May, July and September

A.8 DATA USED FOR THE CALCULATION K_z FOR THE SAMPLING CAMPAIGN IN 2019

Table A 4 Data used for the calculation K_z for 2019

Month	Depth(m)	Temperature (C°)	ρz (kg m⁻³)	N²(s)	K_z ¹⁴N (m²s⁻¹)	K_z ¹⁵N (m²s⁻¹)
	17	5.7	999.846			
June				0.0000		
	22	5.5	999.877	6	4.35*10⁻⁶	4.291*10⁻⁶

	10	6.3	999.717			
June(2)				0.0001		
	23	5.5	999.877	2	$3.11*10^{-6}$	$3.072*10^{-6}$
	11	6.4	999.690			
July				0.0001		
	23	5.6	999.862	4	$2.89*10^{-6}$	$2.849*10^{-6}$
	12	6.4	999.690			
August				0.0001		
	23	5.6	999.862	5	$2.77*10^{-6}$	$2.728*10^{-6}$
	12	6.75	999.583			
Septembe				0.0002		
r	23	5.8	999.828	2	$2.32*10^{-6}$	$2.287*10^{-6}$

A.9 METHANE ISOTOPES AND CONCENTRATIONS

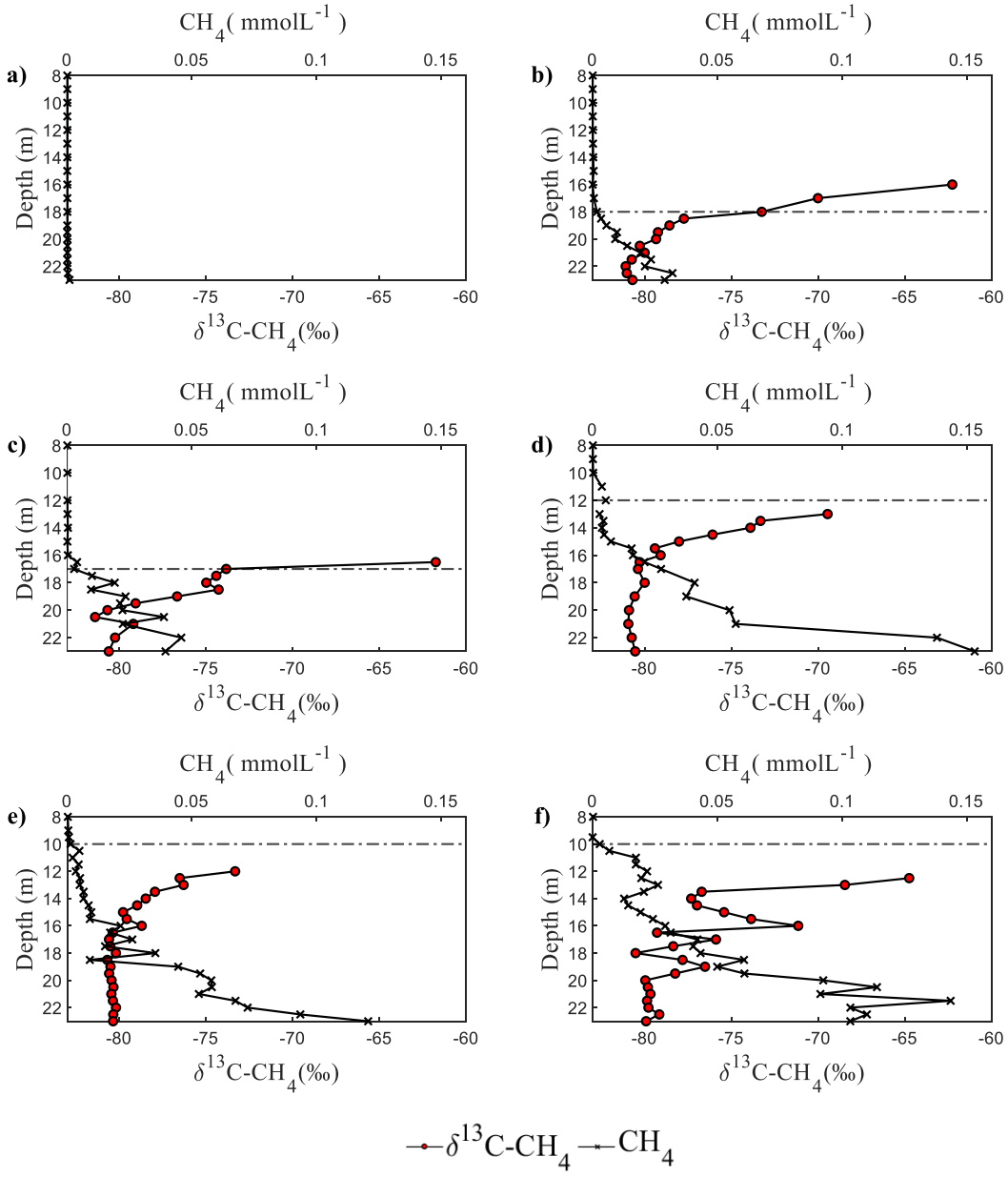

Figure A 6 Monthly δ¹³C in methane and methane concentrations in 2019 for: a) April, b) beginning of June, c) end of June, d) July, e) August, f) September

A.10 ENRICHMENT FACTORS FOR $^{15}N\text{-}NH_4^+$

To test whether anaerobic ammonium oxidation was predominant, we calculated stable isotope enrichment factors for anammox from the data from samples obtained in April, June and September using a closed system approach i.e closed-system Rayleigh model (Mariotti et al., 1981).

For July and August, no relationship was observed between the decrease in the ammonium concentrations and the increase of $\delta^{15}N\text{-}NH_4^+$ making a robust calculation of enrichment factors impossible ($R<0.6$).

$\varepsilon_{ana-NH_4^+}$ was -4.3‰, which is similar to $\varepsilon_{ana-NH_4^+}$ in the water column reported by Wenk et al. (2014) for anaerobic ammonium oxidation in lake Lugano. However, ε values could be affected to a low efflux-to-uptake ratio, overprinting by effects from micro-aerobic nitrification (Wenk et al., 2014), and other physical processes such as diffusion and convection instead of only microbial degradation. Thus, the use of $\varepsilon_{ana-NH_4^+}$ alone fell short for identifying anaerobic ammonium oxidation.

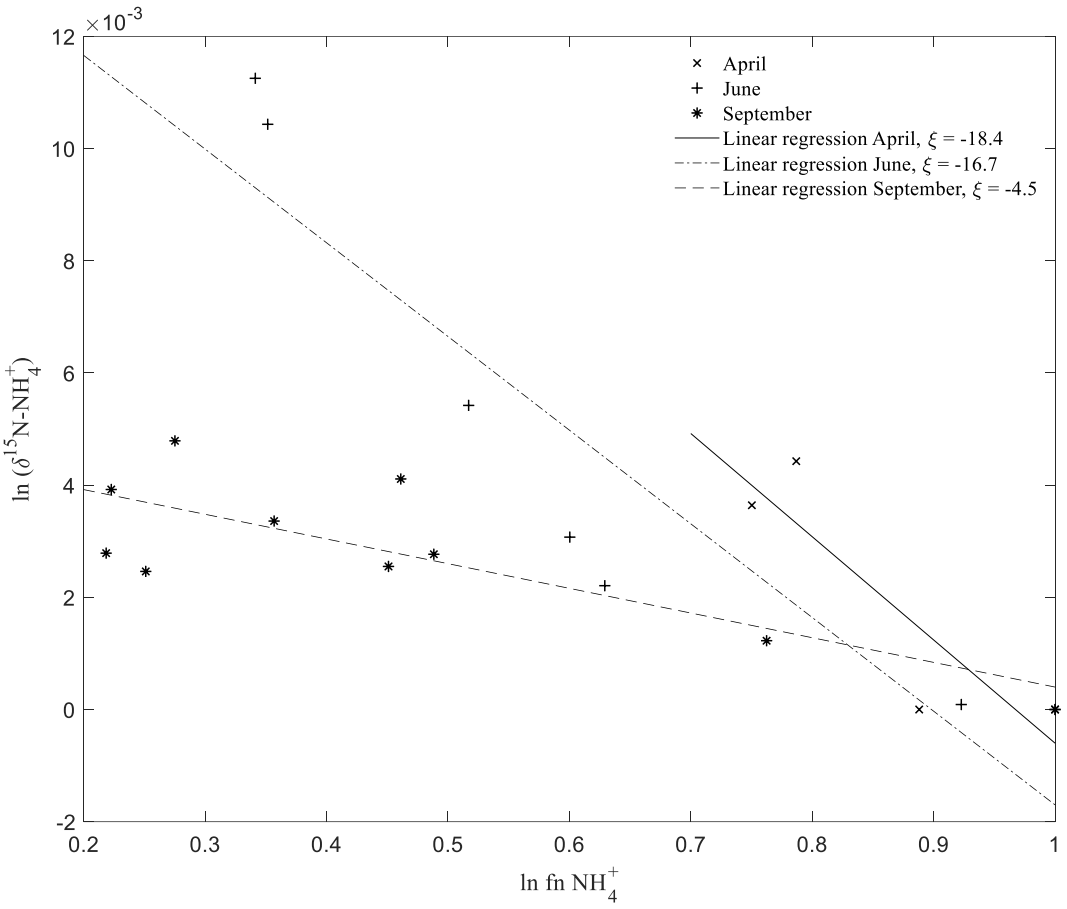

Figure A 7 Calculation of apparent nitrogen isotope enrichment factor (E) for ammonium (closed system approach) observed for April (crosses), June (plus signs) and September (asterisk)

A.11 DATA SET FOR 2019

Table A 5 Collected chemical and isotope data in the water column of Lake Fohnsee during the sampling campaigns. n.d refers to concentration values under the detection limit. Blank spaces were left where measurements were not conducted or where the results did not meet the quality standards.

Date	Depth (m)	O_2 ($mmolL^{-1}$)	NO_3^- ($mmolL^{-1}$)	SO_4^{2-} ($mmolL^{-1}$)	NH_4^+ ($mmolL^{-1}$)	CH_4 ($mmolL^{-1}$)	$\delta^{13}C$-CH_4 ‰	$\delta^{15}N$-NO_3^- ‰	$\delta^{18}O$-NO_3^- ‰	$\delta^{15}N$-NH_4^+ ‰
16.04.2019	8	0.30531	0.10562	0.09760	0.01273			8.06	2.38	
16.04.2019	9	0.26969	0.10463	0.09776	0.01608	n.d				
16.04.2019	10	0.24563	0.10424	0.09833	0.01729	n.d		8.12	2.55	
16.04.2019	11	0.22375	0.10438	0.09782	0.01717	n.d		8.03	2.43	
16.04.2019	12	0.21094	0.10346	0.09849	0.01897	n.d				
16.04.2019	13	0.20906	0.10307	0.09843	0.01956	n.d		8.00	2.58	
16.04.2019	14	0.19750	0.10254	0.09840	0.01966	n.d		7.66	2.34	
16.04.2019	15	0.18281	0.10205	0.09845	0.02013	n.d		7.64	2.29	
16.04.2019	16	0.17156	0.10004	0.09855	0.02051	n.d		7.46	2.55	
16.04.2019	17	0.16188	0.09527	0.09848	0.02225	n.d		7.38	2.40	

16.04.2019	18	0.14594	0.09345	0.09881	0.02239	n.d	6.33	3.06	
16.04.2019	19	0.13406	0.09221	0.09888	0.02564	n.d	6.18	2.20	18.8
16.04.2019	19.5		0.09099	0.09847	0.02351	n.d	6.18	2.34	
16.04.2019	20	0.11438	0.09147	0.09884	0.02445	n.d	6.15	2.35	18
16.04.2019	20.5		0.08194	0.09815	0.02753	n.d	6.08	2.46	
16.04.2019	21	0.08906	0.07972	0.09813	0.02894	n.d	6.06	2.59	13.2
16.04.2019	21.5		0.07494	0.09796	0.03142	n.d	6.11	2.84	
16.04.2019	22	0.07469	0.07273	0.09804	0.03258	n.d	6.16	3.09	14.3
16.04.2019	22.5		0.07019	0.09724	0.03399	0.00027	6.22	3.52	
16.04.2019	23	0.02844	0.06285	0.09581	0.03808	0.00091	6.67	3.70	
05.06.2019	8	0.26563	0.08950	0.09187	0.03454	n.d	6.72	2.30	
05.06.2019	9	0.17500	0.09085	0.09197	0.03609	n.d	6.34	2.09	
05.06.2019	10	0.15000	0.09670	0.09203	0.03349	n.d	5.43	1.48	29.1
05.06.2019	11	0.13750	0.09832	0.09156	0.03660	n.d	5.07	1.17	
05.06.2019	12	0.12063	0.09653	0.09056	0.03066	n.d	4.99	1.09	42.4
05.06.2019	13	0.09625	0.10034	0.09037	0.02956	n.d	5.50	0.89	

05.06.2019	14	0.07656	0.10633	0.09118	0.02736	n.d		6.86	0.69	46.2
05.06.2019	15	0.05750	0.10624	0.09237	0.02643	0.00042		7.11	0.61	
05.06.2019	16	0.03656	0.09944	0.09046	0.01300	0.00034	-62.27	6.79	0.99	31.2
05.06.2019	17	0.00625	0.09022	0.08999	0.02908	0.00052	-70.01	7.18	1.69	37.5
05.06.2019	18	0.00219	0.08136	0.08999	0.03553	0.00175	-73.25	7.79	2.60	27.5
05.06.2019	18.5	n.d	0.07740	0.08939	0.03507	0.00340	-77.74	8.09	2.94	
05.06.2019	19	n.d	0.07333	0.08907	0.03627	0.00554	-78.57	8.43	3.49	25.06
05.06.2019	19.5	n.d	0.06251	0.08888	0.04074	0.00979	-79.23	9.47	4.49	
05.06.2019	20	n.d	0.06272	0.08861	0.04121	0.00906	-79.34	9.37	4.35	19.97
05.06.2019	20.5	n.d	0.04588	0.08807	0.04733	0.01384	-80.28	11.59	5.70	
05.06.2019	21	n.d	0.04546	0.08786	0.04985	0.01921	-80.00	11.72	5.73	18.02
05.06.2019	21.5	n.d	0.02153	0.08690	0.06330	0.02340	-80.74	15.81	5.88	
05.06.2019	22	n.d	0.02888	0.08702	0.06003	0.02095	-81.09	14.52	6.26	17.22
05.06.2019	22.5	n.d	0.01514	0.08618	0.06764	0.03203	-81.03	17.31	5.94	
05.06.2019	23	n.d	0.02239	0.08638	0.06348	0.02890	-80.70	15.37	10.02	14.72
18.06.2019	8	0.15781	0.09039	0.09072	n.d	n.d	n.d	6.61	1.92	

18.06.2019	9	0.11625	0.09191	0.09037	n.d	n.d	n.d	6.02	1.68	
18.06.2019	10	0.09125	0.09396	0.09066	n.d	n.d	n.d	5.88	1.27	
18.06.2019	11	0.08313	0.10071	0.09078	n.d	n.d	n.d	5.97	1.01	
18.06.2019	12	0.06438	0.10207	0.09071	n.d	n.d	n.d	6.40	0.89	
18.06.2019	13	0.04938	0.10533	0.09069	n.d	n.d	n.d	7.30	0.83	
18.06.2019	14	0.03313	0.10556	0.09089	n.d	n.d	n.d	7.73	0.63	
18.06.2019	15	0.01313	0.10230	0.09013	n.d	n.d	n.d	7.63	0.85	
18.06.2019	15.5	0.00469	0.00000	0.00000	n.d	n.d	n.d			
18.06.2019	16	0.00250	0.09404	0.09088	n.d	0.00025	-67.72	8.45	2.48	
18.06.2019	16.5	0.00156	0.08546	0.09024	n.d	0.00395	-61.76	9.13	2.95	
18.06.2019	17	n.d	0.07822	0.08980	0.02609	0.00278	-73.84	9.99	4.25	25.1
18.06.2019	17.5	n.d	0.07749	0.09030	0.02659	0.00994	-74.34	10.10	4.09	
18.06.2019	18	n.d	0.07767	0.09012	0.02687	0.01906	-74.99	10.02	3.82	24.3
18.06.2019	18.5	n.d	0.07394	0.08976	0.02821	0.00954	-74.28	10.27	4.37	
18.06.2019	19	n.d	0.05643	0.08914	0.03952	0.02340	-83.73	12.33	5.70	19.1
18.06.2019	19.5	n.d	0.05598	0.08906	0.03957	0.02117	-79.06	12.42	6.07	

18.06.2019	20	n.d	0.04638	0.08830	0.04589	0.02214	-80.68	13.73	6.87	16.8
18.06.2019	20.5	n.d	0.03829	0.08827	0.05096	0.03877	-81.39	15.05	7.65	
18.06.2019	21	n.d	0.03240	0.08780	0.04809	0.02228	-79.19	16.21	8.50	15.9
18.06.2019	22	n.d	0.00938	0.08641	0.07053	0.04573	-80.24	24.53	12.28	13.7
18.06.2019	23	n.d	0.00142	0.08581	0.07643	0.03940	-80.60	34.07	8.77	13.6
18.06.2019	23.5	n.d								
25.07.2019	8	0.06813	0.10034	0.09353	n.d	0.00011		6.89	1.32	
25.07.2019	9	0.03688	0.10180	0.09339	n.d	0.00012		7.18	1.22	
25.07.2019	10	0.00469	0.09359	0.09340	n.d	0.00025		8.54	2.08	
25.07.2019	11	0.00063	0.08357	0.09338	0.01099	0.00372		9.91	3.12	
25.07.2019	11.5	n.d	0.08396	0.09313	0.01325					
25.07.2019	12	n.d	0.08753	0.09397	0.01218	0.00529		10.01	3.07	
25.07.2019	12.5	n.d	0.08510	0.09333	0.01362			9.97	2.48	
25.07.2019	13	n.d	0.08584	0.09331	0.01286	0.00280	-69.46	9.98	2.45	
25.07.2019	13.5	n.d	0.08741	0.09359	0.01154	0.00434	-73.33	10.90	3.13	
25.07.2019	14	n.d	0.08541	0.09320	0.01086	0.00374	-73.91	10.73	3.10	

25.07.2019	14.5	n.d	0.08478	0.09322	0.02107	0.00459	-76.09	13.24	5.17	
25.07.2019	15	n.d	0.07623	0.09272	0.02005	0.00734	-78.02	12.25	4.28	18.06
25.07.2019	15.5	n.d	0.06888	0.09202	0.01181	0.01564	-79.41	10.13	3.14	
25.07.2019	16	n.d	0.06822	0.09228	0.02399	0.01617	-79.08	13.53	5.39	15.97
25.07.2019	16.5	n.d				0.02086	-80.29			
25.07.2019	17	n.d	0.05269	0.09172	0.03217	0.02747	-80.38	16.16	7.35	19.94
25.07.2019	18	n.d	0.04533	0.09179	0.03747	0.04088	-80.00	18.03	8.86	20.97
25.07.2019	19	n.d	0.03330	0.09144	0.04552	0.03756	-80.58	20.55	9.71	17.41
25.07.2019	20	n.d	0.01642	0.09092	0.05687	0.05491	-80.90	25.48	13.76	19.63
25.07.2019	21	n.d	0.00164	0.08966	0.06892	0.05738	-80.94			19.49
25.07.2019	22	n.d	n.d	0.08084	0.08551	0.13807	-80.75			17.24
25.07.2019	23	n.d	0.00430	0.07108	0.09354	0.15318	-80.55			11.11
13.08.2019	8	0.02563	0.09623	0.09403	0.00000	0.00024		7.05	1.10	
13.08.2019	9	0.00219	0.09409	0.09395	0.00000	0.00044		7.90	1.50	
13.08.2019	9.5	0.00094	0.08422	0.09390	0.00000	0.00067		10.21	2.38	
13.08.2019	10	n.d	0.08016	0.09384	0.01239	0.00133		11.05	3.17	

13.08.2019	10.5	n.d	0.07223	0.09323	0.01701	0.00489		12.77	4.08	
13.08.2019	11	n.d	0.07635	0.09385	0.01399	0.00217		11.87	3.81	16.14
13.08.2019	11.5	n.d	0.07623	0.09407	0.01457	0.00458		12.02	3.78	
13.08.2019	12	n.d	0.07678	0.09375	0.01375	0.00343	-73.32	11.85	3.85	16.05
13.08.2019	12.5	n.d	0.07529	0.09380	0.01552	0.00516	-76.52	12.28	4.25	
13.08.2019	13	n.d	0.07489	0.09377	0.01441	0.00500	-76.29	12.40	4.61	14.92
13.08.2019	13.5	n.d	0.07238	0.09371	0.01711	0.00657	-77.94	13.08	4.55	
13.08.2019	14	n.d	0.07072	0.09355	0.01662	0.00653	-78.48	13.35	4.81	15.85
13.08.2019	14.5	n.d	0.06477	0.09287	0.02229	0.00858	-78.97	14.50	5.59	
13.08.2019	15	n.d	0.06251	0.09285	0.02226	0.00967	-79.78	15.17	6.14	13.67
13.08.2019	15.5	n.d	0.06233	0.09265	0.04030	0.00905	-79.57	15.22	6.60	
13.08.2019	16	n.d	0.05072	0.09192	0.02816	0.02140	-78.71	17.68	8.45	15.7
13.08.2019	16.5	n.d	0.04924	0.09222	0.02967	0.01719	-80.38	17.82	8.49	
13.08.2019	17	n.d	0.04032	0.09181	0.03441	0.02610	-80.59	20.65	10.48	15.17
13.08.2019	17.5	n.d	0.04307	0.09182	0.03261	0.01516	-80.52	19.81	10.53	
13.08.2019	18	n.d	0.03105	0.09182	0.03816	0.03535	-80.19	22.94	11.78	14.93

13.08.2019	18.5	n.d	0.03171	0.09164	0.03867	0.00906	-80.69	23.13	12.17	
13.08.2019	19	n.d	0.01325	0.09030	0.05097	0.04451	-80.51	29.94	18.60	16.17
13.08.2019	19.5	n.d	0.01835	0.08803	0.05065	0.05330	-80.58	24.96	13.65	
13.08.2019	20	n.d	0.00640	0.08666	0.06533	0.05777	-80.44	28.03	18.18	17.1
13.08.2019	20.5	n.d	n.d	0.08644	0.06502	0.05797	-80.34			
13.08.2019	21	n.d	n.d	0.08024	0.07809	0.05277	-80.46			15.57
13.08.2019	21.5	n.d	0.00433	0.08021	0.07837	0.06745	-80.37			
13.08.2019	22	n.d	0.00508	0.07111	0.09300	0.07232	-80.19			15.79
13.08.2019	22.5	n.d	0.01038	0.07530	0.09416	0.09345	-80.35			
13.08.2019	23	n.d	n.d	0.06739	0.09807	0.12065	-80.36			14.53
25.09.2019	8	0.01069	0.06500	0.09282	0.00000	n.d		12.72	5.52	
25.09.2019	9	0.00803	0.05209	0.09306	0.01629			18.24	8.13	
25.09.2019	9.5	n.d	0.05372	0.09332	0.01521	n.d		18.15	8.15	
25.09.2019	10	n.d	0.05363	0.09263	0.02803	0.00286		18.18	9.11	15.06
25.09.2019	10.5	n.d	0.05290	0.09269	0.02055	0.00671		18.25	9.46	
25.09.2019	11	n.d	0.05113	0.09225	0.02605	0.01737		18.27	8.59	

25.09.2019	11.5	n.d	0.05039	0.09207	0.02169	0.01733		18.60	9.00	
25.09.2019	12	n.d	0.04980	0.09238	0.02226	0.02184		18.65	8.54	13.03
25.09.2019	12.5	n.d	0.04964	0.09203	0.02507	0.01952	-64.75	18.91	8.58	
25.09.2019	13	n.d	0.04923	0.09185	0.02558	0.02623	-68.46	19.13	8.95	12.7
25.09.2019	13.5	n.d	0.04983	0.09191	0.02381	0.02056	-76.71	19.25	9.29	
25.09.2019	14	n.d	0.05334	0.09278	0.02269	0.01262	-77.32	19.29	10.45	14.18
25.09.2019	14.5	n.d	0.05020	0.09276	0.02385	0.01426	-76.98	19.36	9.75	
25.09.2019	15	n.d	0.04553	0.09178	0.04698	0.01921	-75.43	21.16	12.54	14.37
25.09.2019	15.5	n.d	0.04408	0.09168	0.03249		-73.87	21.65	13.31	
25.09.2019	16	n.d	0.03579	0.09208	0.03635	0.02913	-71.15	23.65	15.73	13.61
25.09.2019	16.5	n.d	0.02612	0.09112	0.04376	0.03129	-79.29	25.65	16.99	
25.09.2019	17	n.d	0.02345	0.09138	0.04595	0.04204	-75.89	27.02	17.98	12.79
25.09.2019	17.5	n.d	0.01806	0.09156	0.05105	0.04030	-78.35	28.37	20.37	
25.09.2019	18	n.d	0.01751	0.09142	0.04976	0.04329	-80.52	28.81	19.81	13.01
25.09.2019	18.5	n.d	0.00806	0.09131	0.05749	0.06071	-77.82	34.11	23.23	
25.09.2019	19	n.d	0.00488	0.09149	0.06225	0.04996	-76.52	41.00	27.42	

25.09.2019	19.5	n.d	0.00000	0.08845	0.07404	0.06087	-78.24		
25.09.2019	20	n.d	0.00000	0.08212	0.07768	0.09247	-79.96		11.45
25.09.2019	20.5	n.d	0.00000	0.06875	0.09344	0.11401			
25.09.2019	21	n.d	0.00000	0.07183	0.11472	0.09133	-79.67		10.21
25.09.2019	21.5	n.d	0.00000	0.05919	0.11510	0.14355	-79.86		
25.09.2019	22	n.d	0.00000	0.05776	0.11481	0.10335	-79.78		9.61
25.09.2019	22.5	n.d	0.00000	0.05468	0.12808	0.10997	-79.16		
25.09.2019	23	n.d	0.00000	0.05939	0.10189	0.10331	-79.92		10.21